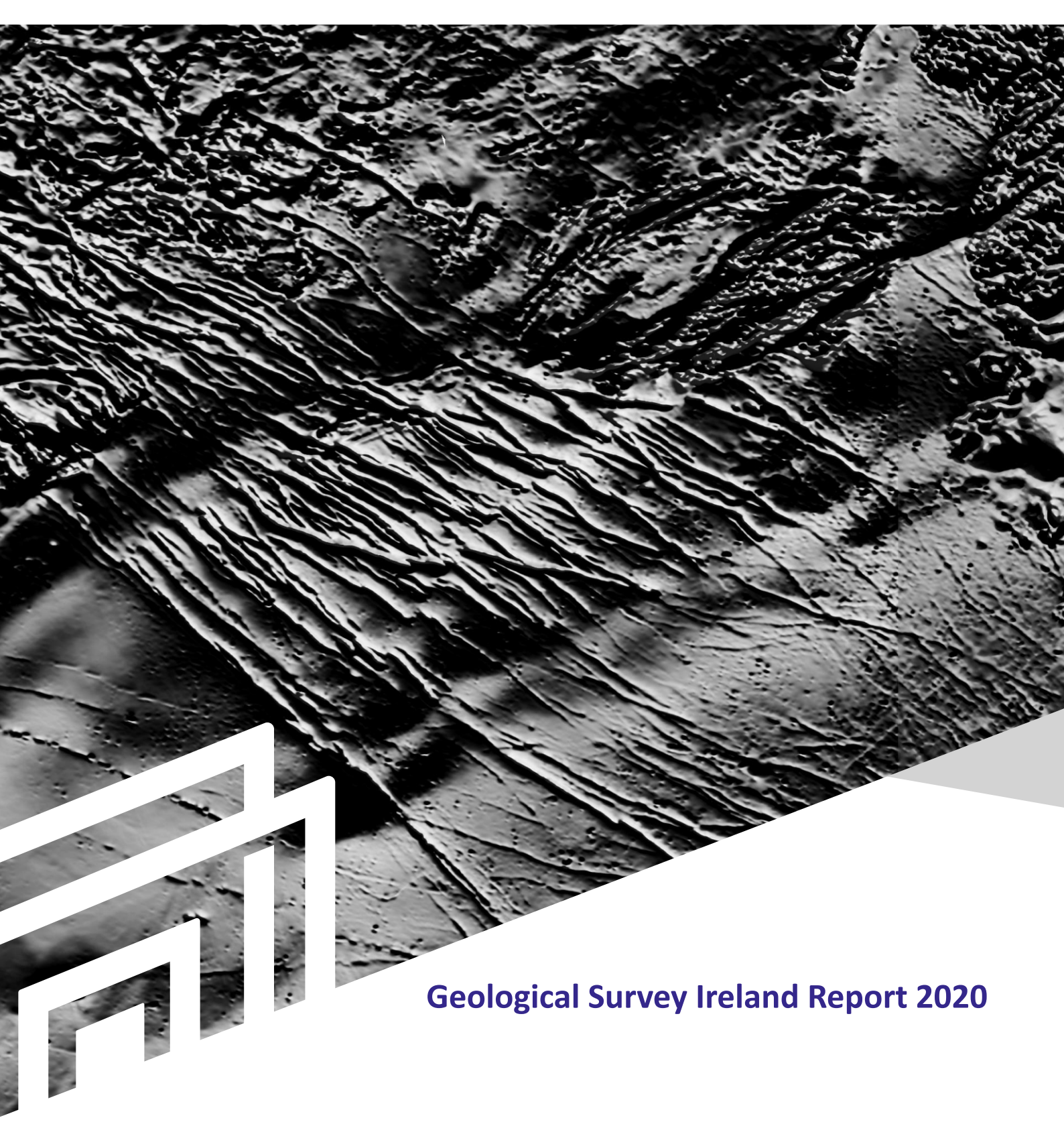




Tellus Interpretation Guide to Airborne Geophysics



Document Information

Project title: Tellus Interpretation Guide to Airborne Geophysical Data Date: 16/10/2020

Prepared By	Date	Comment
M. Ture	27/05/2020 - 30/09/2020	Draft versions: V1.0 – V7.0
M. Ture / M. Muller	15/10/2020	V8.0

Reviewed By	Date	Comment
J. Hodgson, M. Muller	26/08/2020	Review of V6.0
J. Hodgson	30/09/2020	Review of V7.0

Approved By	Date	Comment
J. Hodgson	16/10/2020	V8.0

Version History

Ver. No.	Ver. Date	Comment	Revised By
8.0	16/10/2020	First Published Version	J. Hodgson



Contents

1. I	ntroduction	8
	1.1. The Tellus Survey	8
	1.2. Display	8
2.	Interpretation Guide to Magnetic Data	. 10
	2.1. Magnetic Anomaly Patterns	. 10
	2.2. Magnetic Noise	. 12
	2.3. Image Enhancement in Magnetic Interpretation	. 14
	2.3.1. Upward continued map	. 15
	2.3.2. Pole-reduced (RTP) map	. 17
	2.3.3. First vertical derivative (1VD) map	. 18
	2.3.4. Second vertical derivative (2VD) map	19
	2.3.5. Analytic signal (AS) map	. 20
	2.3.6. Tilt derivative (TDR) map	. 21
	2.4. Examples from Tellus Magnetic Data	. 23
	2.4.1. Tyrone Igneous Complex (illustrating geological features & formations)24
	2.4.2. Galway Granite (illustrating faults and fractures)	. 28
	2.4.3. Galway Roundstone Granite (illustrating internal zonation)	. 31
	2.4.4. Slishwood Division, Sligo-Leitrim (illustrating deep & shallow features)	33 (
	2.4.5. Enniskillen – Monaghan area (illustrating dykes and inferred faults)	. 36
	2.5. Magnetics – Conclusions	. 39
3.	Interpretation Guide to EM Data	. 41
	3.1. Introduction	. 41
	3.2. EM Anomaly Patterns	41
	3.3. Depth of investigation	42
	3.4. EM noise	43
	3.4.1. Cultural noise	44
	3.4.2. Rock petrophysical parameters	44
	3.4.3. High flight altitude	44
	3.4.4. Data processing noise	. 45
	3.5. Resistivity Values Related to 1:500K Geology	46
	3.6. EM Examples from Tellus Data	. 51
	3.6.1. Moffat Shale (illustrating mapping of conductors)	. 52



		3.6.2. Ox Mountains (illustrating litho-stratigraphic variations)	55
		3.6.3. Waterford (illustrating litho-stratigraphic variations)	59
	3.7	. EM Inversion Resistivity Models	62
		3.7.1. Inversion method and models	62
		3.7.2. Enhancement of resistivity models for layer boundary identification	63
		3.7.3. Case-study example: Alluvial sediments, River Maigue, Co. Limerick	64
4.	Int	erpretation Guide to Radiometric Data	69
	4.1	. Introduction	69
	4.2	. Measurement of Gamma Radiation	69
	4.3	. Radiometric Noise and Errors	70
	4.4	. Interpretational Tips for Radiometric Maps	71
	4.5	. Depth of Investigation	72
	4.6	. Radionuclide Concentrations Related to 1:500K Geology	72
	4.7	. Tellus Bundoran Test Line Experiment	79
	4.8	. Radiometric Examples from Tellus Data	81
		4.8.1. Quaternary sediment mapping	86
		4.8.2. Bedrock mapping	91
		4.8.3. Radiogenic heat mapping	94
5. F	Refe	rences	97
Αp	pend	lix 1. Supplementary Information - Magnetics	99
	1. F	irst Vertical Derivative	99
	2. S	econd Vertical Derivative	99
	3. A	analytic Signal	99
	4. T	ïlt Derivative	99
	5. T	otal Horizontal Derivative of Tilt Derivative	L00
Αp	pend	lix 2. Supplementary Information - Electromagnetics 1	L 01
	1.	EM Method	L 01
	2.	Electrical Conductivity of Porous Rocks	L01
	3.	Depth of Investigation1	L01
	4.	EM Noise	102



Figures

FIGURE 1. TELLUS AIRBORNE GEOPHYSICS SURVEY BLOCKS. LEGEND SHOWS SURVEY DATES FOR EACH BLOCK.
BACKDROP, WHERE VISIBLE, SHOWS TOPOGRAPHY.
$ \hbox{Figure 2. Colours, textures and shapes in magnetic map interpretation. Figure numbers indicated for } \\$
EACH EXAMPLE REFER TO FIGURES FOUND LATER IN THE GUIDE
FIGURE 3. NOISE IN MAGNETIC DATA. (A. AND B.) MAGNETIC DATA AND AIR-PHOTO OVER COOMNAGORAGH
MOUNTAIN WINDFARM, CO. CORK IN A6 SURVEY BLOCK. TWO DASHED CIRCLES INDICATE COINCIDENT
LOCATIONS IN BOTH MAPS. NOTE THAT AIR-PHOTO PRE-DATES THE MAGNETIC SURVEY — NOT ALL WINDMILLS
PRESENT IN THE MAGNETIC MAP ARE PRESENT IN THE PHOTO. (C.) GAS PIPELINE AROUND RATHKEALE, CO.
LIMERICK IN A5 SURVEY BLOCK
FIGURE 4. LEVELLING ERRORS IN MAGNETIC DATA IN A5 BLOCK. THE NOISE IS ORIENTED IN THE DIRECTION OF THE
FLIGHT-LINES (NNW-SSE BANDING). THE EXAMPLE SHOWN HERE IS FOR ILLUSTRATIVE PURPOSES ONLY — IT
SHOWS DATA PRIOR TO TIE-LINE LEVELLING AND MICRO-LEVELLING, WHICH ARE GENERALLY EFFECTIVE IN
REMOVING FLIGHT-LINE LEVELLING ARTEFACTS
FIGURE 5. A6 BLOCK TOTAL MAGNETIC INTENSITY (TMI) MAP. HIGH VALUES IN RED ARE POSITIVE AND LOW VALUES
IN BLUE ARE NEGATIVE
FIGURE 6. (A.) A6 BLOCK MAGNETIC MAP UPWARD CONTINUED BY 300 M IN COMPARISON WITH (B.) TMI MAP,
ILLUSTRATING SIGNIFICANT REDUCTION IN CULTURAL MAGNETIC NOISE. HIGH VALUES IN RED ARE POSITIVE AND
LOW VALUES IN BLUE ARE NEGATIVE
FIGURE 7. POLE-REDUCED (RTP) MAGNETIC MAP FOR A6 BLOCK, WITH PRIOR APPLICATION OF 300 M UPWARD
CONTINUATION. HIGH VALUES IN RED ARE POSITIVE AND LOW VALUES IN BLUE ARE NEGATIVE
Figure 8. First Vertical Derivative (1VD) of upward-continued and pole-reduced magnetic grid of $A6$
BLOCK. HIGH VALUES IN RED ARE POSITIVE AND LOW VALUES IN BLUE ARE NEGATIVE
FIGURE 9. SECOND VERTICAL DERIVATIVE (2VD) OBTAINED FROM UPWARD-CONTINUED AND POLE-REDUCED
MAGNETIC GRID OF A6 BLOCK. CULTURAL NOISE IS ALSO RELATIVELY ENHANCED IN THE 2VD. HIGH VALUES IN
RED ARE POSITIVE AND LOW VALUES IN BLUE ARE NEGATIVE
Figure 10. Analytic Signal (AS) for A6 block derived from the TMI data. High values (in red) and low
VALUES (IN BLUE) ARE ALL POSITIVE
FIGURE 11. TILT DERIVATIVE (TDR) OF A6 BLOCK MAGNETIC DATA DERIVED FROM UPWARD CONTINUED AND POLE-
REDUCED TMI GRID. HIGH VALUES IN RED ARE POSITIVE AND LOW VALUES IN BLUE ARE NEGATIVE. VALUES IN
YELLOW ARE AROUND ZERO RADIANS
FIGURE 12. HORIZONTAL DERIVATIVE OF TILT DERIVATIVE (HD-TDR) OF A6 BLOCK MAGNETIC DATA. HIGH VALUES
(IN RED) AND LOW VALUES (IN BLUE) ARE ALL POSITIVE
FIGURE 13. MAGNETIC FEATURES OVER TYRONE IGNEOUS COMPLEX. (A.) EXTRACT FROM 1:250,000 GEOLOGICAL
MAP. (B.) COMPARISON BETWEEN GEOLOGICAL MAP AND SIX DIFFERENT MAGNETIC MAP PRODUCTS. (C. AND
D.) HIGHLIGHTED CHARACTERISTICS AND GEOLOGICAL FEATURES IN SIX DIFFERENT MAGNETIC MAPS. INTERNAL
ARCHITECTURE OF THE IGNEOUS COMPLEX IS PARTICULARLY WELL SHOWN IN THE 2VD AND TDR MAPS 2
FIGURE 14. MAGNETIC FEATURES OVER GALWAY GRANITE. (A.) EXTRACT FROM 1:100,000 GEOLOGICAL MAP. (B.)
COMPARISON BETWEEN GEOLOGICAL MAP AND SIX DIFFERENT MAGNETIC MAP PRODUCTS. (C.) HIGHLIGHTED
CHARACTERISTICS AND GEOLOGICAL FEATURES IN TMI-RTP AND 1VD MAGNETIC MAPS
FIGURE 15. MAGNETIC FEATURES OVER ROUNDSTONE GRANITE, CO. GALWAY. (A.) EXTRACT FROM 1:100,000
GEOLOGICAL MAP. (B.) COMPARISON BETWEEN GEOLOGICAL MAP AND SIX DIFFERENT MAGNETIC MAP
PRODUCTS. INTERNAL ZONATION WITHIN THE OTHERWISE UNIFORMLY MAPPED GRANITE IS WELL ILLUSTRATED
IN THE 1VD AND TDR MAPS
FIGURE 16. MAGNETIC FEATURES OVER SLISHWOOD DIVISION, BETWEEN COOLANEY, CO. SLIGO (SW) AND THUR
MOUNTAINS, CO. LEITRIM (NE). (A.) EXTRACT FROM 1:100,000 GEOLOGICAL MAP. (B.) COMPARISON
BETWEEN GEOLOGICAL MAP AND SIX DIFFERENT MAGNETIC MAP PRODUCTS. (C.) HIGHLIGHTED
CHARACTERISTICS AND GEOLOGICAL FEATURES IN TMI-RTP AND 2VD MAGNETIC MAPS
FIGURE 17. MAGNETIC RESPONSE OVER ENNISKILLEN AND MONAGHAN AREA. (A.) EXTRACT FROM 1:100,000
GEOLOGICAL MAP. (B.) COMPARISON BETWEEN GEOLOGICAL MAP AND SIX DIFFERENT MAGNETIC MAP
PRODUCTS. (C.) DETAIL OF MAGNETIC RESPONSE OF DYKES AND INFERRED FAULT STRUCTURES IN 2VD MAPS
AND LINE INTERPRETATION OF THESE FEATURES
FIGURE 18. APPROXIMATE DEPTHS OF INVESTIGATION FOR TYPICAL IRISH ROCK RESISTIVITIES, FOR THE FOUR TELLUS
SYSTEM FREQUENCIES, DERIVED USING THE HALF-SKIN-DEPTH ESTIMATOR



FIGURE 19. EIVI DATA EXTRACT FROM AZ BLOCK COMPARING (A.) 5 KMZ RESISTIVITY DATA WITHOUT MICRO-	
LEVELLING AND (B.) MICRO-LEVELLED 3 KHZ RESISTIVITY DATA. FLIGHT-LINE PARALLEL LINEAMENTS ARE	
PRESENT IN (A.) BUT ARE REDUCED BY MICRO-LEVELLING IN (B.).	46
FIGURE 20. EM 3 KHZ RESISTIVITIES: PLOT OF MEAN RESISTIVITY VALUE VERSUS LITHOLOGICAL UNIT IN 1: 500K	
GEOLOGY MAP	50
FIGURE 21. EM RESISTIVITY RESPONSE OVER THE MOFFAT SHALE GROUP. (A.) EXTRACT FROM 1:100,000	
GEOLOGICAL MAP. (B.) COMPARISON BETWEEN GEOLOGICAL MAP AND FIVE DIFFERENT EM RESISTIVITY MA	۱P
PRODUCTS. (C.) ANNOTATED DETAIL OF THE CONDUCTIVE ANOMALY ASSOCIATED WITH BLACK SHALES	
(KEHERNAGHKILLY FORMATION AND CORDERRYBANE SHALE FORMATION) OF THE MOFFAT SHALE GROUP.	54
FIGURE 22. EM RESISTIVITY RESPONSE OVER THE OX MOUNTAINS AREA. (A.) EXTRACT FROM 1:100,000	
GEOLOGICAL MAP. (B.) COMPARISON BETWEEN GEOLOGICAL MAP, 3-12-25 KHZ RESISTIVITY TERNARY IMA	\GE
AND RESISTIVITY MAPS AT FOUR FREQUENCIES. (C.) RESISTIVITY MAPS AT FOUR FREQUENCIES WITH ANNOTA	ATED
STRATIGRAPHY. (D.) FRACTIONAL VERTICAL DERIVATIVE MAP (OF ORDER 0.25) AT 3 KHZ WITH ANNOTATED)
STRATIGRAPHY AND 3-12-25 KHZ RESISTIVITY TERNARY IMAGE.	58
FIGURE 23. EM RESISTIVITY RESPONSE OVER A PORTION OF CO. WATERFORD. (A.) EXTRACT FROM 1:100,000	
GEOLOGICAL MAP. (B.) COMPARISON BETWEEN GEOLOGICAL MAP AND RESISTIVITY MAPS AT FOUR	
FREQUENCIES. (C.) RESISTIVITY MAPS AT FOUR FREQUENCIES WITH ANNOTATED STRATIGRAPHY. (D.)	
Fractional vertical derivative maps (of order 0.25) at 12 and 3 kHz with annotated	
STRATIGRAPHY. GEOLOGICAL LINE-WORK (GREY LINES) IS SHOWN IN 0.9 AND 25 KHZ RESISTIVITY MAPS TO)
PROVIDE A GEOLOGICAL FRAME OF REFERENCE	62
FIGURE 24. EXAMPLE 1-D INVERSION MODEL FROM FLIGHT-LINE L5264.1, AT FIDUCIAL NUMBER 314, IN A5 BLOCK	
(LEFT PANEL) RESISTIVITY VERSUS DEPTH, WITH RESISTIVITY VALUES PLOTTED ON A \log_{10} SCALE. (MIDDLE))
VERTICAL DERIVATIVE OF RESISTIVITY VERSUS DEPTH. (RIGHT) ABSOLUTE VALUE OF VERTICAL DERIVATIVE	
VERSUS DEPTH. THE RESISTIVITY STRUCTURE AT THIS LOCATION CONSISTS OF FOUR DISTINCT LAYERS.	
BOUNDARIES BETWEEN LAYERS MAY BE INFERRED FROM VERTICAL DERIVATIVE VALUES CLOSE TO ZERO	64
FIGURE 25. EM INVERSION RESISTIVITY MODELS OVER RIVER MAIGUE ALLUVIAL SEDIMENTS, CO. LIMERICK. (A.)	
EXTRACTS FROM 1:100,000 BEDROCK GEOLOGY AND QUATERNARY MAPS. (B.) COMPARISON BETWEEN	
BEDROCK GEOLOGY AND QUATERNARY MAPS AND RESISTIVITY MAPS AT FOUR DEPTHS. (C.) COMPARISON	
BETWEEN BEDROCK GEOLOGY AND QUATERNARY MAPS AND CROSS-SECTIONS ON L5147 SHOWING	
RESISTIVITY, VERTICAL DERIVATIVE AND ABSOLUTE VALUE OF VERTICAL DERIVATIVE. (D.) INTERPRETATIVE	
GEOLOGICAL SKETCH OF LINE L5147 CROSS-SECTIONS	
FIGURE 26. TYPICAL AIRBORNE GAMMA RAY SPECTRUM (FROM IAEA, 2003)	
FIGURE 27. BUNDORAN TEST LINE GAMMA RAY SPECTROMETRY DATA. (A.) COMPARISON OF AIRBORNE AND GRO	
TOTAL-COUNT DATA AND (B.) GROUND SPECTROMETER TOTAL-COUNT DATA AND MEASURED PEAT THICKNE	
FIGURE 28. COMPARISON BETWEEN AIRBORNE AND GROUND TOTAL-COUNT RADIOMETRIC DATA AND QUATERNA	ιRY
PEAT ALONG BUNDORAN TEST LINE. (A.) EXTRACT FROM 1:100,000 QUATERNARY GEOLOGY MAP. (B.)	
TOTAL-COUNT MEASUREMENTS ALONG GROUND PROFILE. (C.) TOTAL-COUNT GRID FROM AIRBORNE DATA	
SHOWING LOCATION OF GROUND PROFILE. NUMBERS 1, 2 AND 3 INDICATE COINCIDENT LOCATIONS IN ALL	
FIGURES.	_
FIGURE 29. TERNARY IMAGES OF RADIOMETRIC DATA. (A.) CONCENTRATIONS: K-ETH-EU. (B.) CONCENTRATIO	
RATIOS: RTK-RUK-RUT. (c.) Sum-normalised abundances: Kn-THn-Un.	84
FIGURE 30. GUIDE TO COLOURS GENERATED USING RGB COLOUR PALETTE FOR TERNARY DISPLAYS. (A. AND B.)	1
ILLUSTRATE THE STANDARD COLOUR ALLOCATION USED IN THE CONCENTRATION TERNARIES: RED = MAXIMU	
CONCENTRATION IN THE DATASET, GREEN = MAXIMUM THORIUM CONCENTRATION AND BLUE = MAXIMUM	
URANIUM CONCENTRATION. (C., D. AND E.) ILLUSTRATE THE COLOUR VARIATION FROM, ON LEFT-HAND SID	
MAXIMUM CONCENTRATION IN ONE ELEMENT AND ZERO CONCENTRATION IN THE OTHER TWO, TO, ON RIGH	
HAND SIDE, ZERO CONCENTRATION IN THE SAME ONE ELEMENT AND MAXIMUM CONCENTRATION IN THE OT	HER
TWO. (F.) ILLUSTRATES THE COLOUR VARIATION THAT ARISES WHEN THE CONCENTRATIONS IN ALL THREE	
ELEMENTS INCREASE SIMULTANEOUSLY FROM ZERO ON LEFT-HAND SIDE (BLACK) TO THEIR MAXIMA ON RIGH	
HAND SIDE (WHITE).	
FIGURE 31. PEAT BOGS MAPPED BY AIRBORNE TOTAL-COUNT DATA. THICK PEAT (RED) AREAS ARE MAPPED WHER	iΕ
TOTAL-COUNT ≤400 c/s. ORANGE POLYGONS (TOTAL-COUNT ≤1000 c/s) MAP THE MAJORITY OF PEAT DEPOSITS ON THE QUATERNARY MAP	ი-
DEPUSITS ON THE QUATERNARY WAP	o/



FIGURE 32. RADIOMETRIC RESPONSE OVER RIVER MAIGUE ALLUVIAL SEDIMENTS, CO. LIMERICK, SHOWING EXTRACT
FROM 1:100,000 QUATERNARY GEOLOGY MAP, TERNARY IMAGE OF CONCENTRATIONS AND COMPOSITE
IMAGE OF SUM-NORMALISED ABUNDANCES
FIGURE 33. RADIOMETRIC RESPONSE OF MULLAGHMORE SANDSTONE, CO. SLIGO AND CO. LEITRIM. (A.) EXTRACT
FROM HIGH-RESOLUTION DTM, AND 1:100,000 GEOLOGICAL AND QUATERNARY MAPS. NOTE ABSENCE OF
MAPPED QUATERNARY GEOLOGY IN NORTHERN IRELAND. (B.) RADIOMETRIC CONCENTRATION TERNARY MAP,
AND 1:100,000 GEOLOGY MAP AND DTM SHOWN WITH RADIOMETRIC TERNARY DATA CLIPPED TO THE
BOUNDARY OF THE MULLAGHMORE SANDSTONE FORMATION
FIGURE 34. RADIOMETRIC RESPONSE OF BARNESMORE GRANITE, CO. DONEGAL. (A.) EXTRACT FROM 1:100,000
GEOLOGICAL MAP IN COMPARISON WITH URANIUM/POTASSIUM CONCENTRATION RATIO MAP. (B.)
COMPARISON BETWEEN GEOLOGICAL MAP AND FIVE DIFFERENT RADIOMETRIC MAPS, EMPHASISING DIFFERENT
ASPECTS OF THE INTERNAL STRUCTURE OF THE GRANITE. OUTLINE OF THE GRANITE DISPLAYED VARIOUSLY IN
DIFFERENT COLOURS ON THE MAPS. U/K RATIO MAP IS CLIPPED TO THE BOUNDARY OF THE GRANITE 92
FIGURE 35. RADIOMETRIC RESPONSE OF SOUTH EASTERN IRELAND. 93
FIGURE 36. RADIOGENIC HEAT PRODUCTION OF NEAR-SURFACE ROCKS IN IRELAND, DERIVED FROM TELLUS RADIO-
ELEMENT (K, U, TH) CONCENTRATIONS. (A.) MAP OF IRISH RADIOGENIC HEAT PRODUCTION, WITH SEVERAL
HIGH HEAT PRODUCTION GEOLOGICAL FORMATIONS HIGHLIGHTED. (B.) EXTRACTS FROM GEOLOGICAL (LEFT-
HAND SIDE) AND RADIOGENIC HEAT PRODUCTION (RIGHT-HAND SIDE) MAPS AT SELECTED GEOLOGICAL
LOCALITIES96



Tables

TABLE 1. 3 KHZ APPARENT RESISTIVITY DATA: MEAN RESISTIVITY AND RESISTIVITY RANGES (MAXIMA AND MINIMA)	
WITH RESPECT TO LITHOLOGICAL UNITS IN THE $1:500\mbox{K}$ GEOLOGY MAP. RESISTIVITY DATA ARE TAKEN FROM TI	ΗE
Tellus '2019B merge' dataset which comprises 41,839,151 data points, of which 40,642,737	
WERE CORRELATED WITH GEOLOGY. 1,250,017 DATA POINTS ARE LOCATED OVER WATER BODIES (COASTAL	
AREAS AND LAKES) AND PROVIDE NO LITHOLOGICAL CORRELATIONS.	46
TABLE 2. GAMMA RAY ENERGY WINDOWS UTILISED IN GAMMA RAY SPECTROMETRY	70
Table 3. Data statistics for Potassium Concentration with respect to lithological units in the 1:500kg	K
GEOLOGY MAP. DATA UNIT: PERCENTAGE	73
TABLE 4. DATA STATISTICS FOR EQUIVALENT THORIUM CONCENTRATION WITH RESPECT TO LITHOLOGICAL UNITS IN	
THE 1:500K GEOLOGY MAP. DATA UNIT: PARTS PER MILLION.	75
TABLE 5. DATA STATISTICS FOR EQUIVALENT URANIUM CONCENTRATION WITH RESPECT TO LITHOLOGICAL UNITS IN	
THE 1:500K GEOLOGY MAP. DATA UNIT: PARTS PER MILLION.	77



1. Introduction

1.1. The Tellus Survey

Tellus is a national programme to gather ground geochemical and airborne geophysical data across the island of Ireland. The project is managed by Geological Survey Ireland and funded by the Department of Environment, Climate and Communications (previously Department of Communications, Climate Action and Environment). The Tellus survey began in Northern Ireland in 2005, followed by mapping in the Republic of Ireland in 2011. Surveys are flown on an annual phased basis collecting data as survey blocks, which are then merged together to form seamless regional/ national datasets.

The airborne geophysical survey collects magnetic, electromagnetic and radiometric data from survey lines spaced 200 m apart, at an orientation of 345 degrees and at a nominal survey altitude of 60 m. All final processed data are made freely available to the public at www.gsi.ie/tellus or www.tellus.ie.

A map of Tellus airborne survey blocks completed to date is shown in Figure 1. Since 2015, survey blocks have been labelled alpha-numerically and sequentially (e.g., A1, A2, etc.), with the exception of the Waterford Block of 2016. Earlier survey blocks were named geographically (abbreviations typically used for these blocks are shown in brackets): the original Tellus block (NI), Tellus Border (TB) and Tellus North Midlands (TNM). Throughout the Guide, survey blocks are referred to as, for example, "A1 Survey Block" or "Block A1".

A number of geophysical products / outputs are routinely or selectively produced from the airborne datasets that can be used to help geological interpretation. This guide is designed to help explain the different geophysical datasets and map images that are produced and how they might assist in geological interpretations, with reference to Tellus data and the geology of Ireland. All examples shown are drawn from existing Tellus datasets

1.2. Display

Geophysical data are typically gridded and plotted to create contour or coloured pixel maps. Different gridding parameters can be used to display the data. Tellus grids are generally produced using the minimum curvature method for magnetic and resistivity data while the inverse distance weighting method is typically used for radiometric datasets. Different gridding parameters can produce slight variations, particularly at a local scale.



A 32 colour ramp (Geosoft 32 colour ramp) is used for most of the grids/maps produced by Tellus. Low values are given in blue and high values in red/purple. Greyscale maps are also produced, often for the magnetic first vertical derivative maps. The choice of colour ramp is often a personnel choice – with different users having different preferences.

Maps can also be displayed with illumination (or shading), where the effect of a light source is simulated, casting shadows across the 'topography' of the data grid. These illuminated maps are useful for enhancing both strong gradients and subtle features within the maps. While different illumination inclinations (height above the horizon, from $0^{\circ} - 90^{\circ}$) and declinations (azimuth with respect to True North, from $0^{\circ} - 360^{\circ}$ E of N) can highlight geological trends with different orientations, a misleading sense of the locations of anomalies may be given, as features may appear to move depending on the orientation of the illumination, particularly at a local scale.

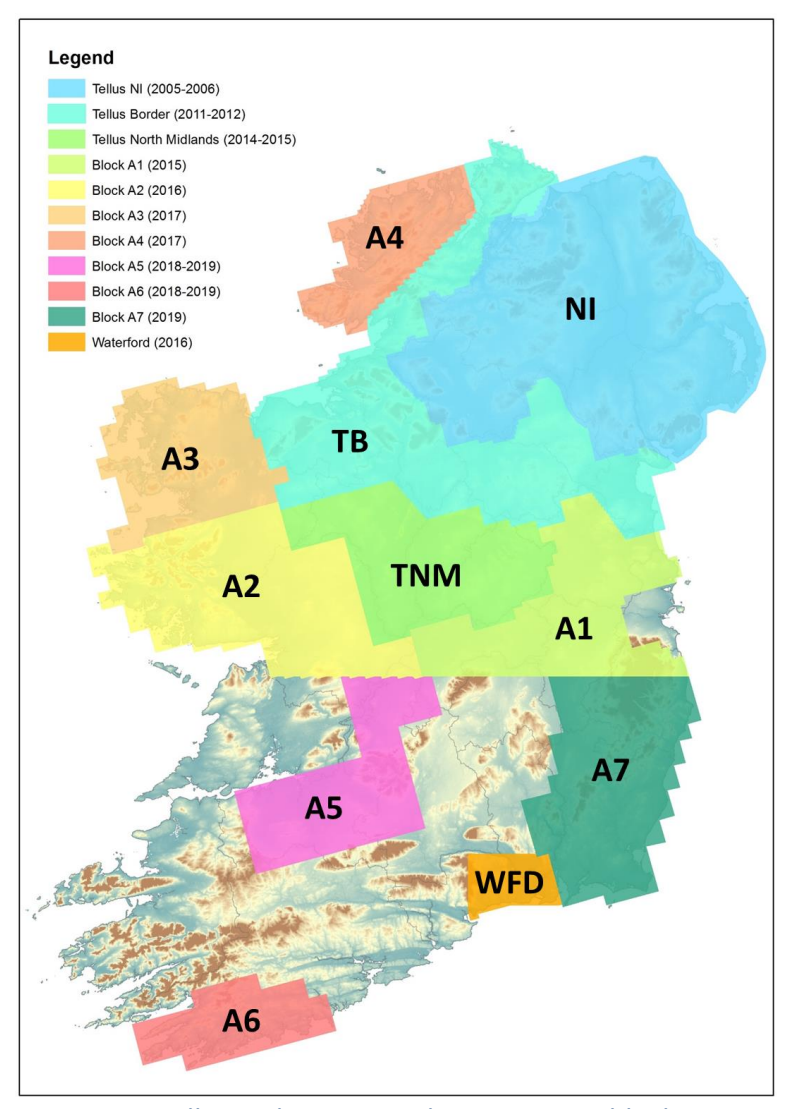


Figure 1. Tellus airborne geophysics survey blocks. Legend shows survey dates for each block. Backdrop, where visible, shows topography.



2. Interpretation Guide to Magnetic Data

2.1. Magnetic Anomaly Patterns

Qualitative interpretation of magnetic maps consists of recognizing and delineating anomaly patterns. These patterns can be classified based on size, shape, texture and amplitude. This simple grouping of anomalies allows an adequate first-pass analysis of most regional magnetic maps, which can then be followed up by further detailed interpretation or numerical modelling where needed. It should be noted that the various different patterns may not necessarily occur isolated from each other, but may be found superimposed (e.g., Parasnis, 1986).

Some typical anomaly patterns and their corresponding geological origin are summarised below:

- Circular features: often associated with granitic and basic intrusions.
- Long narrow anomaly features: frequently due to dykes, tectonic shear zones, elongated ore bodies and isoclinal folds associated with magnetic mineralisation.
- Displacements (lateral offsets of anomalies) are indicative of geological faults.
- Extensive, 'sheet-like' high magnetic intensity areas may show basaltic flows, sills, large gabbro intrusions and greenstone belts.
- 'Quiet' areas with little magnetic relief and with no distinctive pattern may indicate quarzitic, monzonite or limestone rock formations, or areas under thick sedimentary cover.

A consideration of colour and tone, texture and shape may be useful in interpreting magnetic maps (Figure 2):

Colour and tone (in greyscale images)

- High amplitude (positive or negative) anomalies indicate high magnetisation strength and/or shallow depth of burial.
- Low amplitude (positive or negative) anomalies indicate low magnetisation strength and/or greater depth of burial.

Texture

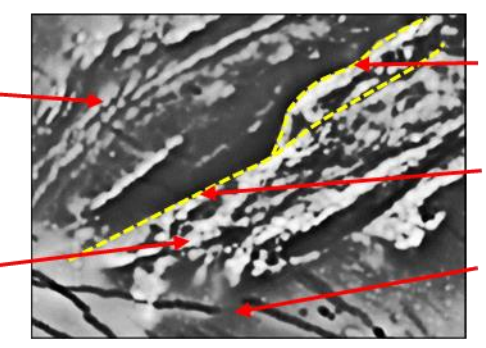
- Look for distinct textural zones or areas.
- Rough textures short wavelength variations indicate shallow magnetic sources or marked internal variation in geological unit.
- Smooth textures long wavelength variations indicate deep magnetic sources or little lateral variation in magnetisation properties.



TONE, TEXTURE AND SHAPE

Moderately duller tone – somewhat deeper magnetic sources

Very bright tone, 'sharp focus' – shallow sources



Explicit linear – stratigraphic contact

Explicit linear – fault and fault contact

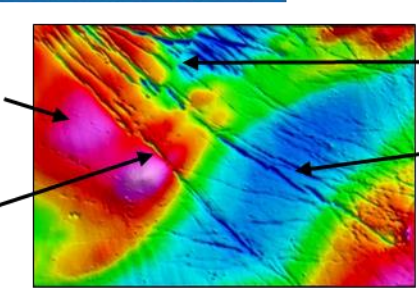
- Implicit linear – fault

1VD - Fig. 13b

TEXTURE, COLOUR AND SHAPE

Broad, long-wavelength variation – deep magnetic sources

Superimposed shortwavelength linears – shallow sources



Implicit linear - fault

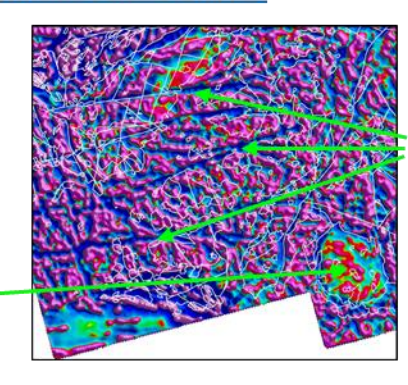
Explicit linears – dykes

TMI-RTP - Fig. 17b

TEXTURE, COLOUR AND SHAPE

Texture and colour changes here define two distinct magnetic bodies (both igneous bodies in this example)

Sub-circular shape – igneous intrusion

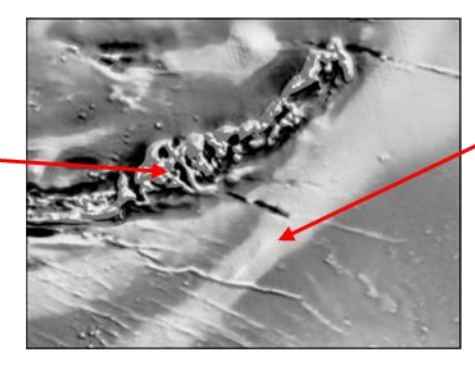


Explicit linears – faults and shear zones

2VD - Fig. 14b

TEXTURE

Short-wavelength variation and 'sharp focus' — shallow magnetic source



Long-wavelength variation and 'less sharp focus' – deeper magnetic source

1VD - Fig. 16b

Figure 2. Colours, textures and shapes in magnetic map interpretation. Figure numbers indicated for each example refer to figures found later in the guide.



Shape

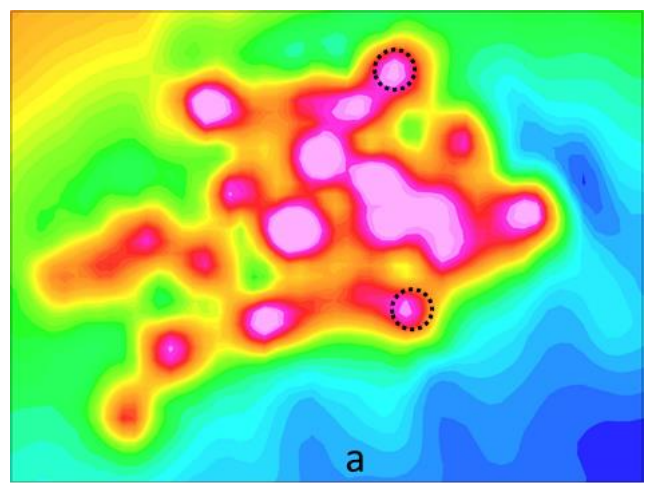
- Explicit linears
 - Narrow features: with distinct magnetisation properties dykes, shear zones.
 - Edges: contacts between units with distinct magnetisation properties – sedimentary or igneous contacts, fault contacts.
- Implicit linears
 - Lined-up anomaly terminations or anomaly displacements faults.
- Sub-circular shapes
 - Often igneous intrusions

The interpretation of various magnetic anomaly patterns on magnetic maps should be made in conjunction with geological maps/observation and consideration of the geological context. Conversely, magnetic mapping is perhaps of greatest importance in constructing or remapping the geology in areas with sparse rock outcrop. The most important element of interpretation of geophysical data is that it makes geological sense.

2.2. Magnetic Noise

Geophysical data record not only the geological responses from rocks but may also record or contain anomalies from different noise sources (e.g., anthropogenic sources, data-acquisition system noise or artefacts from the survey geometry). When interpreting geophysical data, it is important to be aware of potential sources of noise so that noise is not misinterpreted as geological features, for example, misinterpreting a power-line as a fault. Cultural noise refers to effects from anthropogenic, non-geological features such as buildings, windfarms, roads, pipelines, industrial complexes and power-lines, which often give rise to short wavelength bullseye or linear shaped signals in maps. Figure 3 shows magnetic noise relating to a windfarm on Coomnagoragh Mountains, Co. Cork in A6 Survey Block (a, b) and a gas pipeline near Rathkeale, Co. Limerick (c) in A5 Survey Block.







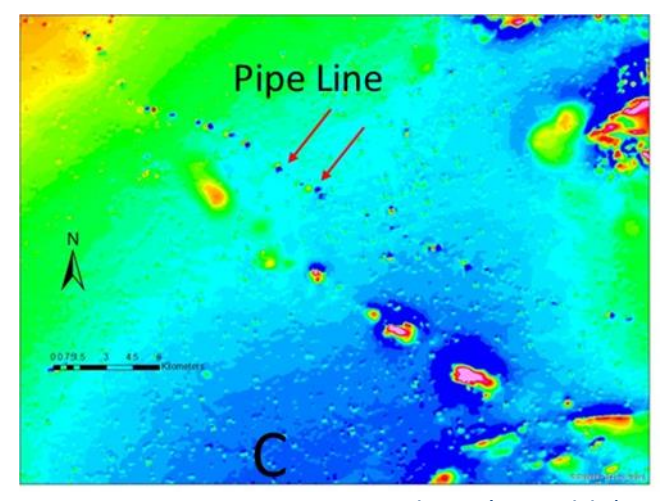


Figure 3. Noise in magnetic data. (a. and b.) Magnetic data and air-photo over Coomnagoragh Mountain windfarm, Co. Cork in A6 Survey Block. Two dashed circles indicate coincident locations in both maps. Note that air-photo pre-dates the magnetic survey – not all windmills present in the magnetic map are present in the photo. (c.) Gas pipeline around Rathkeale, Co. Limerick in A5 Survey Block.

Data processing noise

As a result of the processing of data acquired along discrete flight-lines and in different survey blocks at different times, geophysical grids may show levelling



effects (banding or striping parallel to the flight-line direction) or boundary effects between merged blocks that have proven difficult to remove during processing. Data users are advised to be aware of the flight-line geometry as well as variations in the geophysical signals that may relate to variable survey altitude and variable local terrain and topography.

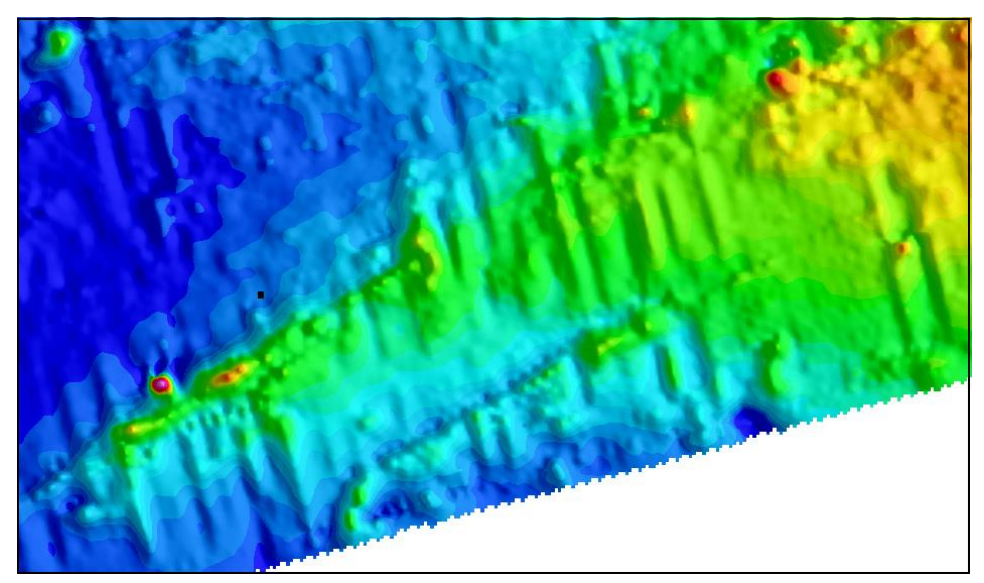


Figure 4. Levelling errors in magnetic data in A5 Block. The noise is oriented in the direction of the flight-lines (NNW-SSE banding). The example shown here is for illustrative purposes only – it shows data prior to tie-line levelling and micro-levelling, which are generally effective in removing flight-line levelling artefacts.

2.3. Image Enhancement in Magnetic Interpretation

Magnetic maps can be processed or filtered in different ways to help enhance different aspects of the image, for example, to sharpen anomalies or to focus on the signal from different depths. Magnetic data from Block A6 in west Cork have been processed to produce six different magnetic maps (Figures 5-12) to illustrate the effects of a range of different applied filters. The Tellus geophysics group commonly produces these maps for GSI users from the original magnetic anomaly data, often referred to as Total Magnetic Intensity data. The maps include (with abbreviations in brackets):

- i) Total Magnetic Intensity (TMI)
- ii) Upward continuation by 150 m or 300 m (Up150 or Up300)
- iii) TMI Reduced-to-Pole (TMI-RTP or RTP)
- iv) First Vertical Derivative of RTP (1VD)
- v) Second Vertical Derivative of RTP (2VD)
- vi) Tilt Derivative of RTP (TDR)
- vii) Total Horizontal Derivative of Tilt Derivative (HD-TDR)
- viii) Analytic Signal of RTP (AS)



The definitions, characteristics and uses of these 'value-added' maps are described below, illustrated by the maps produced using each filter. Mathematical equations describing each filter may be found in Appendix 1. The image processing and filtering starts with the final contractor delivered magnetic data – the Total Magnetic Intensity (TMI) data – as shown in Figure 5.

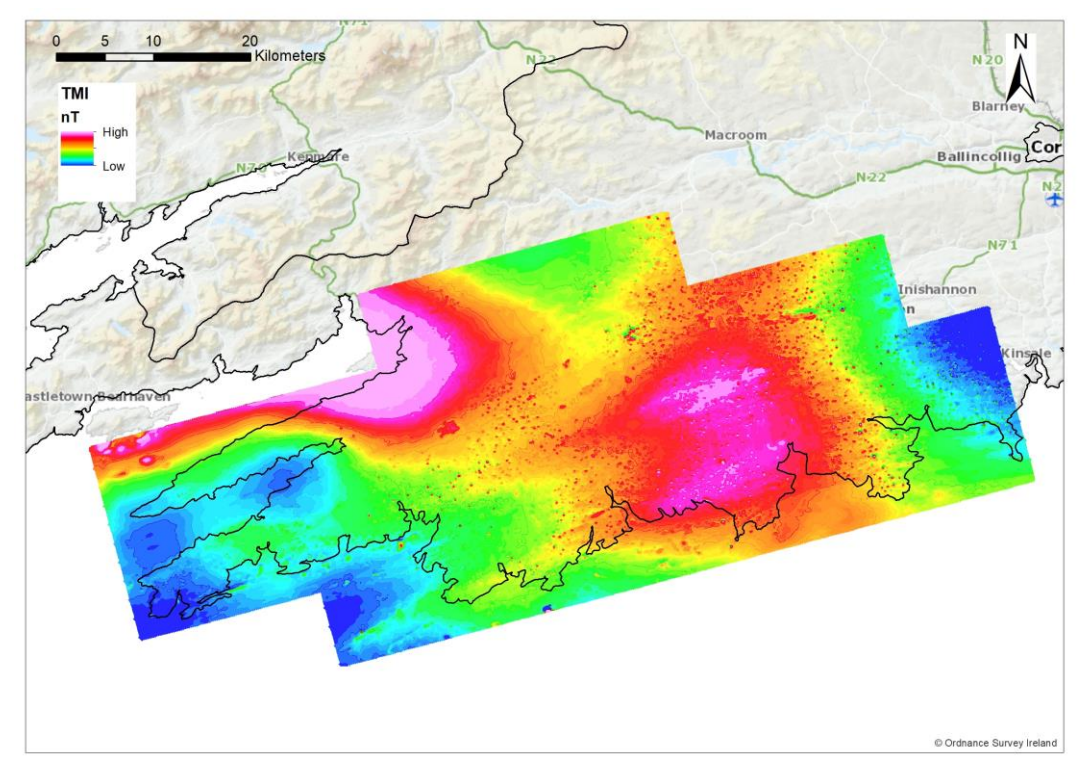


Figure 5. A6 Block Total Magnetic Intensity (TMI) map. High values in red are positive and low values in blue are negative.

There are a number of cultural noise features apparent in the magnetic intensity data in Figure 5, typically from farms and buildings and appearing as high-frequency (short-wavelength) pinpricks or bullseyes. Cultural noise can be removed through applying a 'de-spiking' filter to the flight-line data or through use of a smoothing filter such as upward continuation, which calculates the magnetic field at an elevation higher than that at which it was recorded, effectively removing shallow-source magnetic signals, including those relating to cultural noise.

It is noted again that geological features should be interpreted with caution in the light of possible cultural artefacts.

2.3.1. Upward continued map

Computation of magnetic fields at higher flight altitudes than the data were recorded at is referred to as upward continuation. The process is used to smooth out short-wavelength anomalies and to relatively enhance long-wavelength



anomalies. Upward continuation is useful for suppressing the effects of shallow-sourced anomalies when detail of deeper anomalies is required.

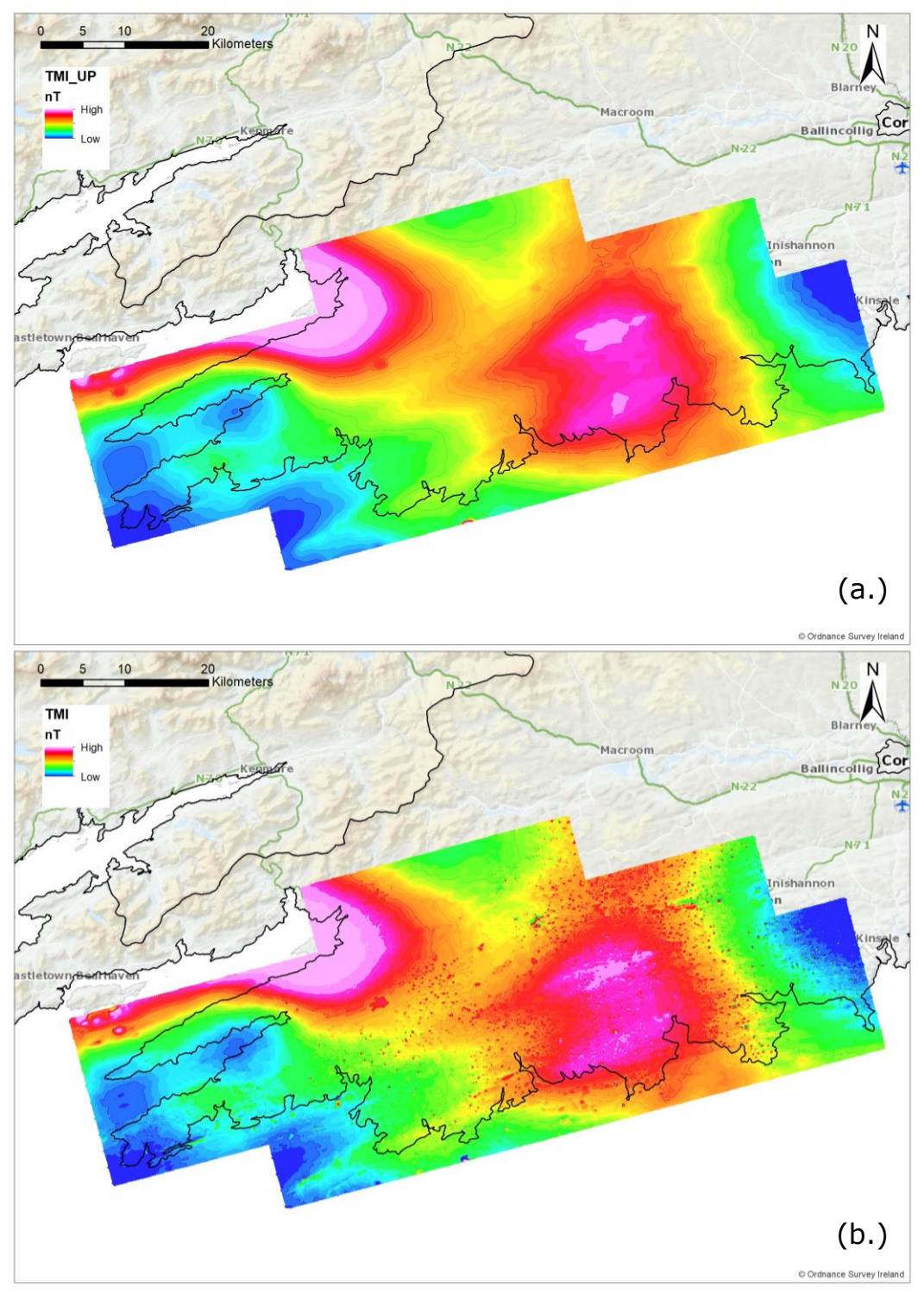


Figure 6. (a.) A6 Block magnetic map upward continued by 300 m in comparison with (b.) TMI map, illustrating significant reduction in cultural magnetic noise. High values in red are positive and low values in blue are negative.



Upward continuation is considered a clean filter because it produces almost no side effects that may require the application of other filters or processes to correct. It is, therefore, often used to remove or minimise the effects of shallow sources and cultural noise in grids. Furthermore, upward continued data may be interpreted numerically and with modelling programs, which is not the case for data produced by many other filters. The upward continuation process illustrated in Figure 6 is used to clean short-wavelength cultural noise. If different high level upward continuations do not successfully remove the observed cultural noise, it may be necessary to remove the noise by manual editing of flight-line data.

2.3.2. Pole-reduced (RTP) map

The magnetic field associated with geological bodies arises from the parallel alignment of domains in magnetic minerals in rocks with the Earth's present-day magnetic field (itself generated in the Earth's deep interior). Such magnetisation of crustal rocks is referred to as induced magnetisation, as it is induced in rocks by the Earth's deep-sourced magnetic field. The strength of the induced magnetisation depends on the magnetic susceptibility property of the rocks. Crustal rocks may also contain a component of remanent magnetisation, in which the magnetic domain alignment is not parallel with the Earth's present-day magnetic field, but reflects the Earth's magnetic field orientation at the time and location of rock formation or metamorphism.

As the shape of induced magnetic anomalies is variable, depending on the location of the geological bodies with respect to the Earth's magnetic poles, a process referred to as 'reduction-to-the-pole' is used to simplify anomaly shapes by calculating the effective magnetic field anomaly at the location of the poles, where the Earth's magnetic field orientation is vertical rather than inclined (Milligan and Gunn, 1997).

When the Earth's field is inclined, induced magnetic anomalies have shapes that are asymmetric with respect to their subsurface sources. However, when the inducing field is vertical, the induced anomalies are located directly and symmetrically over their magnetic sources. Reduction-to-the-pole transforms magnetic intensity data to equivalent data that would have been recorded if the survey was at a magnetic pole, and hence places the magnetic anomalies directly over their causative bodies, greatly simplifying the geological interpretation of the data.

Note that reduction-to-the-pole, however, does not correctly re-position anomalies associated with remanent magnetisation. The possibility of remanence should, therefore, always be considered when interpreting the positions of anomalies and their causative bodies in pole-reduced data.



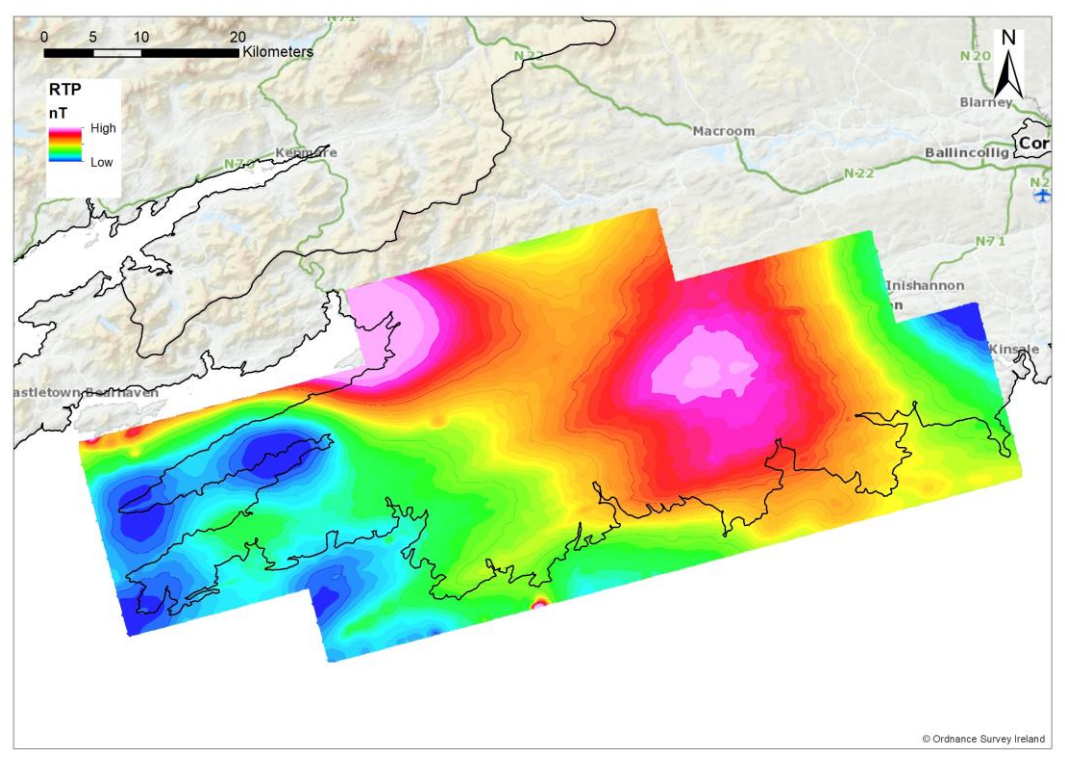


Figure 7. Pole-reduced (RTP) magnetic map for A6 Block, with prior application of 300 m upward continuation. High values in red are positive and low values in blue are negative.

2.3.3. First vertical derivative (1VD) map

The first vertical derivative (1VD) or vertical gradient (Milligan and Gunn, 1997) is the mathematical equivalent to physically measuring the magnetic field simultaneously at two points, with one point located vertically above the other. By subtracting one measurement from the other and dividing the result by the vertical spatial separation of the two measurements, a vertical gradient is derived. The 1VD enhances short-wavelength anomalies, often separating overlapping adjacent anomalies and eliminates long-wavelength regional anomalies. The vertical derivative is commonly applied to total magnetic field data to enhance the shallowest geological sources in the data. As with other filters that enhance the short-wavelength components of the wavelength spectrum, it may be necessary to apply an additional filter, for example a low-pass filter, to subdue short-wavelength noise.



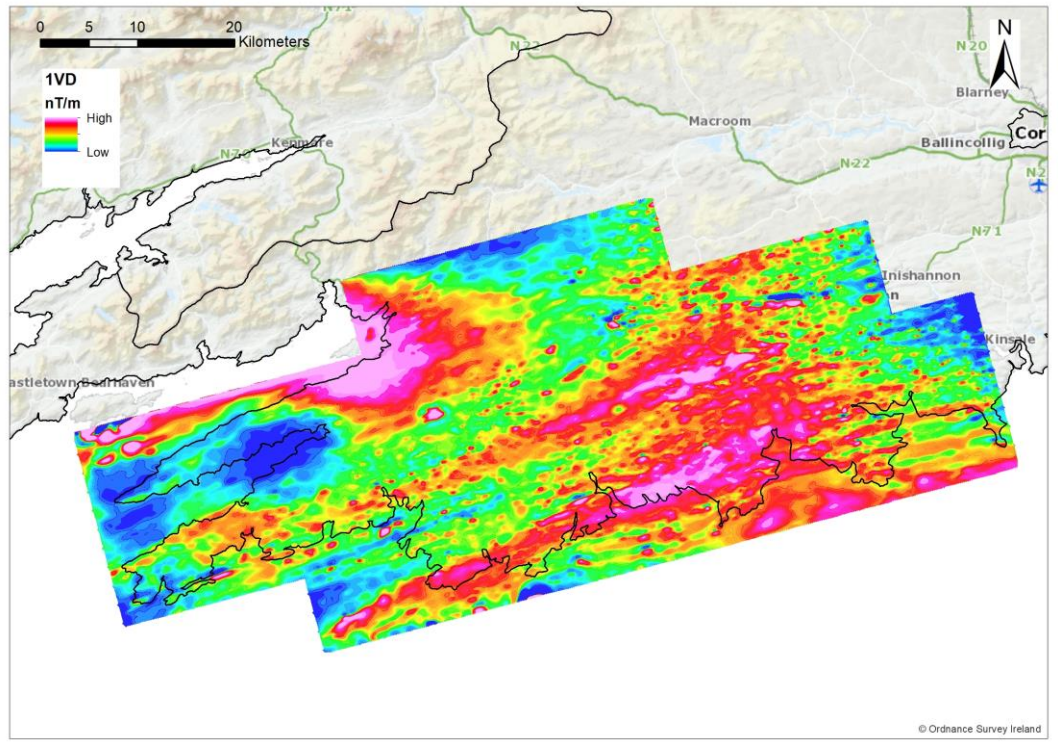


Figure 8. First Vertical Derivative (1VD) of upward-continued and pole-reduced magnetic grid of A6 Block. High values in red are positive and low values in blue are negative.

Figure 8 illustrates that shallow geological boundaries and structures are enhanced and better defined in the first vertical derivative (1VD) when compared to the maps of Figures 5 to 7. Notice that the SSW-NNE linear trends, which reflect the banding of geological units, are present both on-shore and off-shore.

2.3.4. Second vertical derivative (2VD) map

The value of the second vertical derivative (2VD) for magnetic interpretation arises from the fact that the double differentiation with respect to vertical distance tends to emphasize, even further than the 1VD, the anomalies associated with small, shallow geologic structures at the expense of larger, regional features. The 2VD map can help identify additional near-surface anomalies not clearly imaged in the 1VD map.



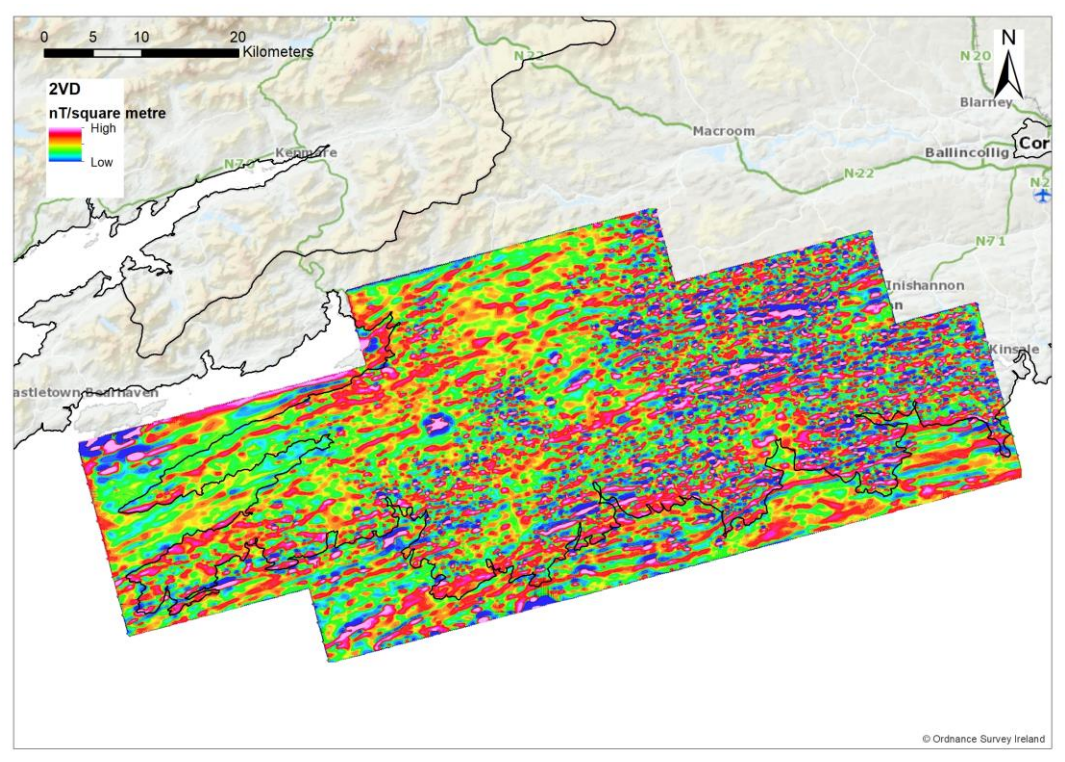


Figure 9. Second Vertical Derivative (2VD) obtained from upward-continued and pole-reduced magnetic grid of A6 Block. Cultural noise is also relatively enhanced in the 2VD. High values in red are positive and low values in blue are negative.

Figure 9 illustrates an increased number of shallow features imaged and delineated in the 2VD map, in comparison with the 1VD map of Figure 8. A large number of geological boundaries and faults are apparent in the 2VD image. Contour maps, as opposed to colour grid images, of the 2VD can also prove effective in highlighting lineaments oriented in different directions.

2.3.5. Analytic signal (AS) map

The analytic signal (AS) (Nabighian, 1972) is calculated by taking the square root of the sum of the squares of each of the three directional first derivatives (in the X and Y horizontal grid directions and in the vertical Z direction). The resulting shape of the analytic signal is independent of the orientation of the magnetisation of the source, whether induced or remanent. The effect is one of transforming the asymmetric shape of the magnetic anomaly, for any magnetisation orientation recorded at any magnetic latitude, to a single positive anomaly (or peak) centred directly over the geologic structure giving rise to the anomaly.

The form of the AS, therefore, greatly simplifies the geological interpretation of the data. AS maps are characterised by 'ridges' located above the geological contacts of larger bodies or at the centre of narrow bodies. Because the AS map is derived using derivatives, anomalies relating to shallow magnetic bodies are sharpened and enhanced with respect to the TMI map. As anomalies associated



with remanent magnetisation are correctly positioned directly over causative bodies in the analytic signal, it offers an advantage in this respect over reduced-to-pole (RTP) maps.

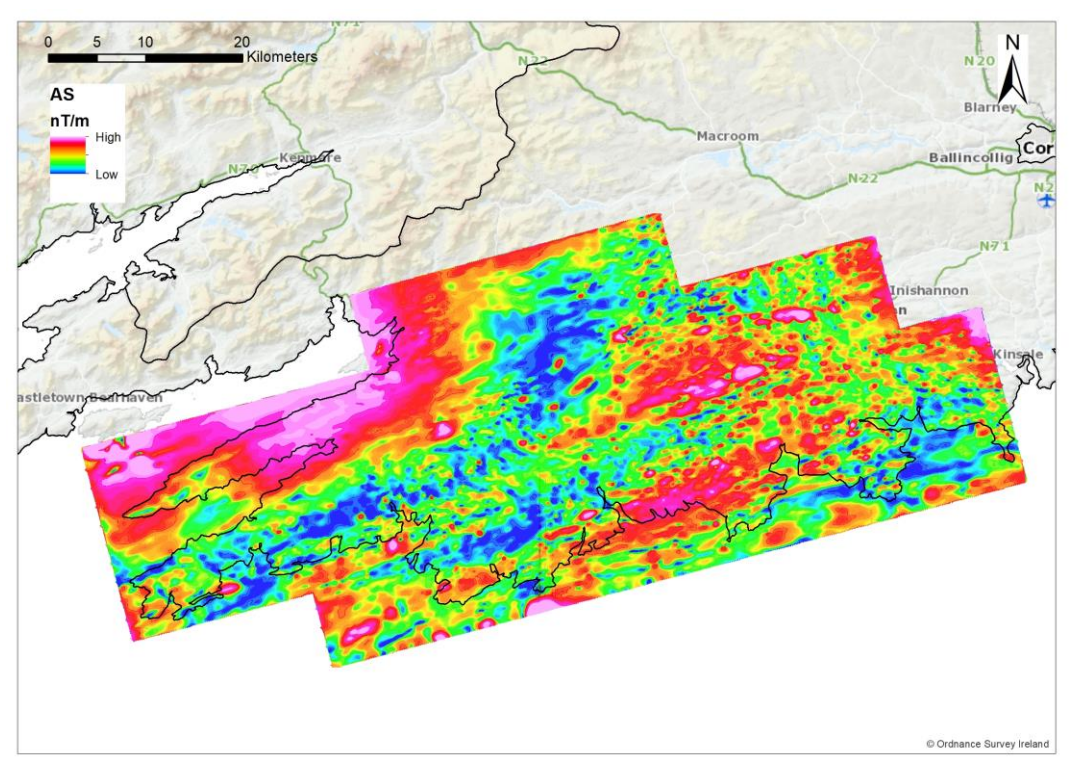


Figure 10. Analytic Signal (AS) for A6 Block derived from the TMI data. High values (in red) and low values (in blue) are all positive.

2.3.6. Tilt derivative (TDR) map

The tilt derivative (TDR) (Verduzco et al., 2004) is defined as the arctangent of the ratio of the vertical derivative of the TMI (numerator) to the total horizontal derivative of the TMI (denominator). The total horizontal derivative is defined as the square root of the sum of the squares of the two horizontal derivatives in the X and Y grid directions. As the TDR is an angle, it is often referred to as the 'tilt angle' or 'local phase' of the magnetic field.

The tilt derivative offers several advantages in the interpretation of magnetic anomalies. First, the dependence of the TDR on magnetisation strength is the same in both the horizontal and vertical derivatives, so weakly magnetic bodies are weighted the same as strongly magnetic bodies – providing a relative enhancement of subtler features present in the TMI data. Second, the TDR has a very simple form, simplifying the geological interpretation of the data. For example, for vertical geological contacts the TDR = 0° contour corresponds with the boundaries of causative magnetic bodies. TDR values are also always positive over the bodies themselves and negative away from them. The lateral distance observed on maps between the TDR = 0° and 45° contours also provides an estimate of the depth to the top of the magnetic body (Salem et al., 2007).



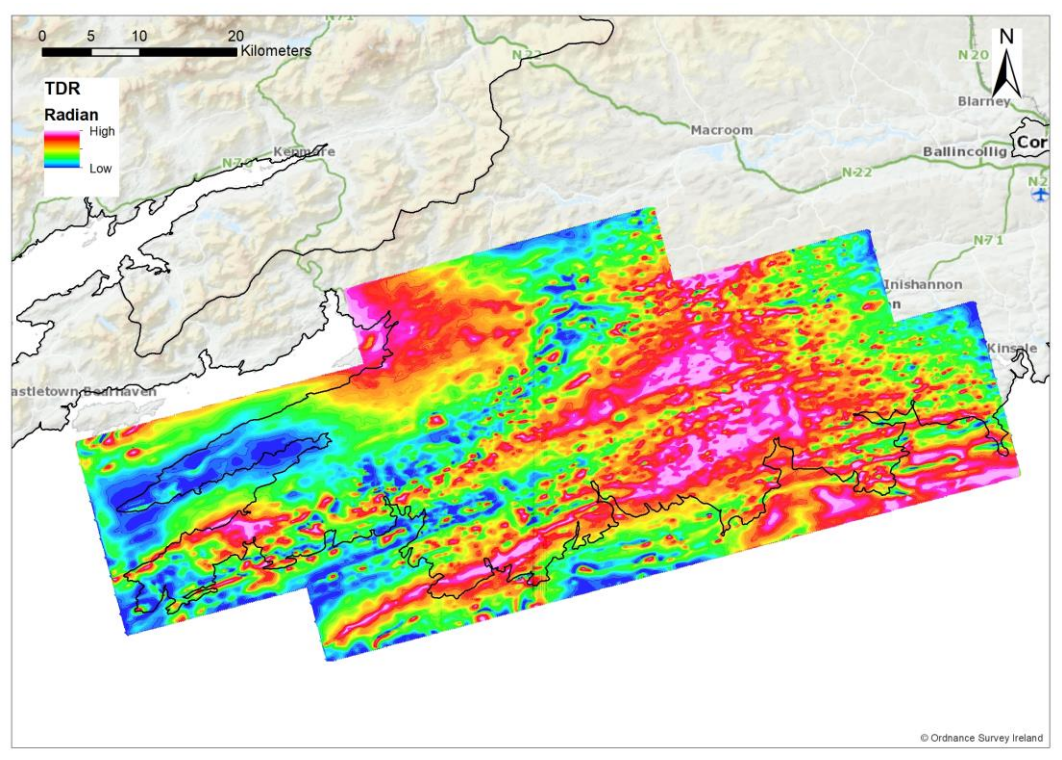


Figure 11. Tilt Derivative (TDR) of A6 Block magnetic data derived from upward continued and pole-reduced TMI grid. High values in red are positive and low values in blue are negative. Values in yellow are around zero radians.

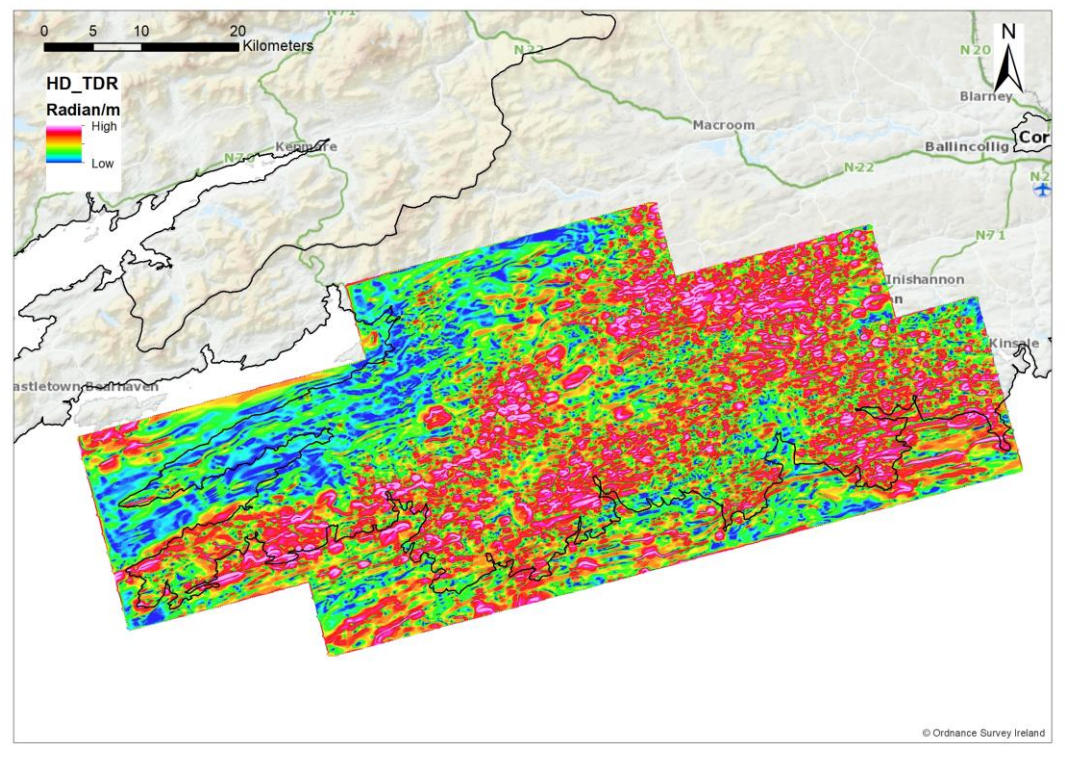


Figure 12. Horizontal Derivative of Tilt Derivative (HD-TDR) of A6 Block magnetic data. High values (in red) and low values (in blue) are all positive.



An additional product may be derived from the TDR, in the form of the total horizontal derivative of the tilt derivative (HD-TDR) (Figure 12). It is defined as the square root of the sum of the squares of the two horizontal derivatives of the TDR in the X and Y grid directions.

The tilt derivative and the total horizontal derivative of the tilt derivative are useful for mapping shallow basement structures and mineral exploration targets (Geosoft Oasis Montaj, undated reference).

Note that the various derivative grids do not enhance all magnetic (geological) features similarly, but may highlight different features depending on, for example, magnetisation strength (which may depend on lithological variation), lateral and vertical size of the causative magnetic body and depth of burial. It is up to the interpreter to identify and use the map most suited to their interpretation needs.

2.4. Examples from Tellus Magnetic Data

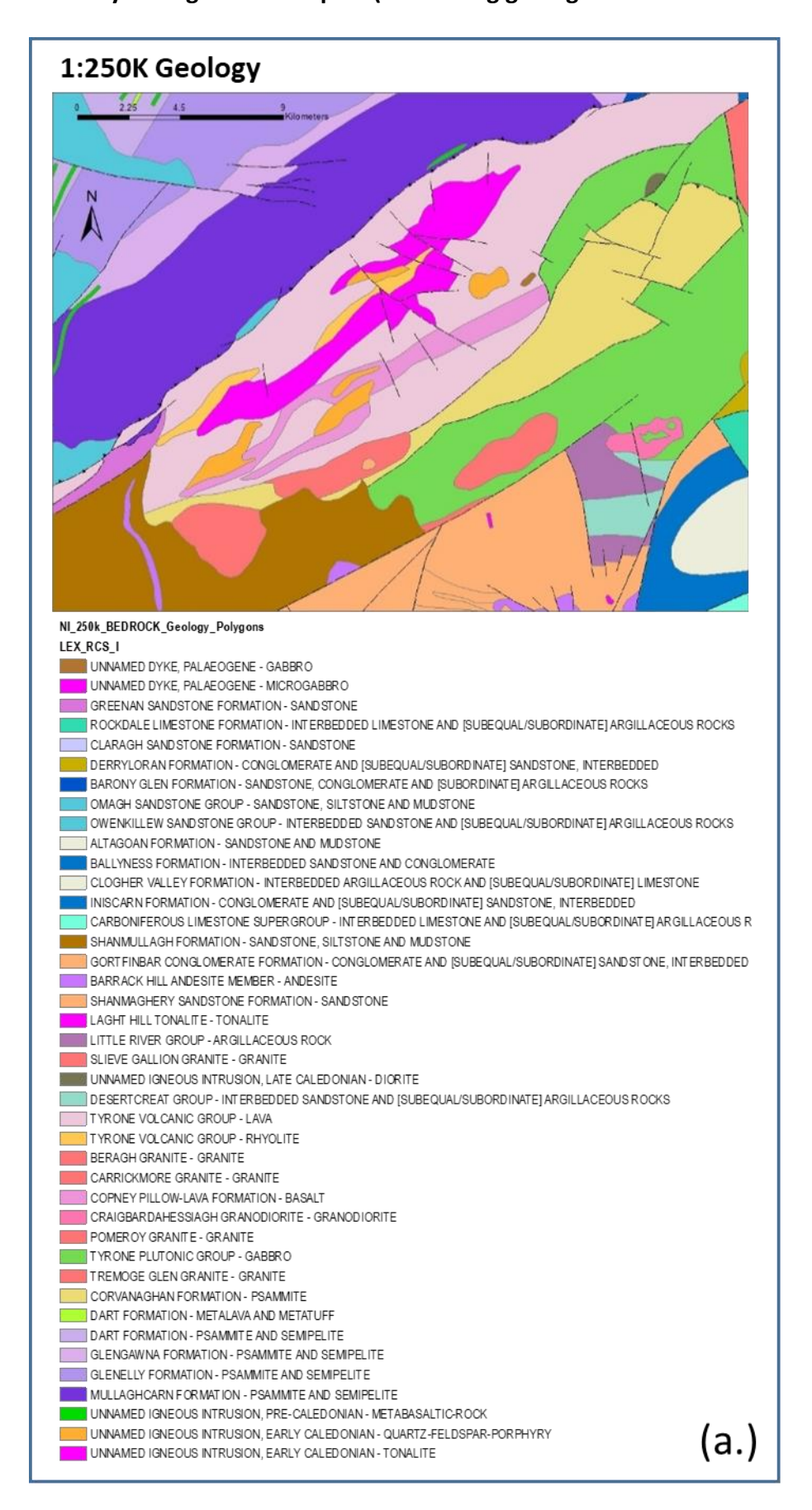
The following examples show how different filtered images can be used to map geology and identify anomalies. The definition of each filter has been described above (sections 2.3.1 to 2.3.6). Five examples were chosen to illustrate interpretation of the following:

- i.) Geological features and formations.
- ii.) Faults and fractures zones.
- iii.) Internal zonation.
- iv.) Differences between deep and shallow features.
- v.) Dykes and inferred faults.

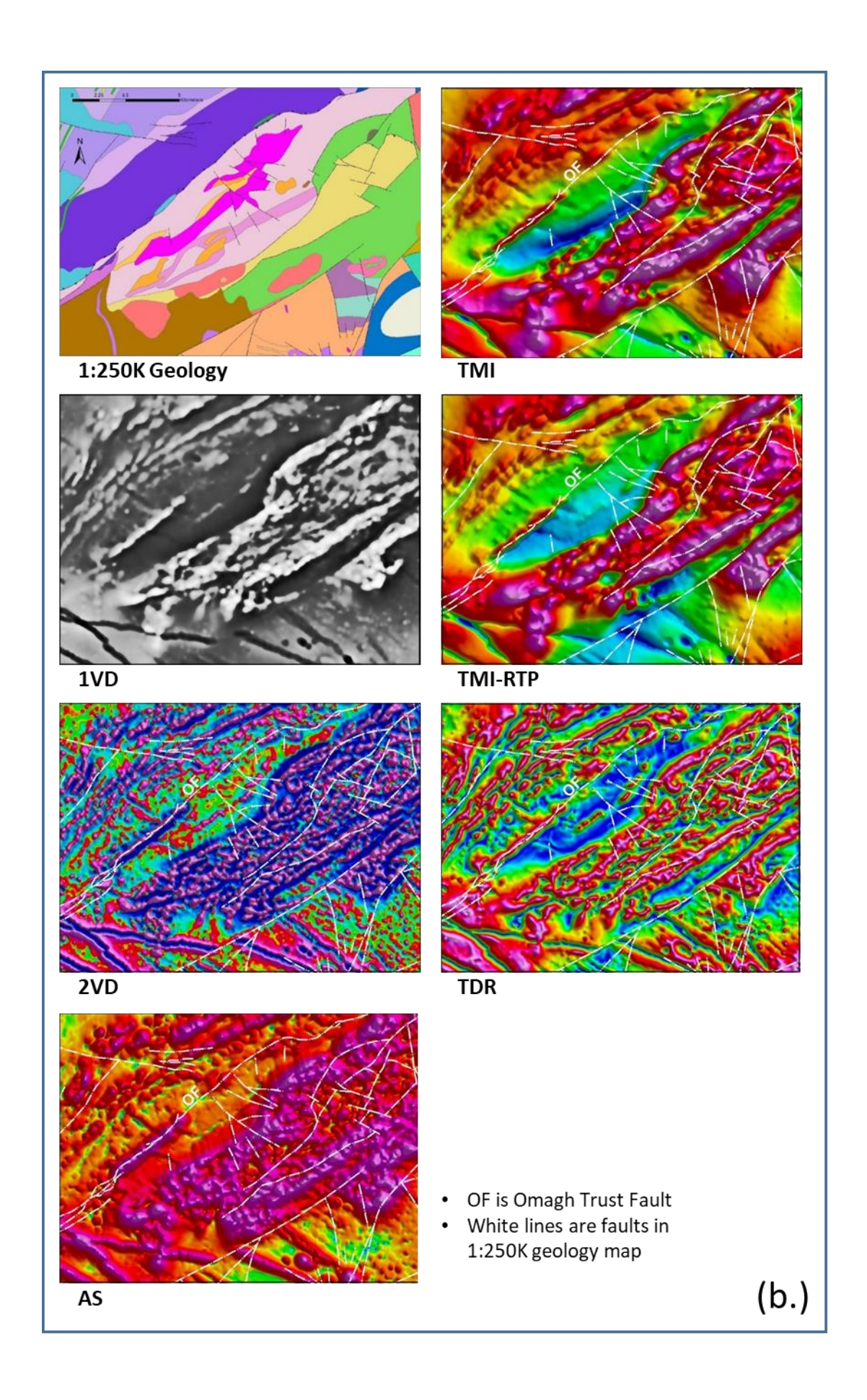
For each case-study example presented below, the geological map with stratigraphic legend is presented in the first panel (extracted from 1:100,000 or 1:250,000 geological maps, as annotated), followed by a composite panel showing maps of geology, Total Magnetic Intensity (TMI) upward continued by 150 m, Reduced-to-Pole (TMI-RTP), First Vertical Derivative (1VD), Second Vertical Derivative (2VD), Tilt Derivative (TDR) and Analytic Signal (AS). The bottom panels show zoomed-in images of the geophysical maps together with interpretational tips and observations, illustrating potential uses of the six magnetic maps for each area.



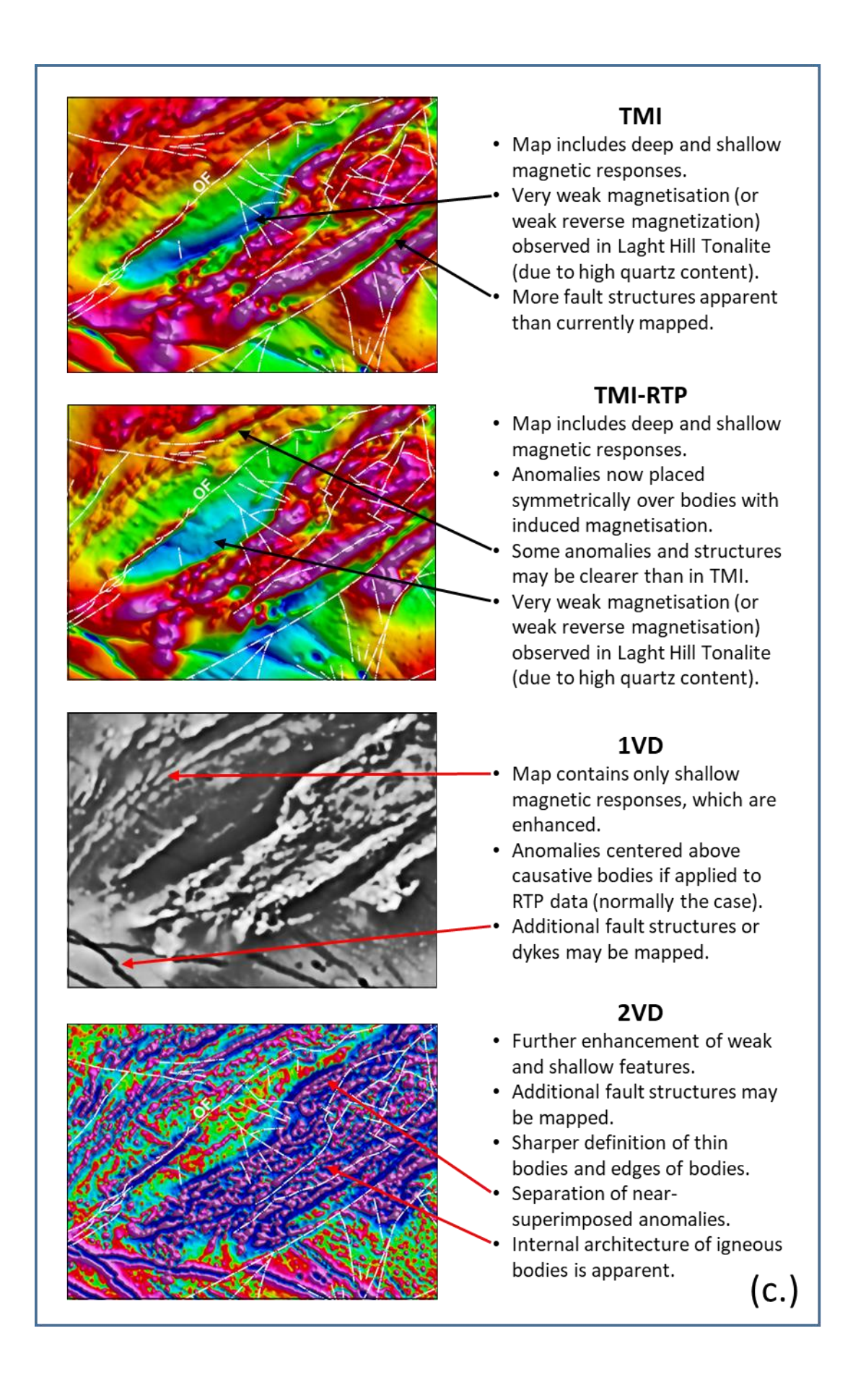
2.4.1. Tyrone Igneous Complex (illustrating geological features & formations)













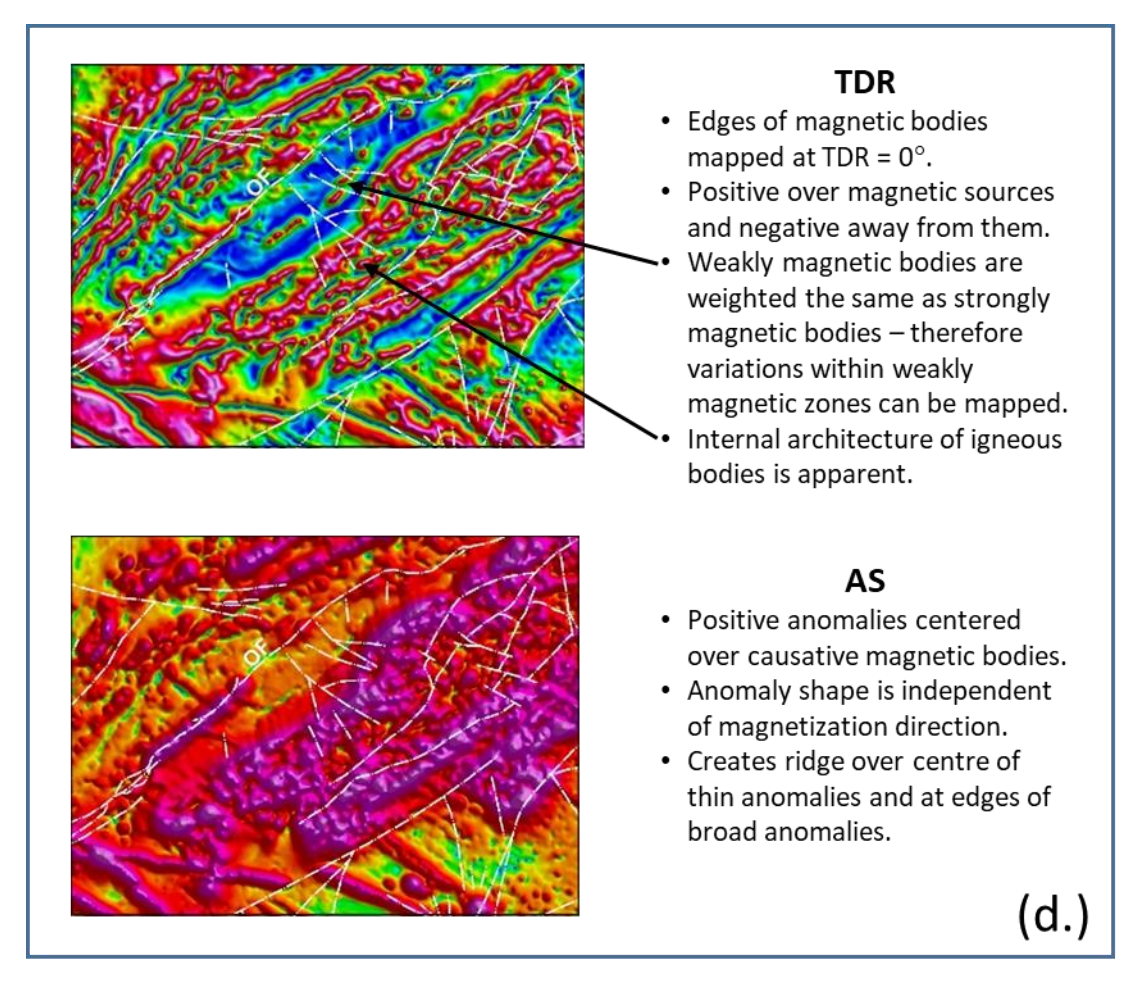
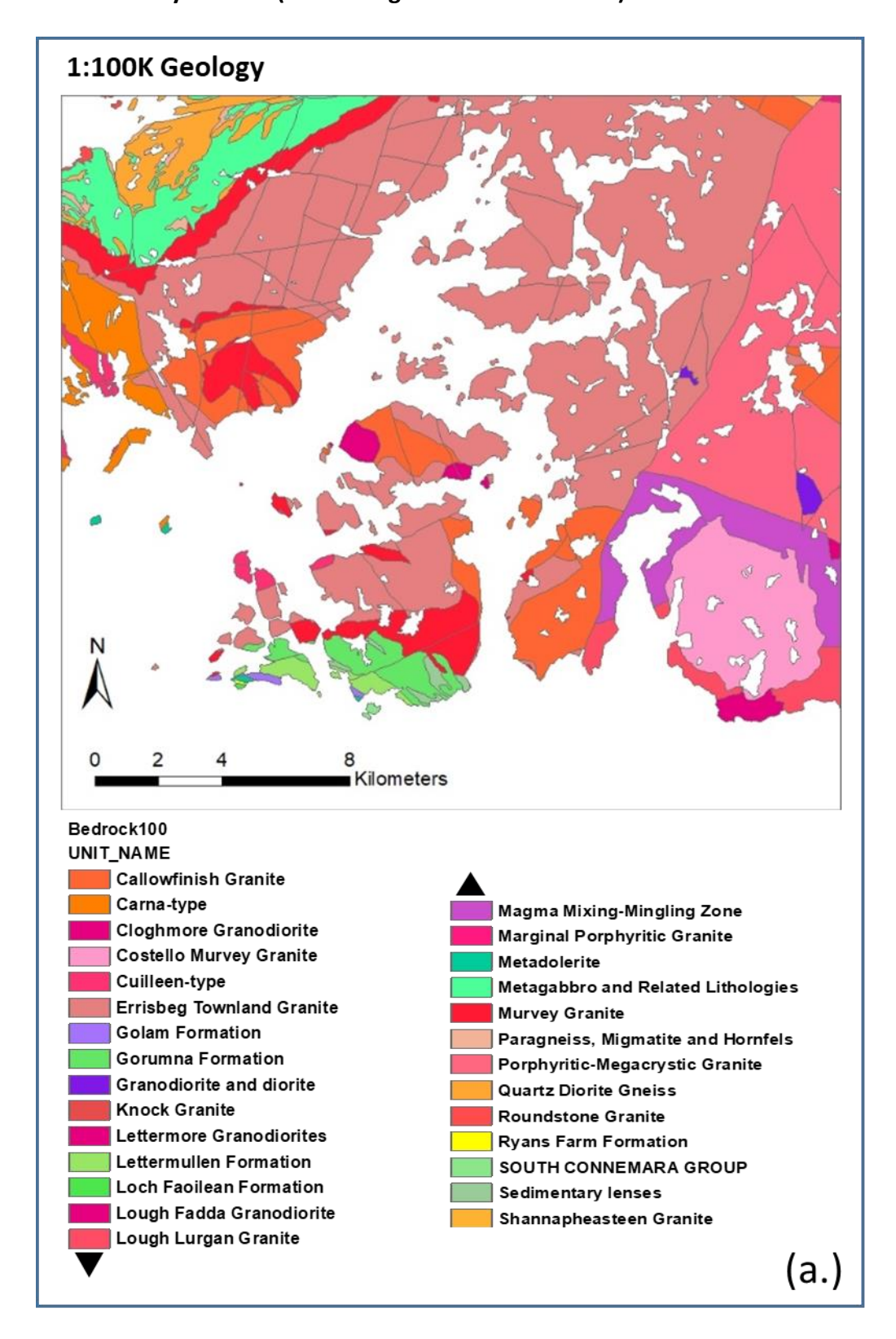


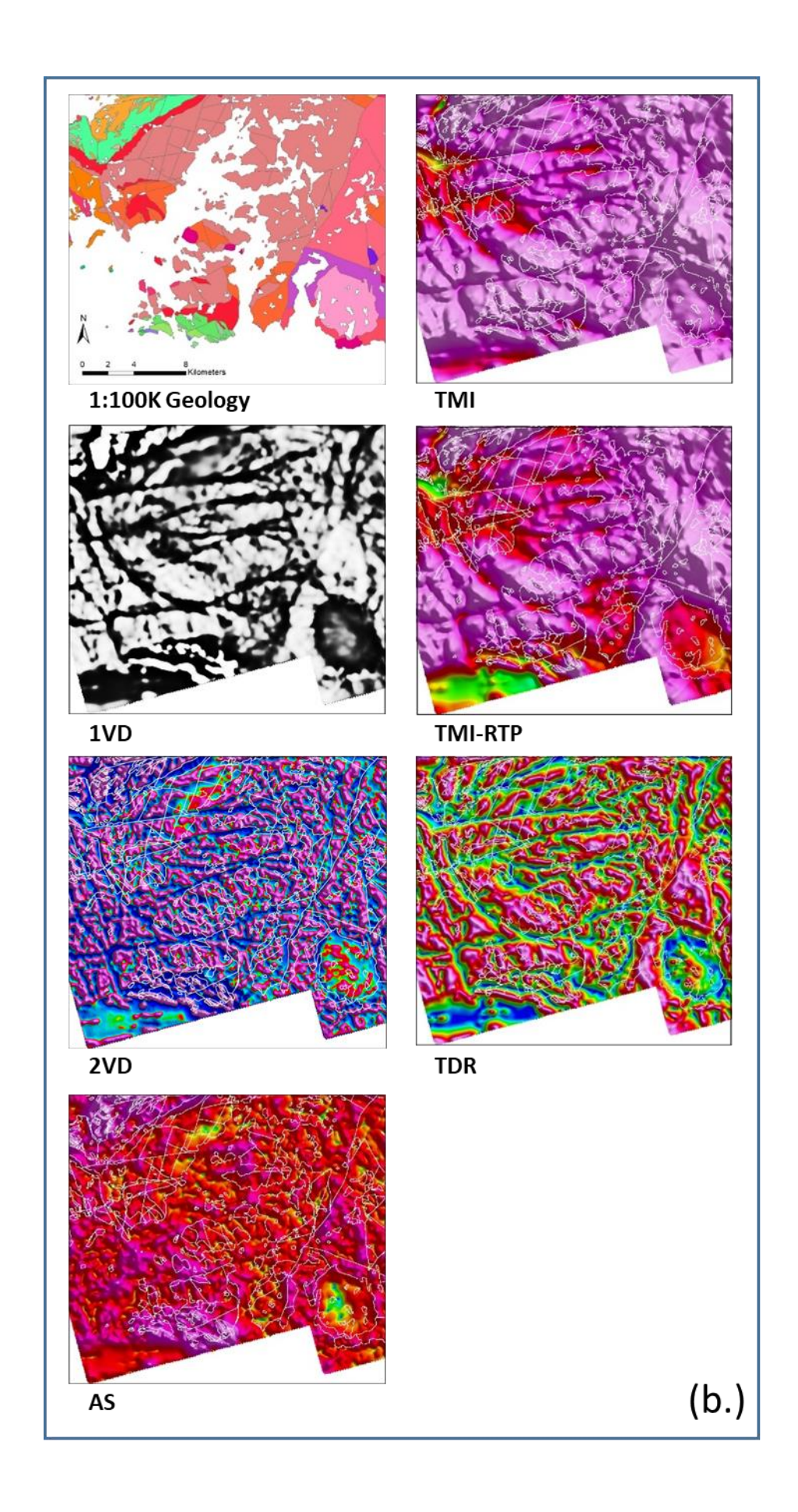
Figure 13. Magnetic features over Tyrone Igneous Complex. (a.) Extract from 1:250,000 geological map. (b.) Comparison between geological map and six different magnetic map products. (c. and d.) Highlighted characteristics and geological features in six different magnetic maps. Internal architecture of the igneous complex is particularly well shown in the 2VD and TDR maps.



2.4.2. Galway Granite (illustrating faults and fractures)









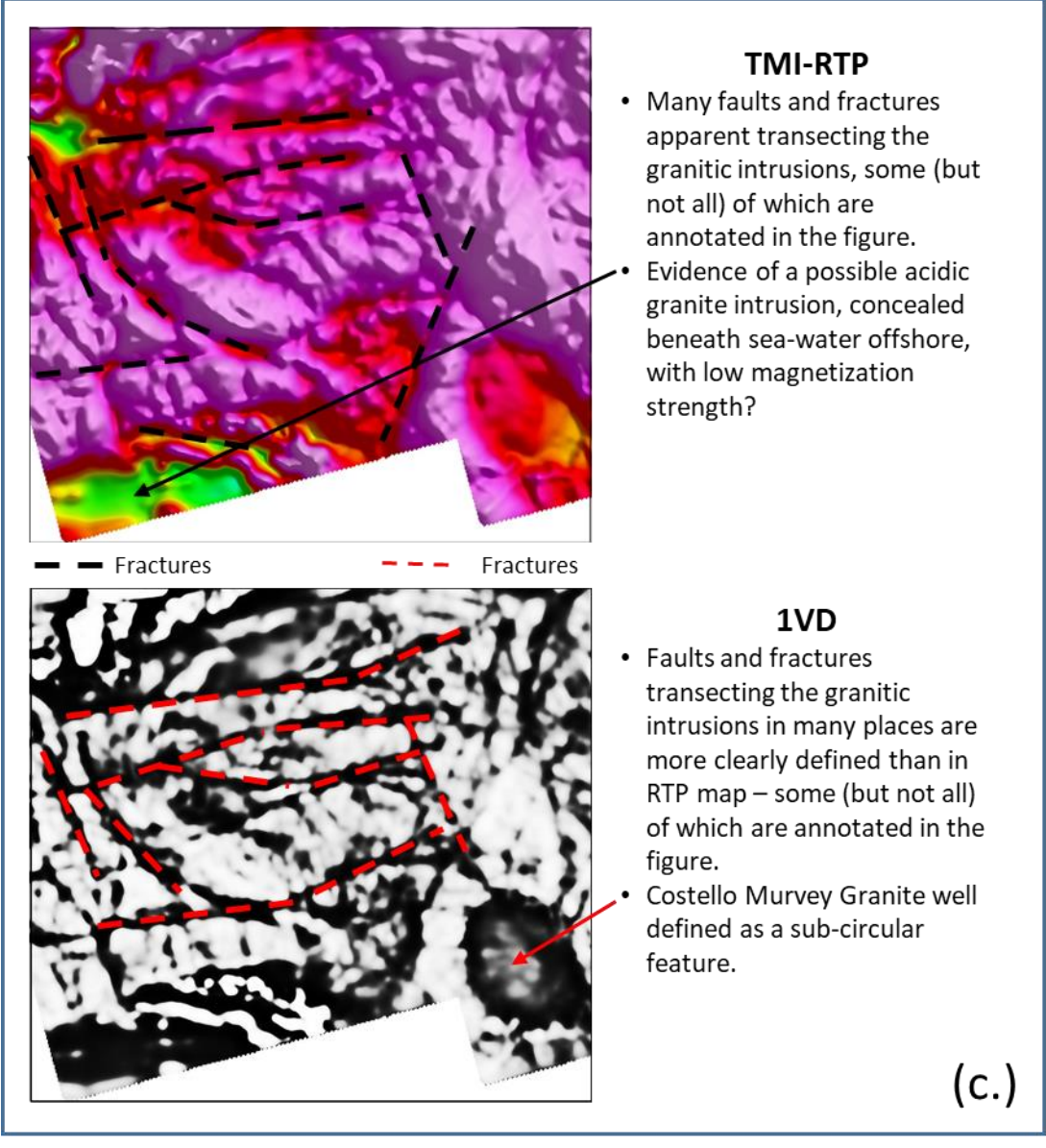
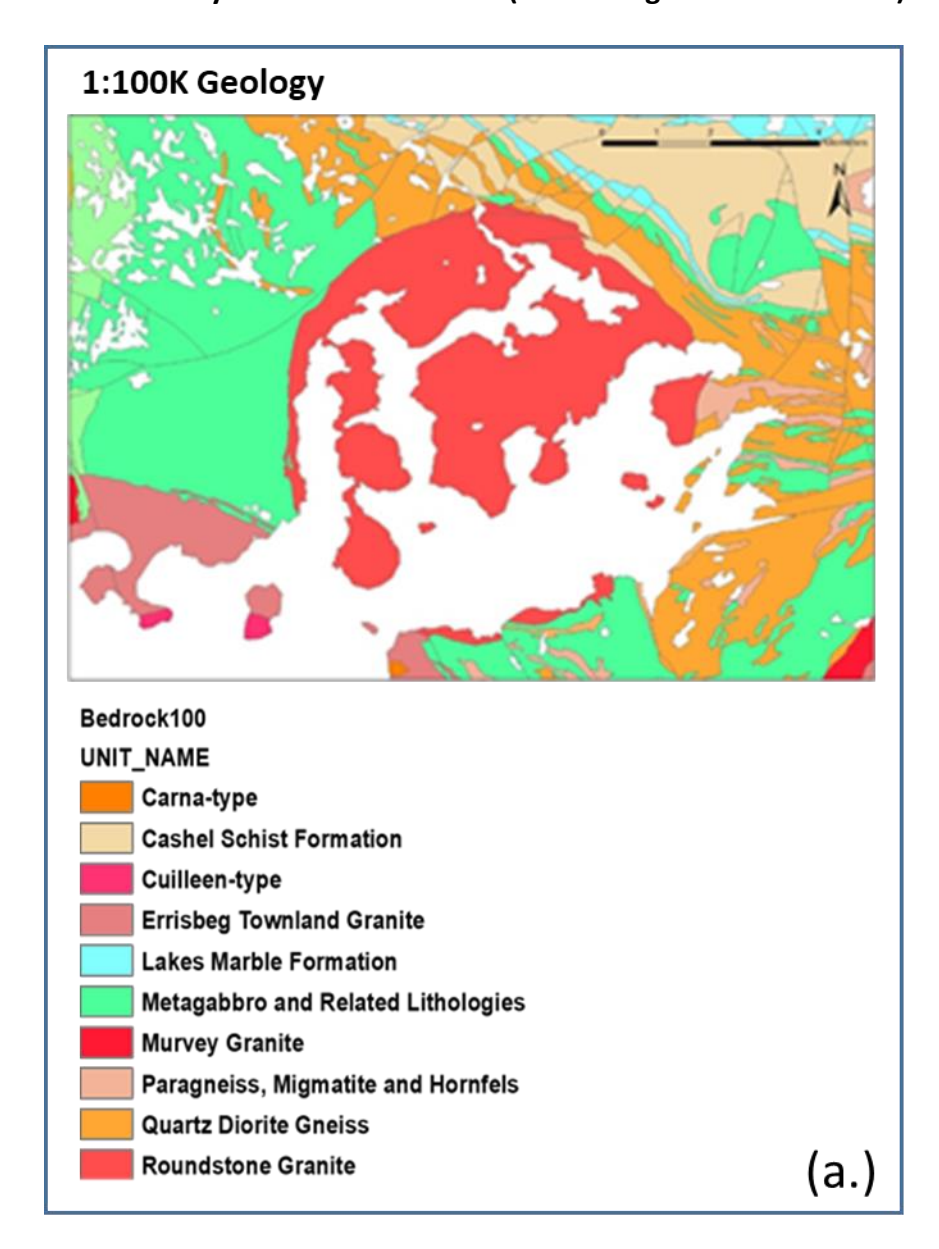


Figure 14. Magnetic features over Galway Granite. (a.) Extract from 1:100,000 geological map. (b.) Comparison between geological map and six different magnetic map products. (c.) Highlighted characteristics and geological features in TMI-RTP and 1VD magnetic maps.



2.4.3. Galway Roundstone Granite (illustrating internal zonation)





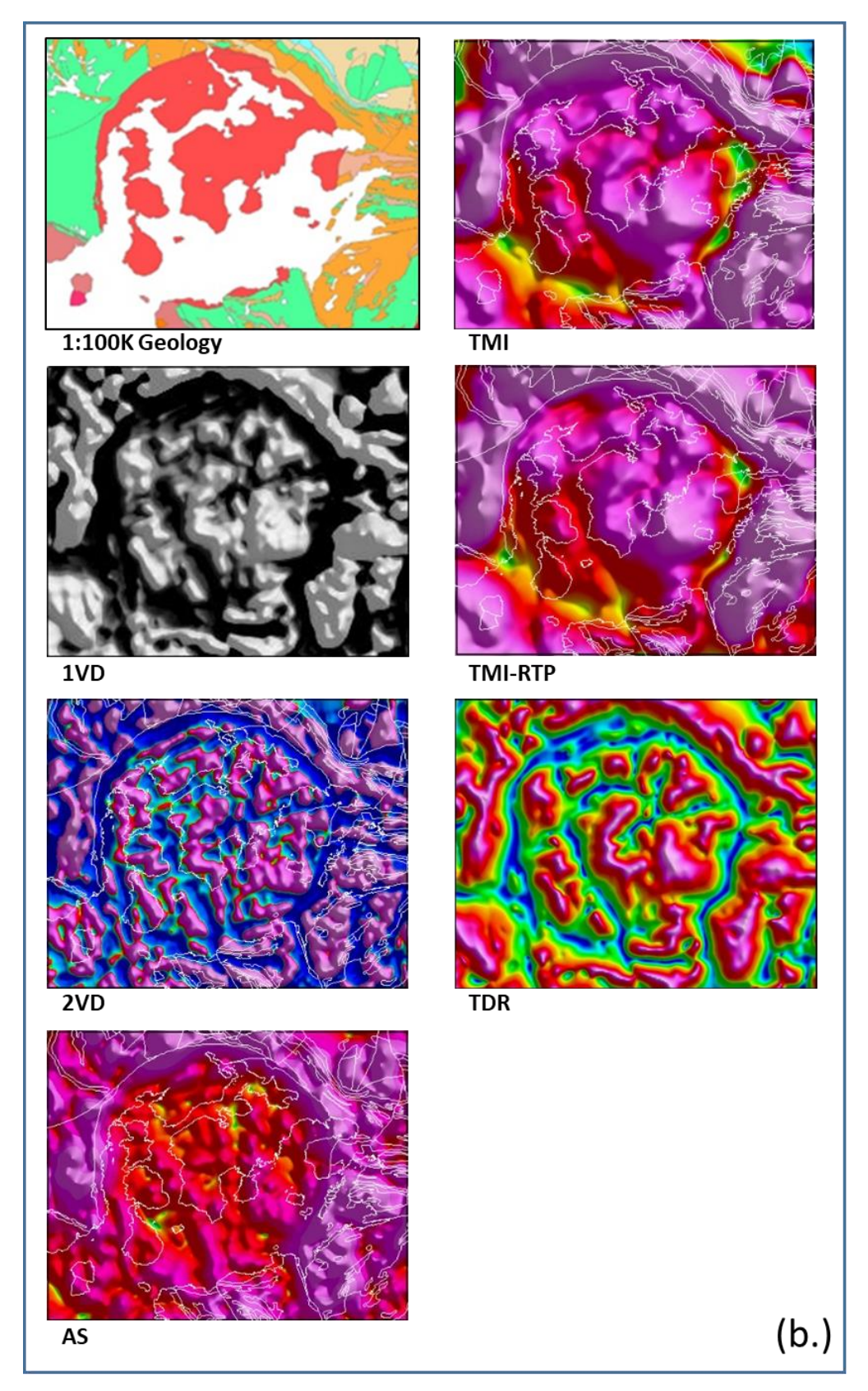
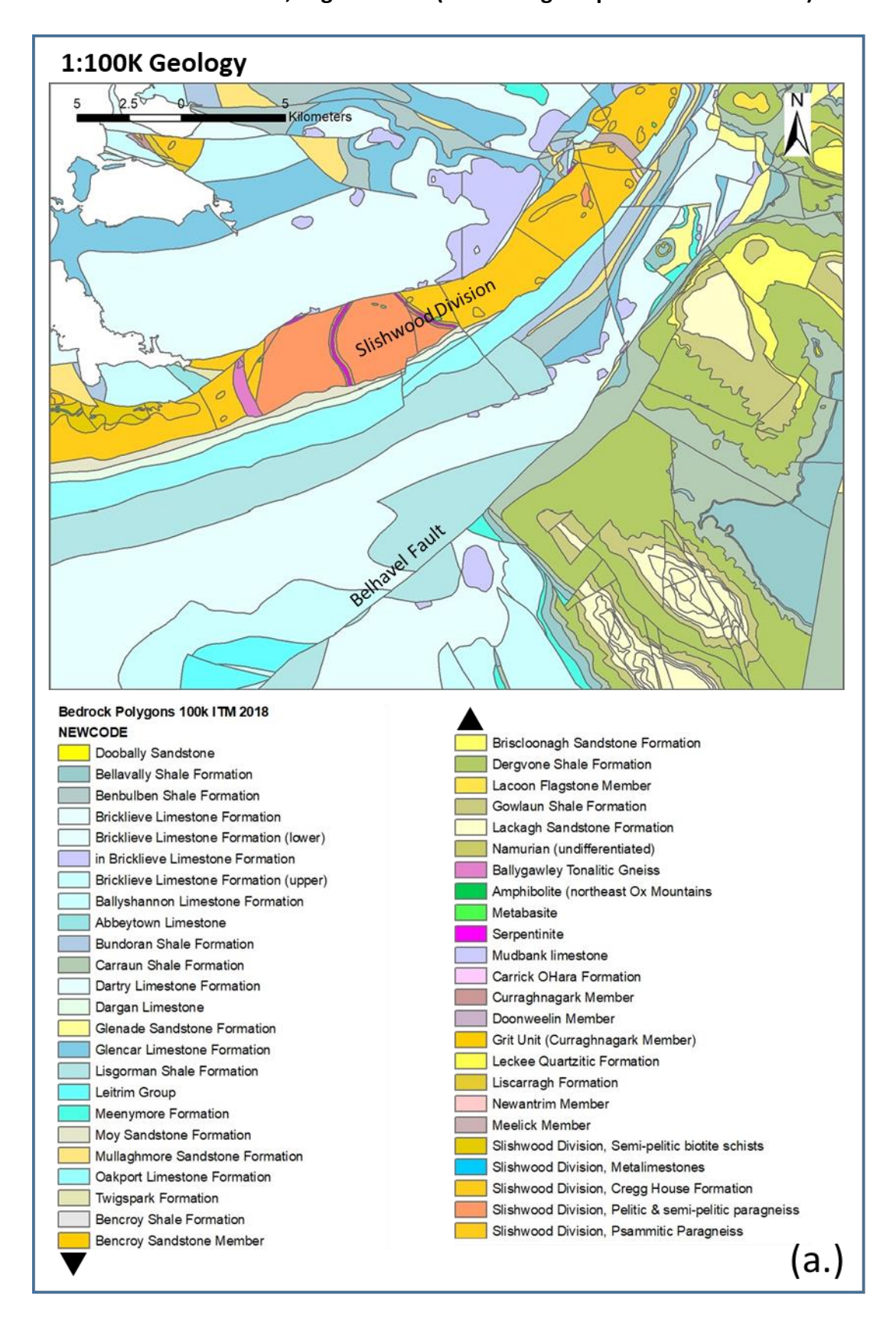


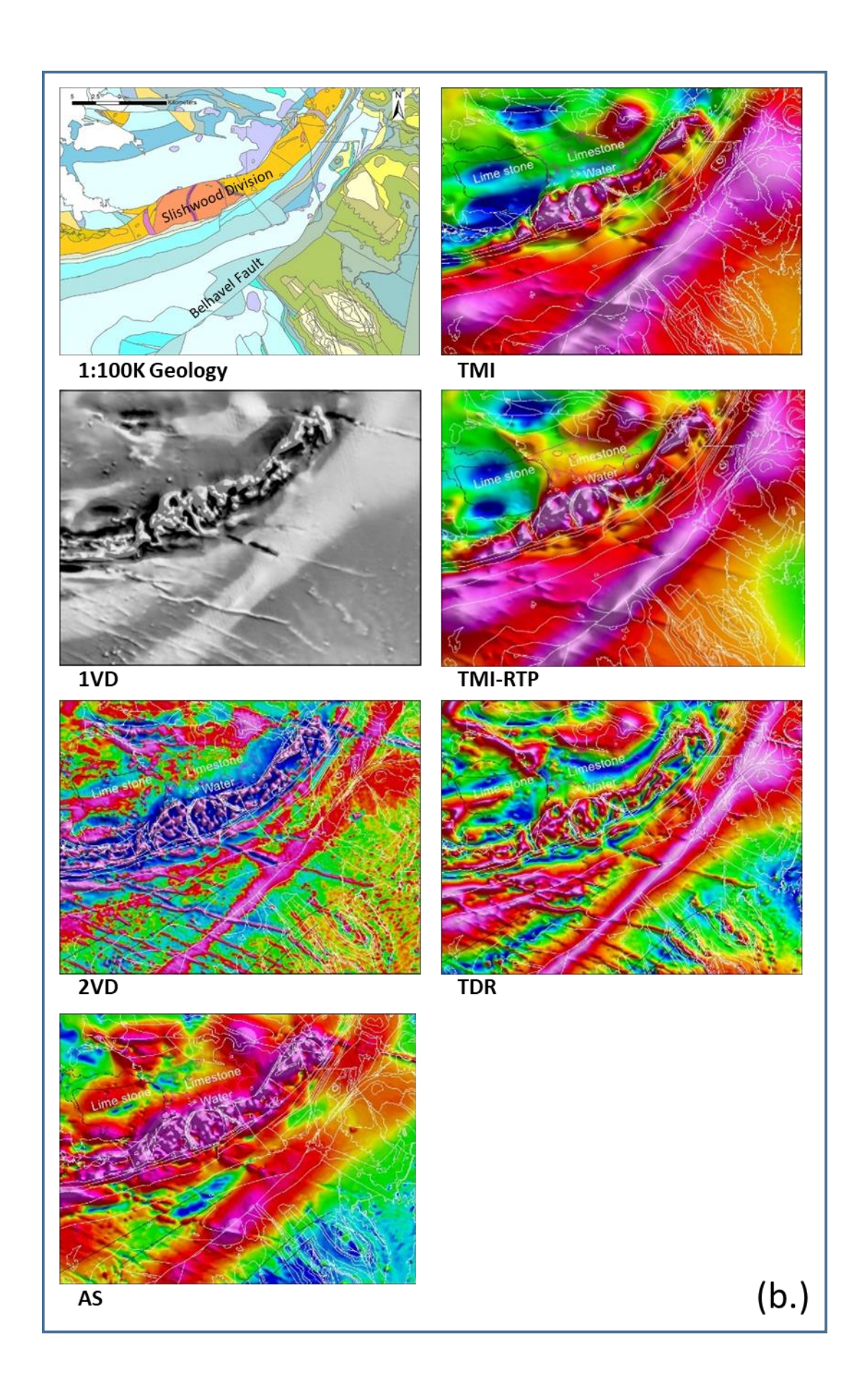
Figure 15. Magnetic features over Roundstone Granite, Co. Galway. (a.) Extract from 1:100,000 geological map. (b.) Comparison between geological map and six different magnetic map products. Internal zonation within the otherwise uniformly mapped granite is well illustrated in the 1VD and TDR maps.



2.4.4. Slishwood Division, Sligo-Leitrim (illustrating deep & shallow features)









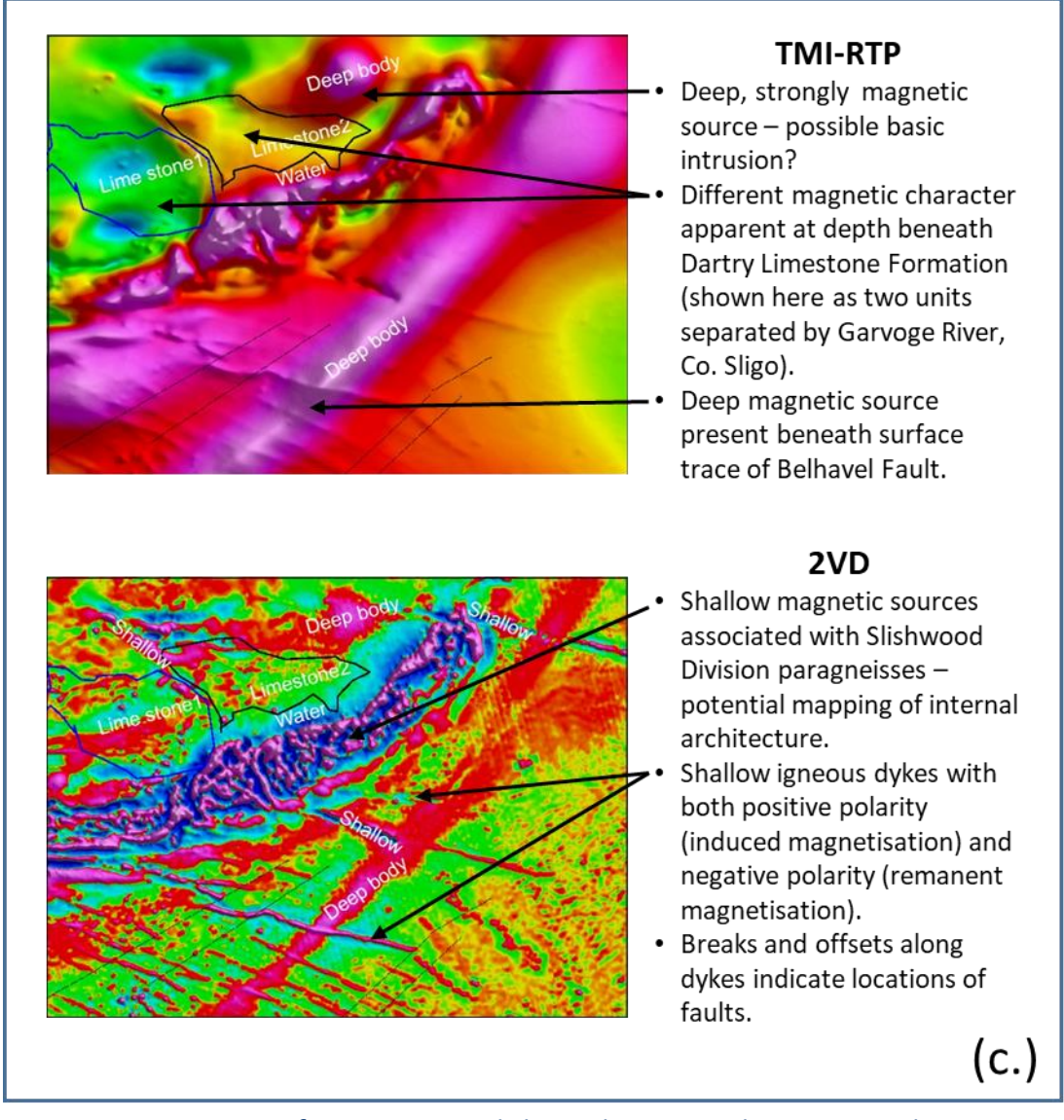


Figure 16. Magnetic features over Slishwood Division, between Coolaney, Co. Sligo (SW) and Thur Mountains, Co. Leitrim (NE). (a.) Extract from 1:100,000 geological map. (b.) Comparison between geological map and six different magnetic map products. (c.) Highlighted characteristics and geological features in TMI-RTP and 2VD magnetic maps.

Magnetic responses from deep features correspond with smooth, long-wavelength anomalies, while shallow, near-surface features give rise to sharp, short-wavelength responses.

Several deep magnetic bodies are mapped in the TMI-RTP data (Figure 16c) that include:

- Highly magnetic response from a deep circular magnetic body, potentially corresponding with a basic intrusive body.
- Major southwest-northeast lineament, visible on all magnetic maps associated with the surface trace of the Belhavel Fault – and corresponding with a deep magnetic source.

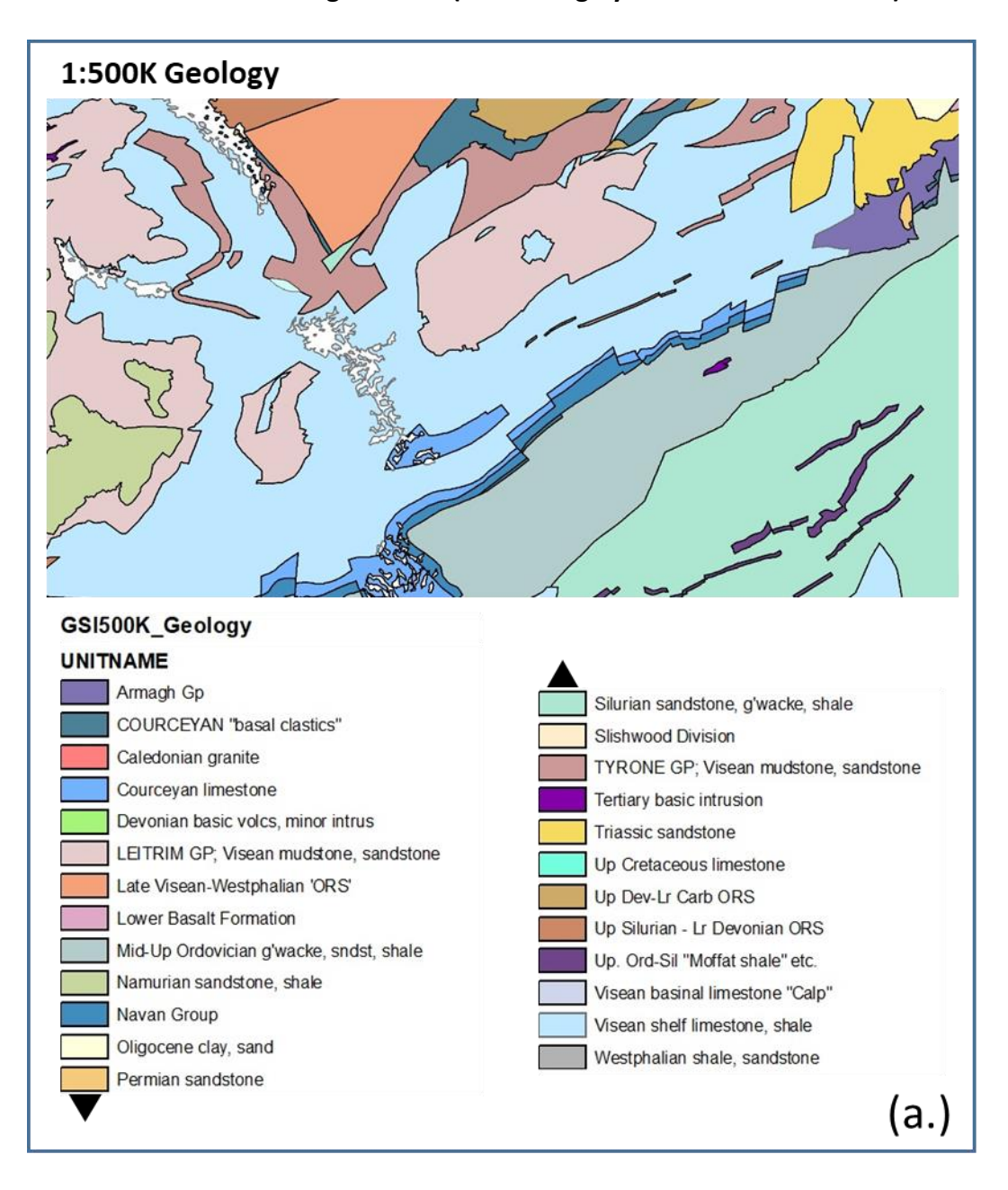


• Some evidence of lateral variation in the magnetic signature at depth below the Limestone Dartry Limestone Formation mapped at surface.

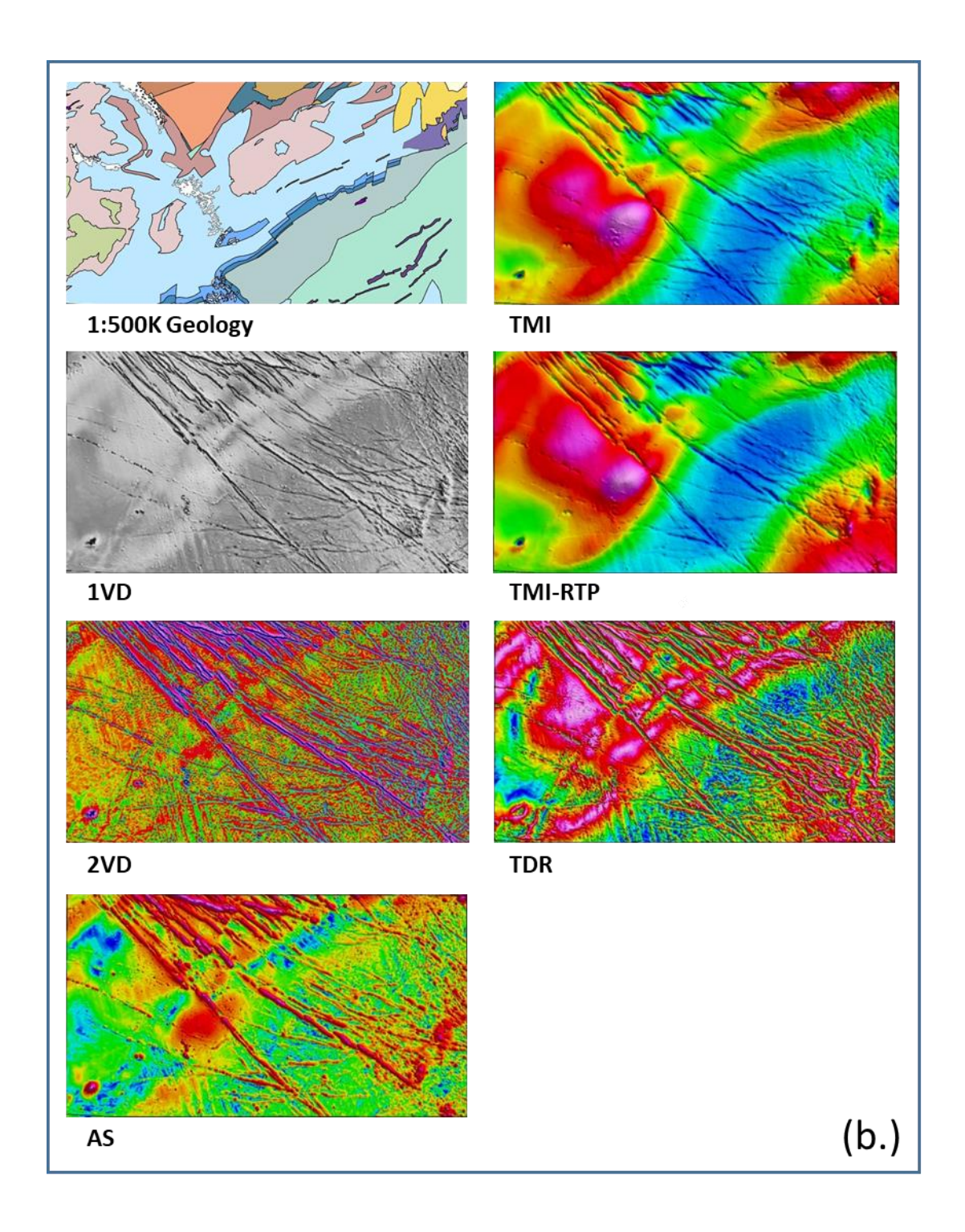
Shallow magnetic responses observed on the 2VD map (Figure 16c) include:

- Shallow dykes with both positive (red) and negatively polarity (blue), corresponding with induced and remanent magnetisation respectively.
- Internal architecture of the Slishwood Division rocks is mapped in detail at shallow depth.

2.4.5. Enniskillen – Monaghan area (illustrating dykes and inferred faults)









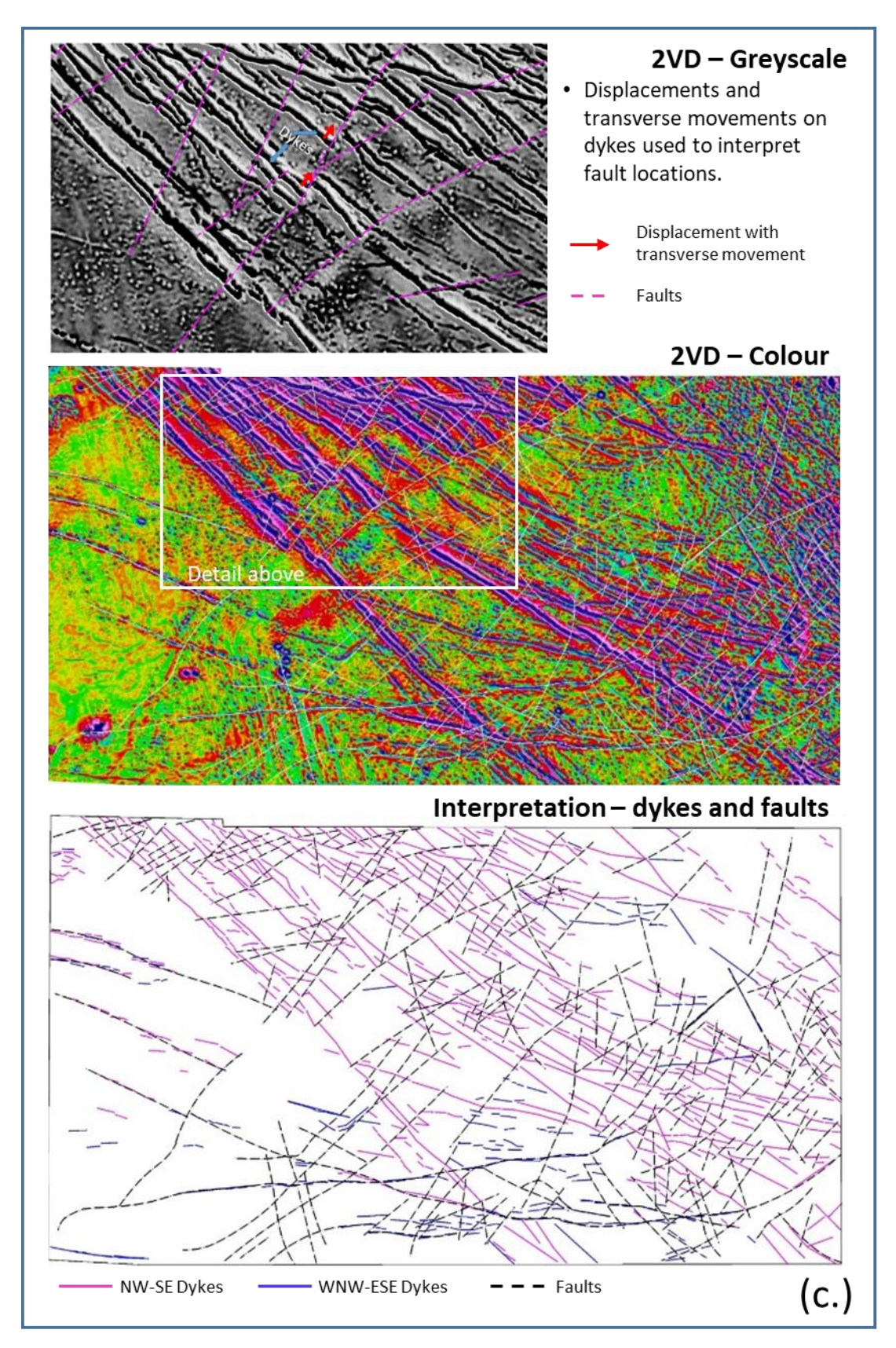


Figure 17. Magnetic response over Enniskillen and Monaghan area. (a.) Extract from 1:100,000 geological map. (b.) Comparison between geological map and six different magnetic map products. (c.) Detail of magnetic response of dykes and inferred fault structures in 2VD maps and line interpretation of these features.



2.5. Magnetics – Conclusions

Magnetic maps are complex in the sense that the shapes of magnetic anomalies, and their relationships with causative bodies at depth, are dependent on depth of burial, alignment of rock magnetisation (induced, remanent, or a combination of the two), location of measurement with respect to Earth's magnetic poles and anthropogenic magnetic noise. The range of different filters applied to the primary magnetic dataset (Total Magnetic Intensity, TMI) aims to simplify the shapes of anomalies by positioning them directly and centrally over magnetic bodies, isolating the magnetic responses originating from different depths and removing noise. A consideration of the following points may help in the understanding of these magnetic responses and their interpretation:

- Background knowledge of the following, relating to the area under interpretation: (i) likely occurrence of magnetic minerals in different rock formations, (ii) tectonic and magmatic episodes of mineralisation, potentially leading to the introduction of magnetic minerals and (iii) likely depths of burial for the stratigraphic succession of an area, based on existing information or geological models.
- Reference to typical ranges of magnetic susceptibility values and to remnant magnetisation data (if available) for a given rock formation may provide an important interpretational aid.
- Magnetic maps obtained from the application of different filters enhance different aspects of the magnetic field or are useful in different ways:
 - Simplification of anomaly shape and positioning of anomalies directly and symmetrically over causative magnetic bodies: Reduction-to-Pole (RTP, successful for induced magnetisation only), Analytic Signal (AS) and Tilt Derivative (TDR). The latter two filters additionally enhance features at shallow depths and subdue features at greater depths.
 - Enhancement of shallow depths of interest: First and Second Vertical Derivatives (1VD and 2VD), as well as AS and TDR referred to above.
 - Enhancement of greater depths of interest by removing shallowsource structures: Upward Continuation (UpXXX, where XXX is the height in metres of the upward continuation).
 - Removal of anthropogenic noise: Upward Continuation (often used prior to applying filters that enhance shallow structures).
 - Enhancement of structures with a particular strike direction: Directional Horizontal Derivatives computed along an azimuth perpendicular to the strike direction of interest. For example, a derivative in the E-W direction will enhance structures with a N-S strike.

The magnetic map products outlined in the Guide provide the basis for qualitative, map-based interpretations. Quantitative interpretation products and



models require the use of 2D and 3D modelling software. In the absence of such software, however, approximate estimates of depths to the tops of magnetic sources at specific locations can be derived using several different 'graphical' approaches applied to the record flight-line data.

It should be remembered that all geophysical data provide an indirect observation of the subsurface and provide the basis for an interpretation. Interpretation of data should make geological sense. It is useful to complement all geophysical interpretation work with available geological information and further with field mapping and direct investigations where possible.



3. Interpretation Guide to EM Data

3.1. Introduction

Airborne electromagnetic (AEM) methods are used as tools for mineral exploration, geological mapping, groundwater exploration, and environmental and civil engineering mapping. Electromagnetic interpretation is commonly based on the mapping of apparent resistivity (or apparent conductivity) following the technique developed by Fraser (1978) using 'half-space' subsurface models. In the half-space approach, the EM responses measured by the aircraft are transformed or modelled to derive a ground resistivity value under the assumption that the subsurface consists of a single, infinitely thick resistivity layer. In the case of the Tellus frequency-domain EM data, resistivity maps are produced independently for each of the four transmission frequencies used (0.9, 3, 12 and 25 kHz), with the lower frequencies providing greater depths of imaging.

The rocks that make up the island of Ireland show considerable variation in their electrical resistivity properties. The contrasting electrical properties help to map different geological formations and their distributions.

The electrical resistivity properties of rocks depend on a combination of factors that include: rock chemistry, mineralogy, porosity and permeability, and temperature and pressure. Porosity is the percentage of pore volume or empty space in a formation that can contain fluids, and the bulk rock resistivity of porous rocks is primarily dependent on the porosity, fluid saturation and conductivity of the pore fluids (See Appendix 2 for more detail). Clay rich rocks (e.g., shales and mudstones) are generally conductive, while quartz rich rocks (e.g., granites and quartzites) and massive limestones/dolomites are generally resistive.

3.2. EM Anomaly Patterns

Qualitative interpretation of EM resistivity maps consists of recognizing and delineating anomaly patterns. These patterns can be classified on both regional and local scales. EM maps can be presented either in resistivity or conductivity units. Conductivity is the inverse of resistivity (i.e., conductivity = 1/resistivity) and the measurement units for resistivity and conductivity are ohm.metres (Ω .m) and Siemens-per-metre (S/m) respectively. For consistency, all Tellus EM maps are published and presented in resistivity units. On such maps warm colours (pink, red and orange) show resistive bodies and cold colours (blue and green) shows less resistive or conductive features. The following features may provide the basis for an adequate first analysis of most EM maps. The various patterns



may not necessarily occur in isolation from each other, but may be found superimposed (e.g., Parasnis, 1986).

- Long narrow features: are frequently associated with conductive structures that may represent shear zones, fault zones, mineralised zones or thin/narrow sedimentary units such as shale horizons.
- Displacements (lateral offsets) of anomalies are indicative of geological faults.
- Extensive high resistivity areas may show massive rocks that are not extensively weathered (e.g., granites and limestones).
- Areas with little resistivity relief (i.e., little spatial variation) and with no
 distinctive pattern may indicate an absence of geological variation, such
 as thick sedimentary cover or, in the case of the high frequency data,
 thick, extensive and uniform overburden.
- Lateral variations: the lower frequency EM data (0.9 and 3 kHz, and potentially 12 kHz) will generally show lateral variations that reflect bedrock geological variation, while the higher frequency data (25 kHz and potentially 12 kHz) may reflect variation in weathered overburden, quaternary deposits and/or bedrock geology.

Airborne electromagnetic maps may help in:

- Locating conductors/resistors (e.g., ore bodies).
- Delineating overburden thickness (e.g., for engineering and archaeological investigations).
- Mapping bedrock geology and structure.
- Application in environmental hazard mitigation by locating, delineating and monitoring subsurface hazards (e.g., pollution plumes).
- Delineating thickness of layered aquifers and/or structures favourable for groundwater flow.

3.3. Depth of investigation

The Tellus program releases resistivity maps separately for each of the four transmitted frequencies. Assessment of these constant-frequency maps requires some consideration of the depth at which the resistivity structures are imaged. A common means of estimating depth of investigation is to use the concept of the electromagnetic skin-depth (P), which is defined as the depth at which the electromagnetic field strength has fallen off to 1/e (~36.8%) of its value at the surface:

$$P = 0.5\sqrt{\frac{1}{\sigma f}} = 0.5\sqrt{\frac{\rho}{f}}km = 503\sqrt{\frac{\rho}{f}}m$$
 (1)

where, ρ is resistivity, σ is conductivity and f is frequency. The first two formulations in (1) provide depth in kilometres and the third formulation in (1) provides depth in metres. It is clear from the formulation in (1) that in any constant-frequency resistivity map, resistive structures are imaged at a greater depth than conductive structures, and this should be kept in mind when interpreting the maps.



An approximate measure of depth of investigation, based on the EM skin-depth and commonly used, is the half-skin-depth (i.e., P/2, where P is defined in Equation 1) (SGL, 2019). The half-skin-depth versus resistivity graph of Figure 18 may be used as a rough depth-of-investigation guide when assessing Tellus constant-frequency resistivity maps. The bulk of Irish rocks fall within the 10 – 1,000 Ω .m resistivity range of Figure 18 (see Table 1).

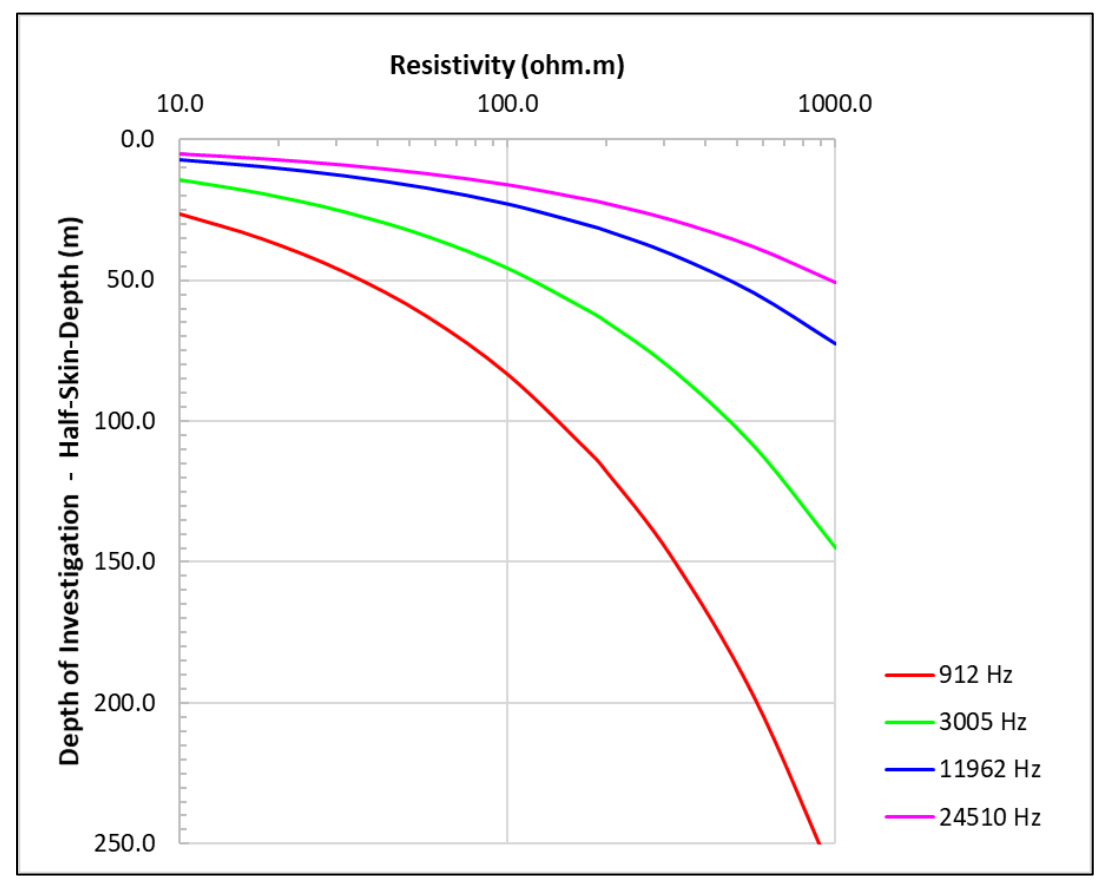


Figure 18. Approximate depths of investigation for typical Irish rock resistivities, for the four Tellus system frequencies, derived using the half-skin-depth estimator.

3.4. EM noise

There are a number of potential sources of noise within EM data, which the user should be aware of when carrying out interpretations. These noise sources include:

- i) System noise.
- ii) Cultural (anthropogenic) noise.
- iii) Rock petrophysical parameters.
- iv) High flight altitude.
- v) Data processing noise.



While a more detailed account of some aspects of EM noise is provided in Appendix 2, the main points of concern with respect to the interpretation of Tellus EM resistivity maps are discussed below.

3.4.1. Cultural noise

Cultural noise is recorded when flying over buildings, industrial complexes, railways, motorways and power-lines. The noise in the data may express itself in two ways in resistivity maps. (i.) Spurious very low or very high resistivity values that may have bullseye (e.g., farm buildings) or linear (e.g., power-lines) forms. Reference to air-photos or infrastructure maps may be useful during interpretation. (ii) In cases, cultural noise may lead to negative values in the recorded EM response data, which in turns leads to negative resistivity values.

While negative values are retained in Tellus resistivity datasets, to provide a means of recognising where noise is present in the data, these negative values are non-geological and should be ignored during geological interpretation.

3.4.2. Rock petrophysical parameters

All current Tellus EM resistivity products are derived on the basis that the observed EM responses are entirely due to resistivity variation. While frequency domain EM responses are primarily sensitive to rock resistivity, they also have some sensitivity to three other petrophysical properties: magnetic permeability, dielectric permittivity and polarization. In most cases, the effect of these three parameters is very small, and will have little impact on Tellus EM resistivity products and on their interpretation.

In specific cases where highly magnetic rock or polarisable rock (e.g., containing disseminated sulphides) is present, understanding of subsurface geology may benefit from a joint modelling of magnetic permeability and/or polarisation with resistivity. The *aempy* EM inversion code that the Tellus program is currently using to generate resistivity-depth models (see Section 3.7 below) has the capacity to implement such joint modelling, and GSI's intention is to carry out joint modelling in selected case-study areas in the future.

3.4.3. High flight altitude

The geological signal strength in recorded EM responses is significantly reduced as flight height above ground level increases. At high flight altitudes, where geological signal strength is reduced to below system noise levels, it is no longer possible to generate valid resistivity estimates from the data. The altitude threshold above which resistivity data are no longer reliable is spatially variable – depending on the depth of the geological source, the ground resistivity and the EM frequency used.



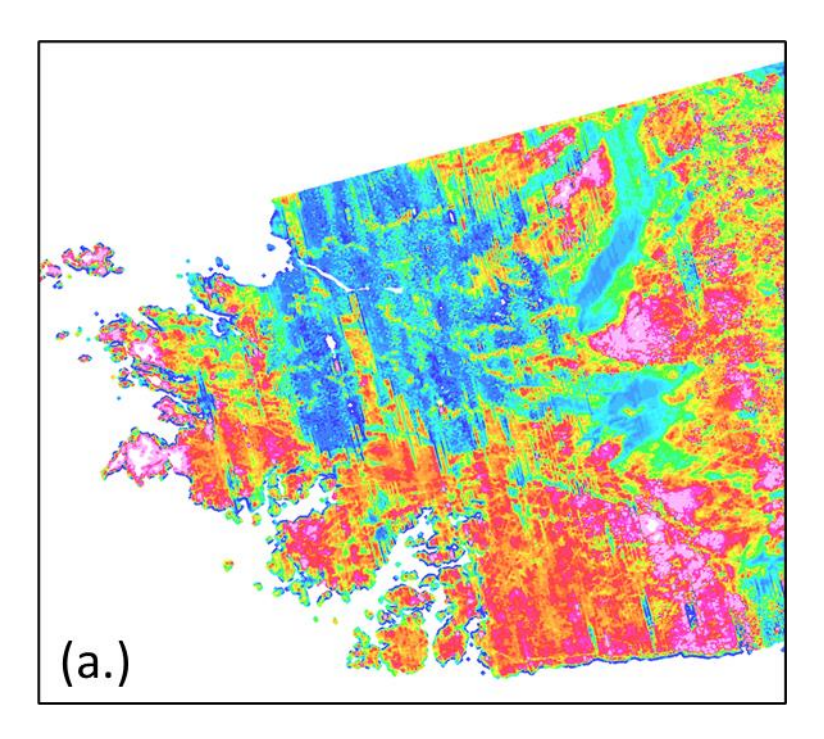
In order to remove potentially unreliable resistivity values from published data, Tellus maps are blanked (nulled) above a flight altitude of 150 m for the island-wide merged datasets and, more conservatively, above 120 m for the data released for each of the individual flight blocks.

As a universal flight altitude threshold is used (either 150 m or 120 m) for nulling the data, it is possible that some unreliable resistivity solutions are retained from lower flight altitudes in some instances. Interpreters are advised to exercise caution in their interpretations in areas immediately adjacent to blanked high-fly zones – especially where 'rims' of unusually high or low resistivity values are seen around blanked areas.

3.4.4. Data processing noise

Data processing noise that the interpreter should be aware of is related to the levelling of resistivity data between different flight blocks or between different flight-lines within a block. This can lead to, in the former case, visible steps across the boundaries of blocks or, in the latter case, stripes in the flight-line direction.

While significant processing effort is made to remove levelling errors/artefacts from the published datasets, a small number of minor, residual levelling artefacts may be present in the maps that the interpreter should remain alert to.





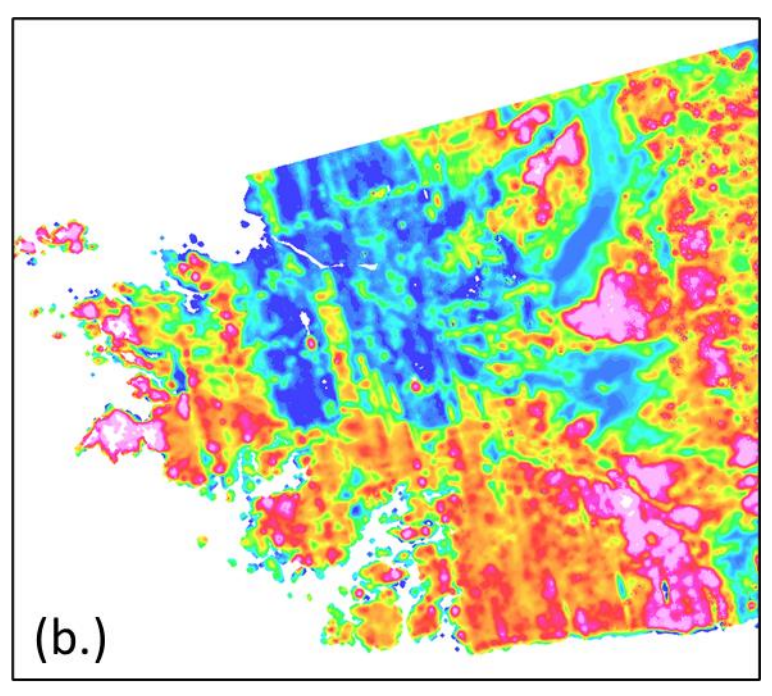


Figure 19. EM data extract from A2 Block comparing (a.) 3 kHz resistivity data without micro-levelling and (b.) micro-levelled 3 kHz resistivity data. Flight-line parallel lineaments are present in (a.) but are reduced by micro-levelling in (b.).

3.5. Resistivity Values Related to 1:500K Geology

Knowledge of typical Irish rock resistivities may help in the interpretation of Tellus EM resistivity data and maps. To this end, the current island-wide merged EM resistivity data at 3 kHz have been correlated with lithologies in the 1:500K geology map of Ireland — yielding mean, minimum and maximum resistivity values for all mapped lithological units (Table 1 and Figure 20). The mean values provide a reasonable bulk value for each lithological unit, while the minimum to maximum range of the data reflects lithological variation within each unit.

Table 1. 3 kHz apparent resistivity data: mean resistivity and resistivity ranges (maxima and minima) with respect to lithological units in the 1:500K geology map. Resistivity data are taken from the Tellus '2019B merge' dataset which comprises 41,839,151 data points, of which 40,642,737 were correlated with geology. 1,250,017 data points are located over water bodies (coastal areas and lakes) and provide no lithological correlations.

Tellus airborne EM 3 kHz resistivity (Merge2019B dataset) versus 1: 500K Geology					
Unit Label	UNIT NAME/Geology	Mean (Ω.m)	Min (Ω.m)	Max (Ω.m)	Number of Data
1	Metadolerite or Amphibolite	443.3	0.5	2999.0	62,944
2	Serpentinite, DX	308.4	1.2	1159.7	5,050
3	Orthogenesis suite, Connemara	1166.8	11.2	2999.9	58,404



4	Ordovician granite	550.6	0.7	2999.2	113,893
5	Metagabbro, metadiorite (Tyrone plu)	687.2	0.8	2999.9	163,323
6	Palaeozoic felsic minor intrusion	627.1	22.5	2979.1	9,575
7	Caledonian appinite suite	573.2	42.0	2998.7	19,024
8	Caledonian granite	588.2	0.0	2999.9	2,320,633
9	Tertiary granite, felsite	338.9	7.5	2762.1	174,208
10	Tertiary rhyolite (Volc & Intru)	55.6	3.8	271.9	24,000
11	Tertiary basic intrusion	300.7	1.9	2977.3	38,592
13	Mullet Gneiss	636.0	0.9	2995.8	12,460
14	Cross point Gneiss	694.9	1.8	2992.3	35,726
15	Doolough Granite and Gneiss	1186.2	202.0	2985.9	1,864
16	Kilmore Quay Group	232.4	7.9	767.2	16,355
17	Greenore point Group	222.7	5.9	572.1	39,966
18	Tyrone C1 (Corvanagh/Slishwood)	584.7	73.1	1107.9	44,833
19	Slishwood Division	576.0	0.4	2999.9	246,826
20	Inishkea Division	693.9	0.5	2992.7	64,062
21	Dalradian Grampian Group	816.9	0.2	2999.9	297,073
22	Dalradian Appin Group quartzite	459.2	0.2	2995.2	104,943
23	Dalradian Appin Group	466.5	0.0	2999.9	463,990
24	Dalradian Argyll Group Paragenesis	890.6	0.7	2963.3	15,671
25	Dalradian Argyll Group Volcanics	772.3	6.3	2996.5	21,520
26	Dalradian Argyll quartzite	541.7	0.1	2999.7	443,292
27	Dalradian Argyll Group	451.1	0.0	2999.9	1,921,296
28	Dalradian S Highland GP Volcanics	602.2	47.4	2995.1	31,224
29	Dalradian S Highland GP	383.1	0.0	2999.9	1,734,853
30	Cambrian quartzite	378.4	1.1	2888.1	25,506
31	Cambrian slate	212.6	0.0	1555.2	103,625
32	Cambrian greywacke, sandst, quartzite	252.7	0.0	2624.3	350,426
33	Lr.Mid Ordovician basic volcanics	385.3	2.5	2998.4	182,338
34	Lr.Mid Ordovician acid volcanics	834.0	0.7	2998.2	29,054



35	Lr.Mid Ordovician slate	282.8	0.0	2999.4	1,490,413
36	Lr.Mid Ordovician greywackes, sandstone	727.2	0.1	3000.0	105,799
37	Mid-Up Ordovician basic volcanics	480.1	0.0	2997.7	85,574
38	Mid-Up Ordovician acid volcanics	457.0	0.1	2999.2	242,115
39	Mid-Up Ordovician slate	249.9	0.0	2999.0	599,747
40	Mid-Up Ordovician g'wacke, sandstone, shale	397.7	0.0	2999.9	901,795
41	Ordovician or Silurian melange	212.2	0.5	968.5	5,776
42	Rathkenny Formation	308.8	1.6	2997.2	134,656
45	Croagh Patrick Succ.	731.6	19.2	2956.4	59,188
46	Silurian quartzite	686.0	48.8	2996.3	6,120
47	Louisburgh-Clare Island. Succ.	491.5	0.0	2997.2	17,294
48	Killary-Joyces Succ.	470.3	5.9	2994.4	35,442
49	Silurian sandstone, g'wacke, shale	316.3	0.0	3000.0	4,293,358
50	Devo basic volcanics, minor intrus	280.7	4.7	2988.0	30,484
52	Up Silurian-Lr Devonian ORS	151.3	1.3	2989.0	375,262
53	Mid Devonian ORS	285.1	7.7	2994.6	80,917
54	UP Devonian Lr Carb OSR	256.8	0.1	2999.5	986,020
56	Dev-Lr Carboniferous volcanics & minor intrus	220.1	0.1	2971.0	82,852
58	Lower limestone, shale	196.1	0.0	2997.4	174,931
59	COURCEYAN "basal clastics"	129.7	0.0	2998.1	724,634
60	Navan Group	231.3	0.0	2999.8	269,360
61	Courceyan limestone	258.0	0.0	3000.0	1,783,645
62	Waulsortian Limestone	471.9	0.0	3000.0	1,600,324
63	Visean "basal clastics"	229.2	0.0	2999.2	337,486
64	Visean shelf limestone, shale	437.2	0.0	3000.0	8,166,831
65	Visean basinal limestone "calp"	375.9	0.0	3000.0	2,687,658
66	TYRONE GP, Visean mudstone, sandstone	160.4	0.0	2980.9	859,542
67	Armagh GP	55.4	4.6	287.2	124,176
68	LEITRIM GP, Visean mudstone, sandstone	60.4	0.0	2960.2	664,272
69	Ballycastle Succ.	89.1	10.8	950.8	12,466



70	Late Visean-Westphalian "ORS"	106.2	15.3	356.1	215,648
71	Namurian sandstone, shale	150.4	0.0	2999.9	763,974
72	Westphalian shale, sandstone	135.1	9.3	296.2	7,601
73	Permian sandstone	54.4	3.4	757.7	17,527
74	Permo-Triassic sandstone	60.0	0.0	269.3	9,082
<i>75</i>	Triassic sandstone	37.5	0.4	966.1	402,462
76	Lr Jurassic mudstone	33.6	3.0	779.1	28,554
77	Up Cretaceous limestone	90.8	2.2	941.3	79,022
78	Tertiary minor volcanics	377.9	86.8	1033.6	4,646
79	Lower basalt formation	69.1	2.8	995.0	1,682,834
80	Interbasaltic formation	81.1	2.2	861.5	35,103
81	Causeway Tholeiite Mbr	66.0	5.3	940.0	73,585
82	Upper basalt formation	91.9	4.2	951.8	965,245
83	Olingocene clay, sand	26.7	3.7	420.4	242,768



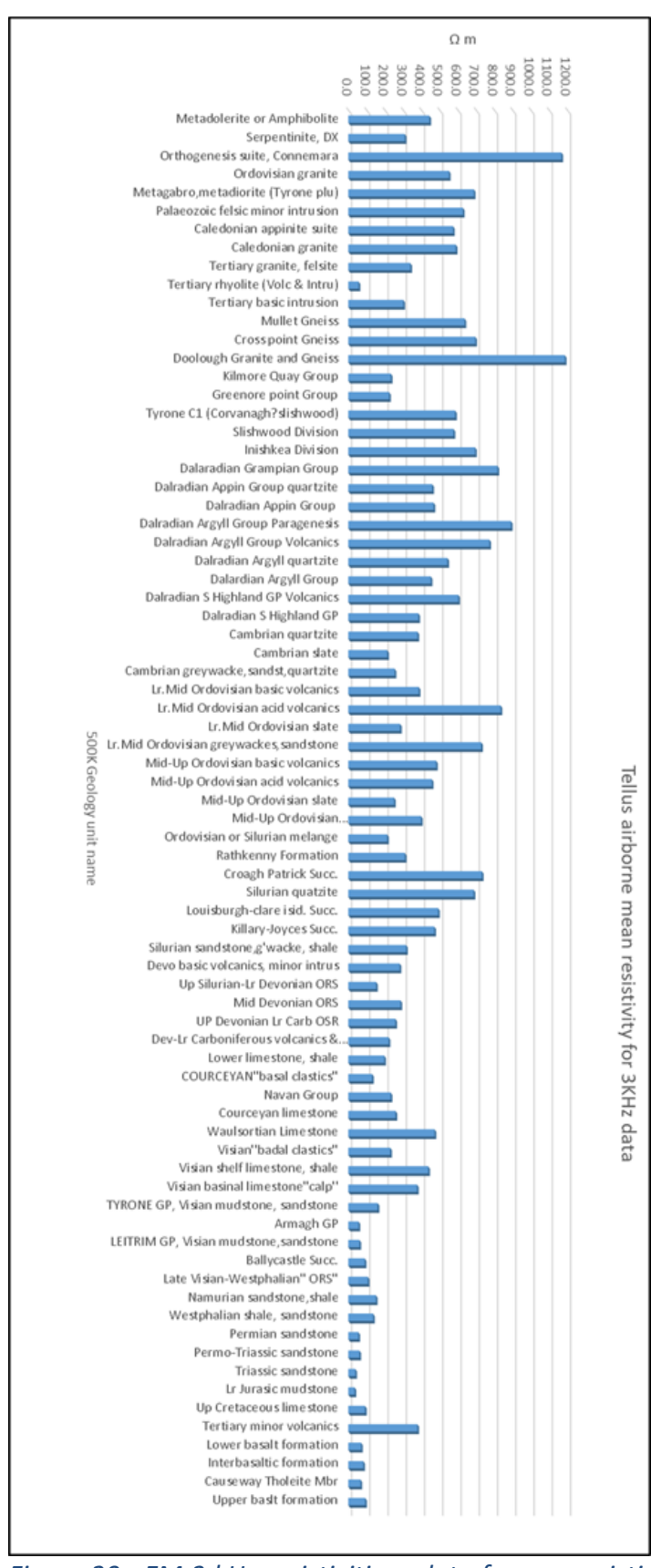


Figure 20. EM 3 kHz resistivities: plot of mean resistivity value versus lithological unit in 1: 500K geology map.



The lithological units with the highest resistivity values mapped to date are:

- Doolough Granite and Gneiss (mean resistivity 1186 Ω .m)
- Connemara Orthogenesis Suite (1167 Ω .m)
- Dalradian Argyll Group Paragenesis (891 Ω .m)
- Lower Mid Ordovician acid volcanics (834 Ω .m)
- Dalradian Grampian Group (817 Ω .m).

The lithological units with the lowest resistivity values mapped to date are:

- Olingocene clay and sand (27 Ω .m)
- Lower Jurassic mudstone (34 Ω .m)
- Triassic sandstone (38 Ω .m)
- Permian sandstone (54 Ω .m)
- Armagh Group (55 Ω .m)
- Tertiary rhyolite (volcanics and intrusives) (56 Ω .m).

A general, but not universal, trend is apparent in which older rocks, having undergone compaction and metamorphic processes over time, are characterized by higher resistivities than younger rocks and units, particularly younger sedimentary successions, which are amongst the most conductive rock units in Ireland.

3.6. EM Examples from Tellus Data

Three example data areas are illustrated below with interpretative observations. Each example shows the geological map together with EM resistivity maps at each of the four system frequencies (0.9, 3, 12 and 25 kHz). In addition, selected fractional vertical derivatives (of order 0.25) and four-frequency composite images are shown.

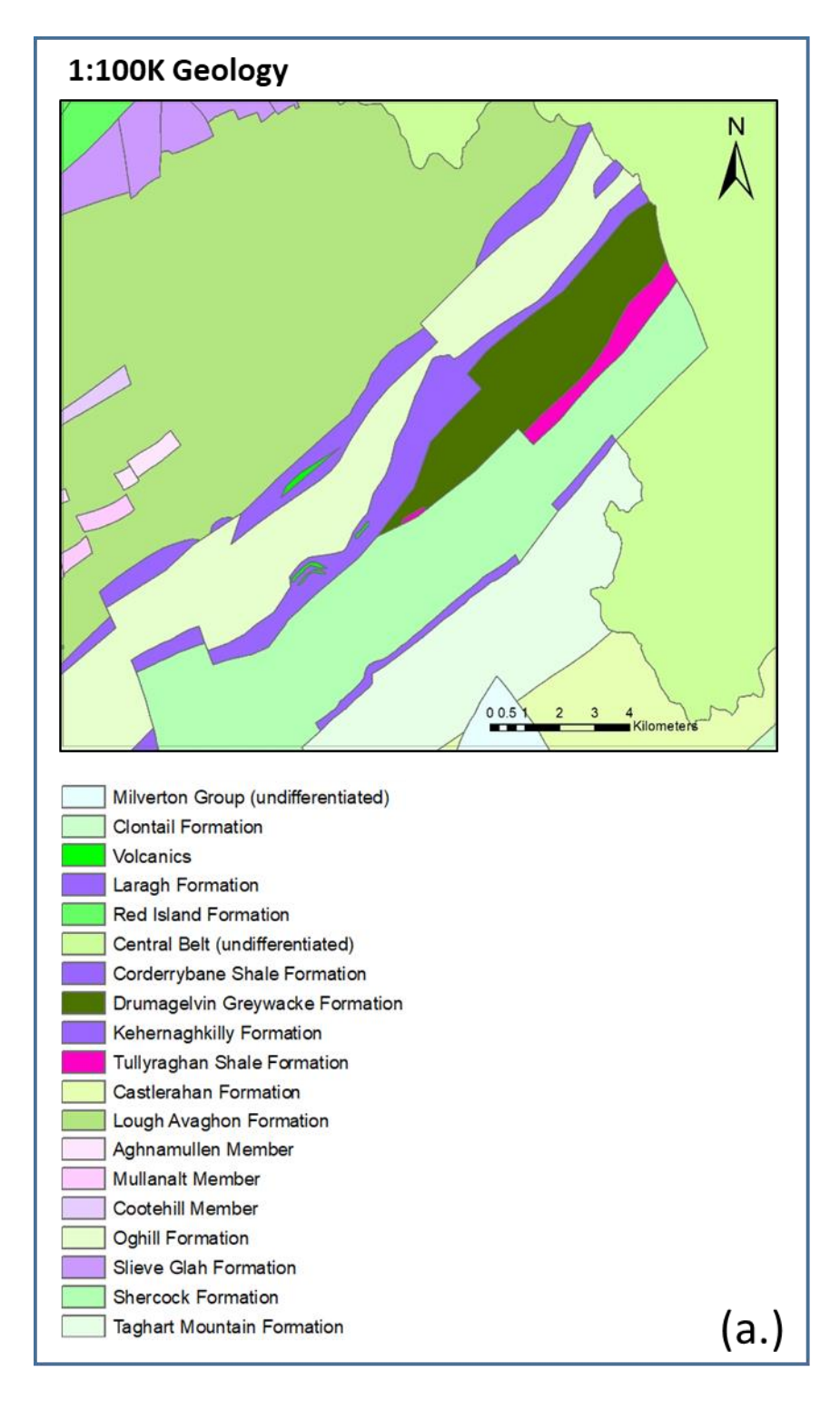
Fractional vertical derivative of order 0.25. While the first and second vertical derivatives (i.e., derivatives of order 1.0 and 2.0 respectively) typically applied to magnetic data are strong sharpening filters, the 0.25 order fractional derivative is applied to the EM resistivity maps with the aim of moderately sharpening up the boundaries between different resistivity units and enhancing subtler features in the grids, without exacerbating any cultural noise in the data.

Four-frequency composite image. A four-frequency composite image is used to display simultaneously on one map the resistivity data from all four EM frequencies. In the scheme, each individual resistivity map is coloured using a standard Geosoft blue-to-red/violet palette, and the composite colour is taken as the sum of each of the four grid colours at each map point. The composite image may reveal or draw attention to geological features not immediately apparent in each of the four individual resistivity maps.

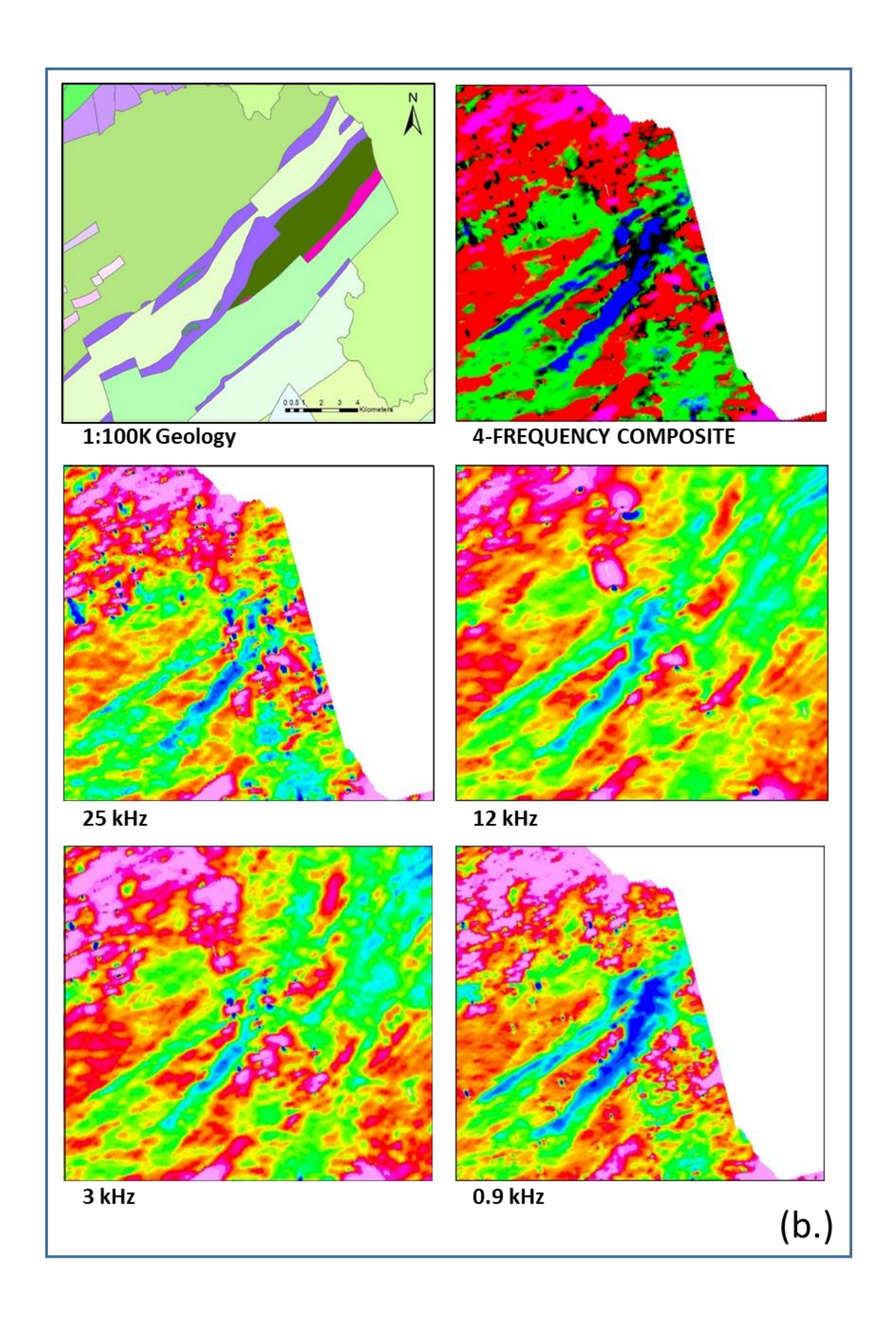


3.6.1. Moffat Shale (illustrating mapping of conductors)

Note that the 1:100K geology map displayed below lacks stratigraphic detail on the Northern Ireland side of the Irish border, accounting for the apparent truncation of stratigraphy at the border in the map. Furthermore, airborne EM data were only acquired at two frequencies (3 and 12 kHz) during the first Tellus survey in Northern Ireland, accounting for the lack of data at 0.9 and 25 kHz in Northern Ireland in the maps below.









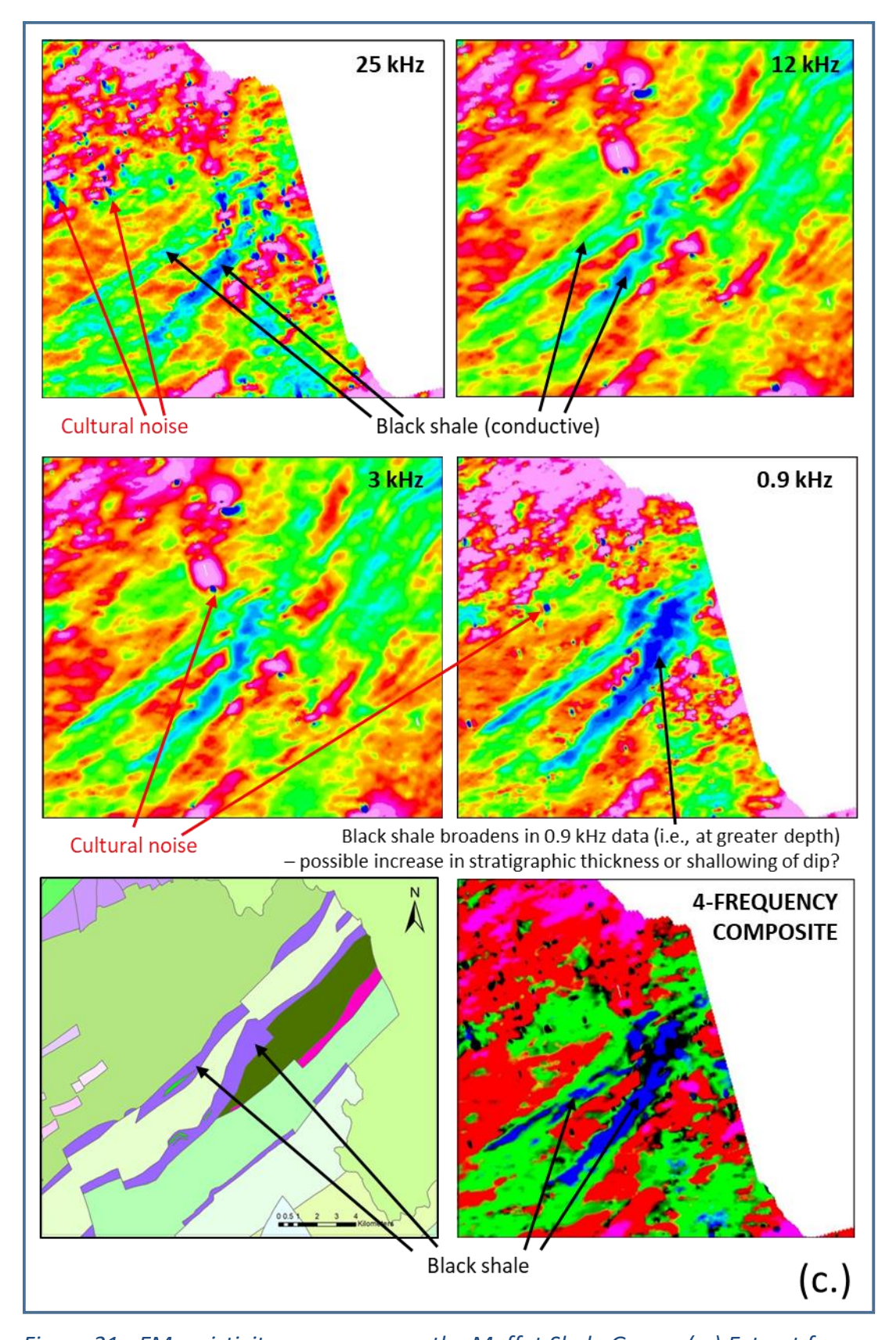
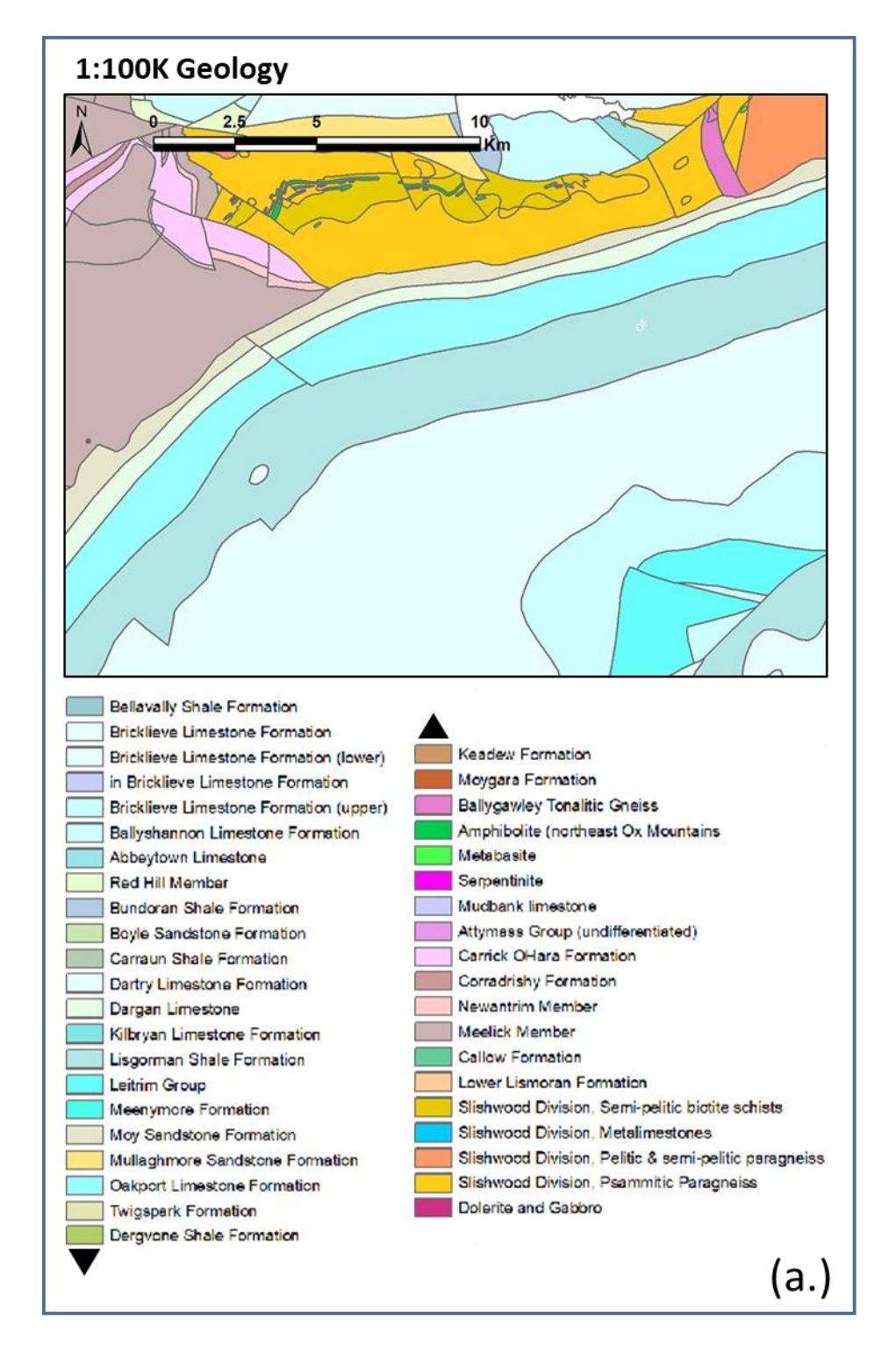


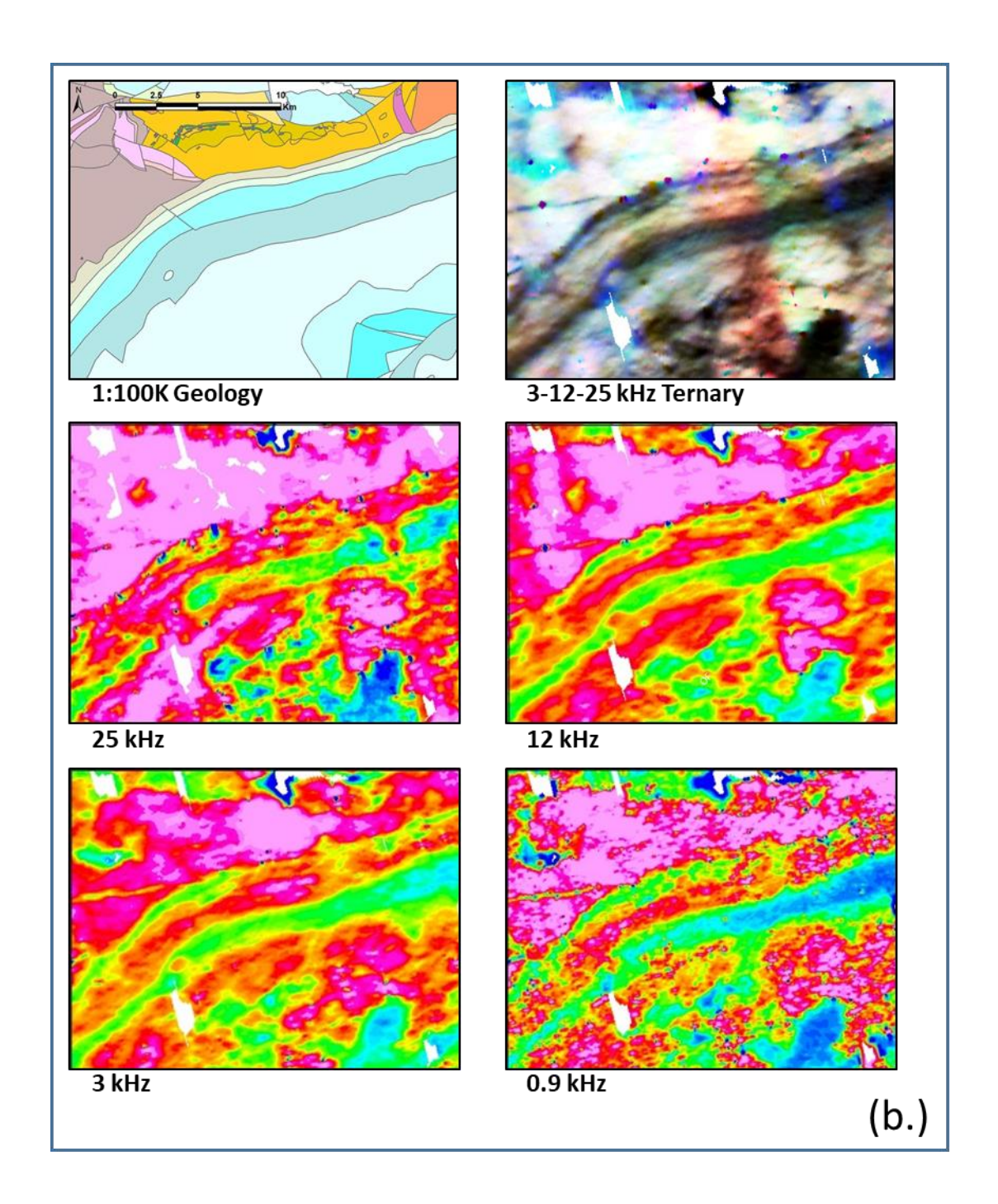
Figure 21. EM resistivity response over the Moffat Shale Group. (a.) Extract from 1:100,000 geological map. (b.) Comparison between geological map and five different EM resistivity map products. (c.) Annotated detail of the conductive



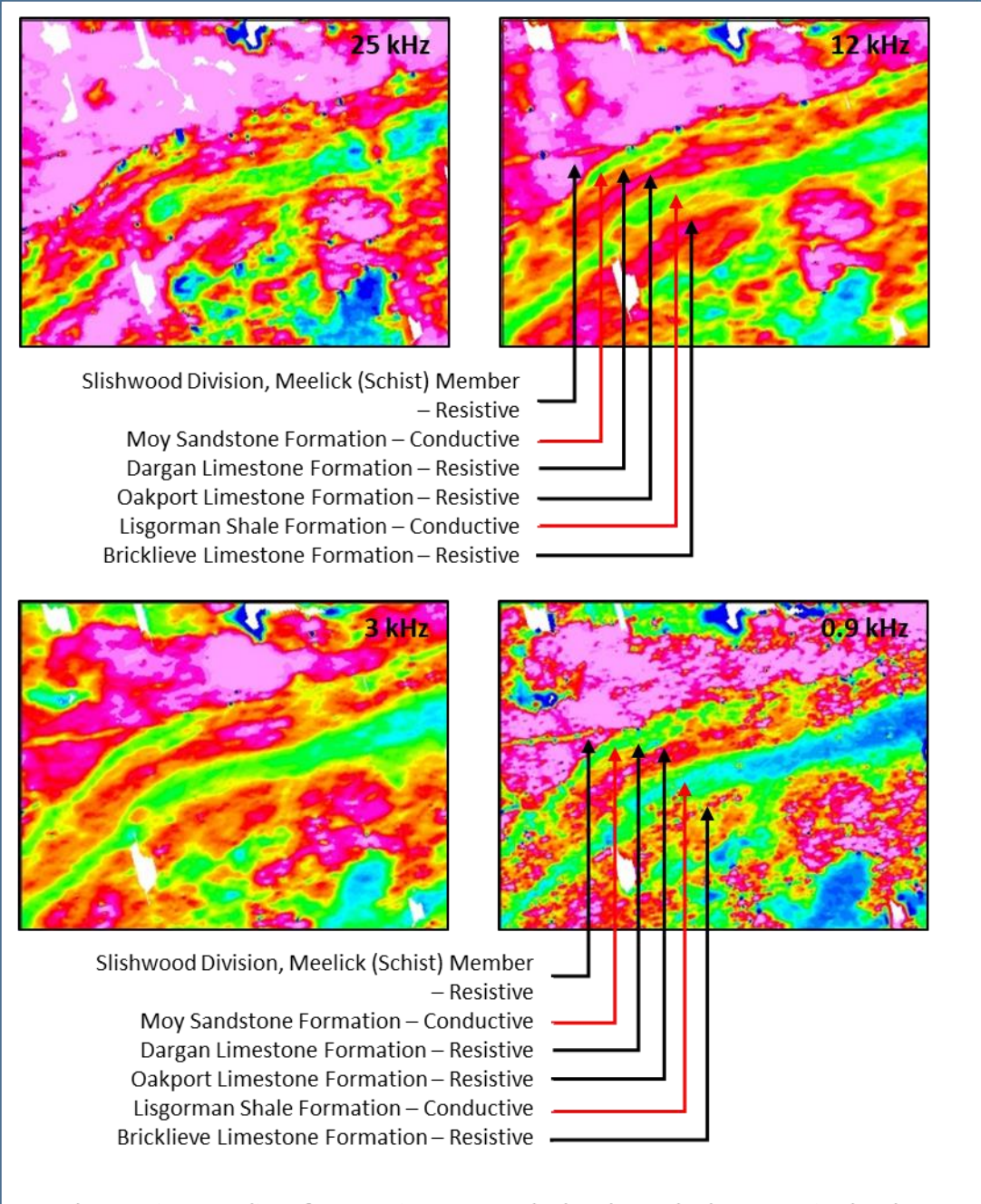
3.6.2. Ox Mountains (illustrating litho-stratigraphic variations)











- The two intermediate frequencies at 12 and 3 kHz have the lowest noise levels.
 0.9 kHz data have the highest noise levels.
- Distinction between Moy Sandstone and Dargan Limestone formations is less clear in 0.9 kHz data, possibly due to noise or thinning or steepening of dip with increasing depth of the latter formation.
- Lisgorman Shale Formation is more conductive in 0.9 kHz map (at greater depth), particularly towards the east of the mapped area.

(c.)



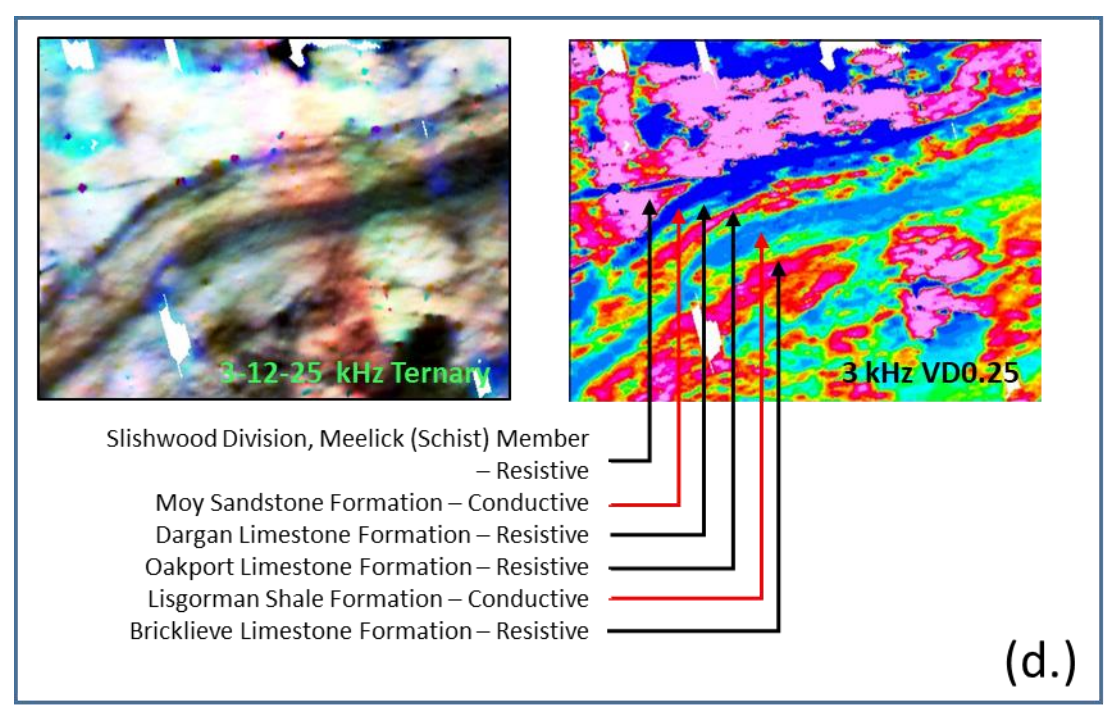
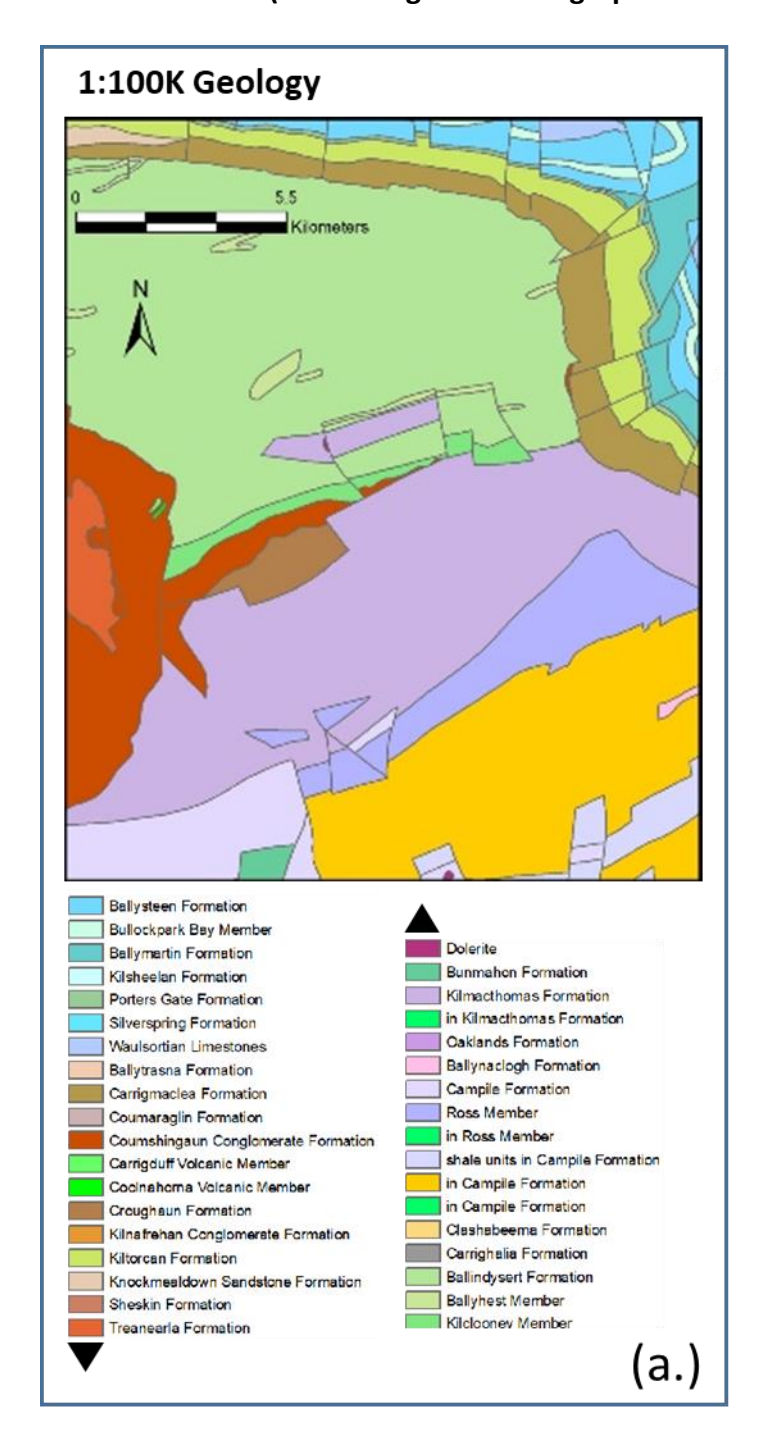


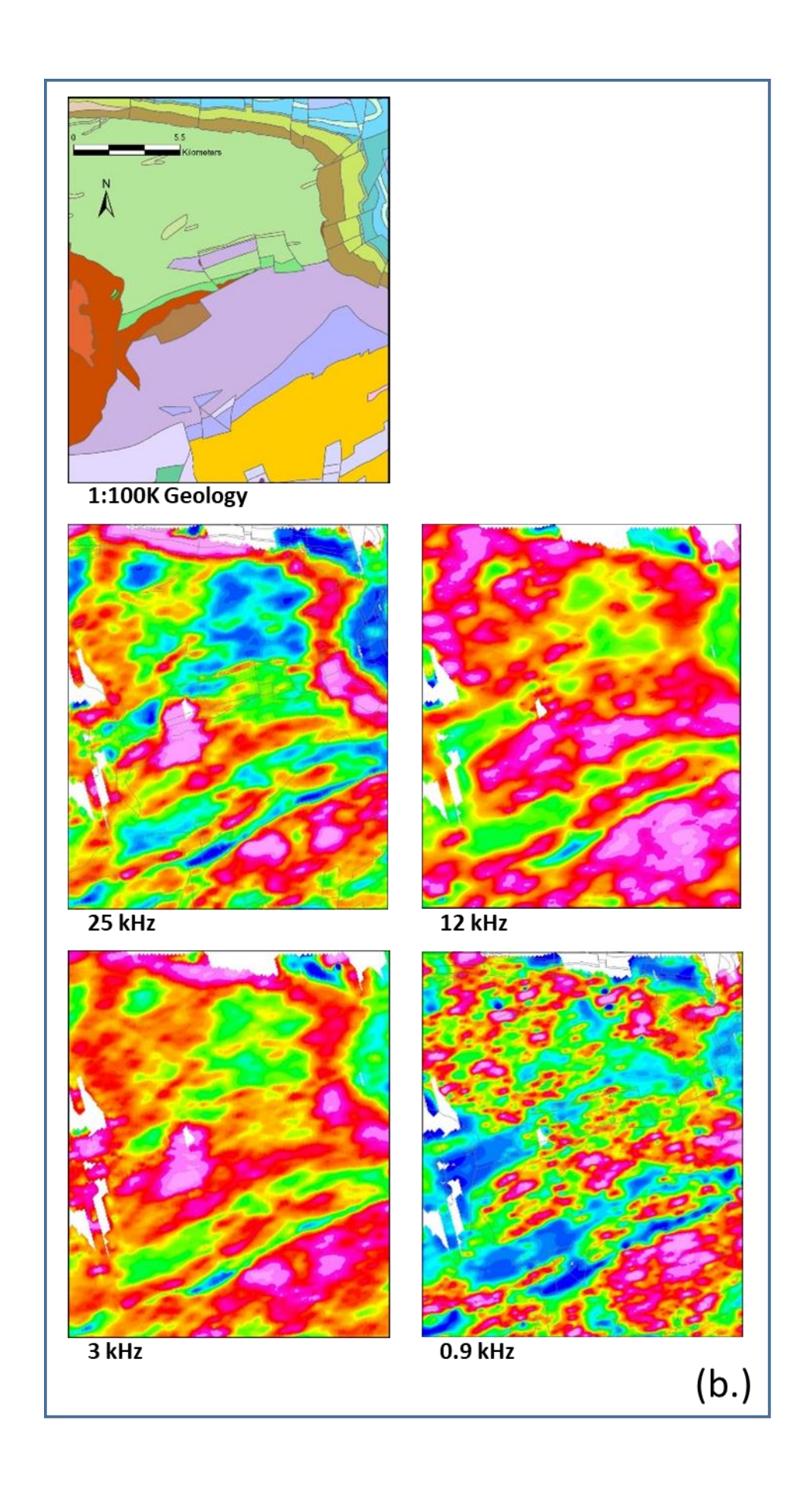
Figure 22. EM resistivity response over the Ox Mountains area. (a.) Extract from 1:100,000 geological map. (b.) Comparison between geological map, 3-12-25 kHz resistivity ternary image and resistivity maps at four frequencies. (c.) Resistivity maps at four frequencies with annotated stratigraphy. (d.) Fractional vertical derivative map (of order 0.25) at 3 kHz with annotated stratigraphy and 3-12-25 kHz resistivity ternary image.



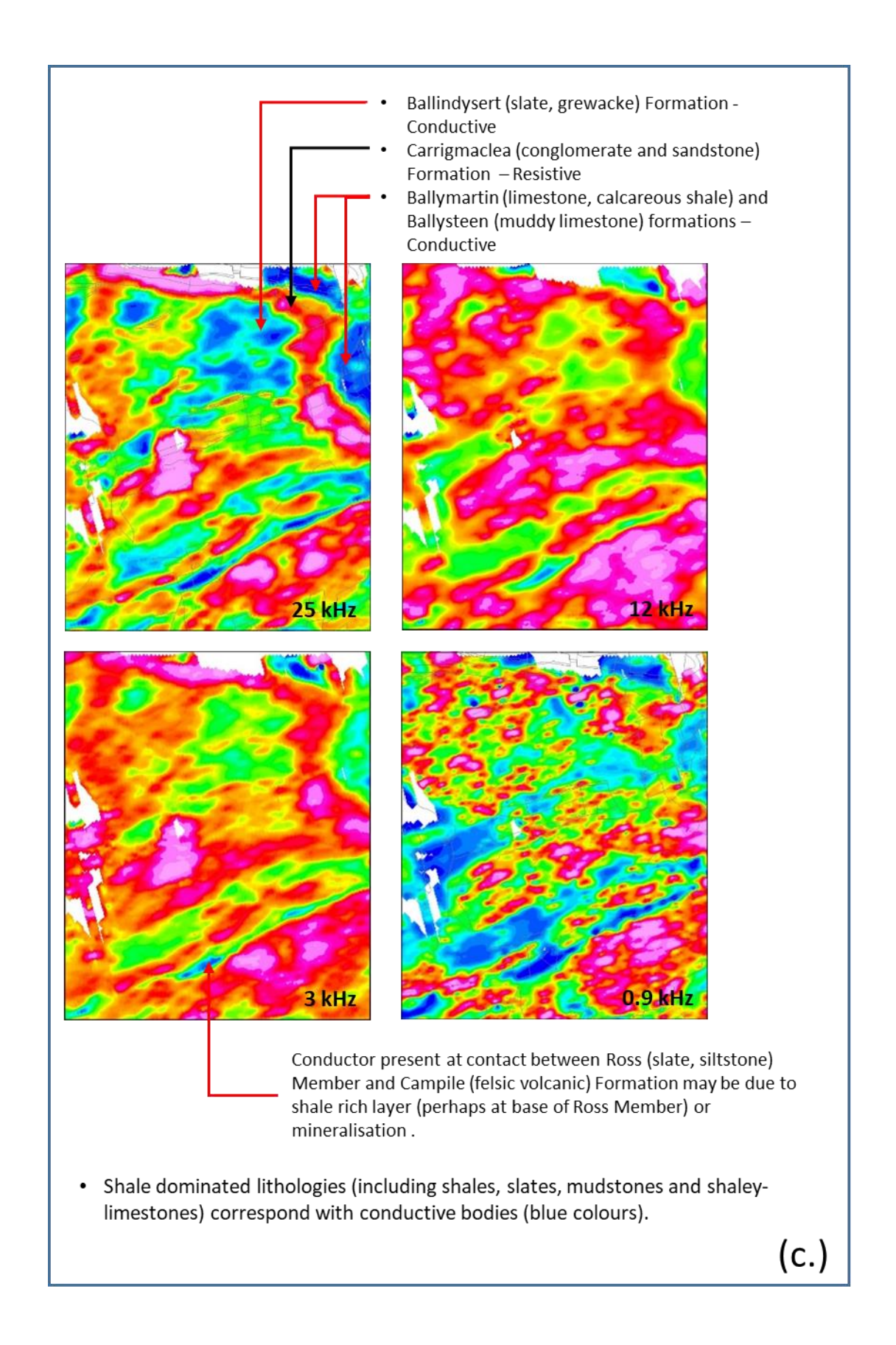
3.6.3. Waterford (illustrating litho-stratigraphic variations)













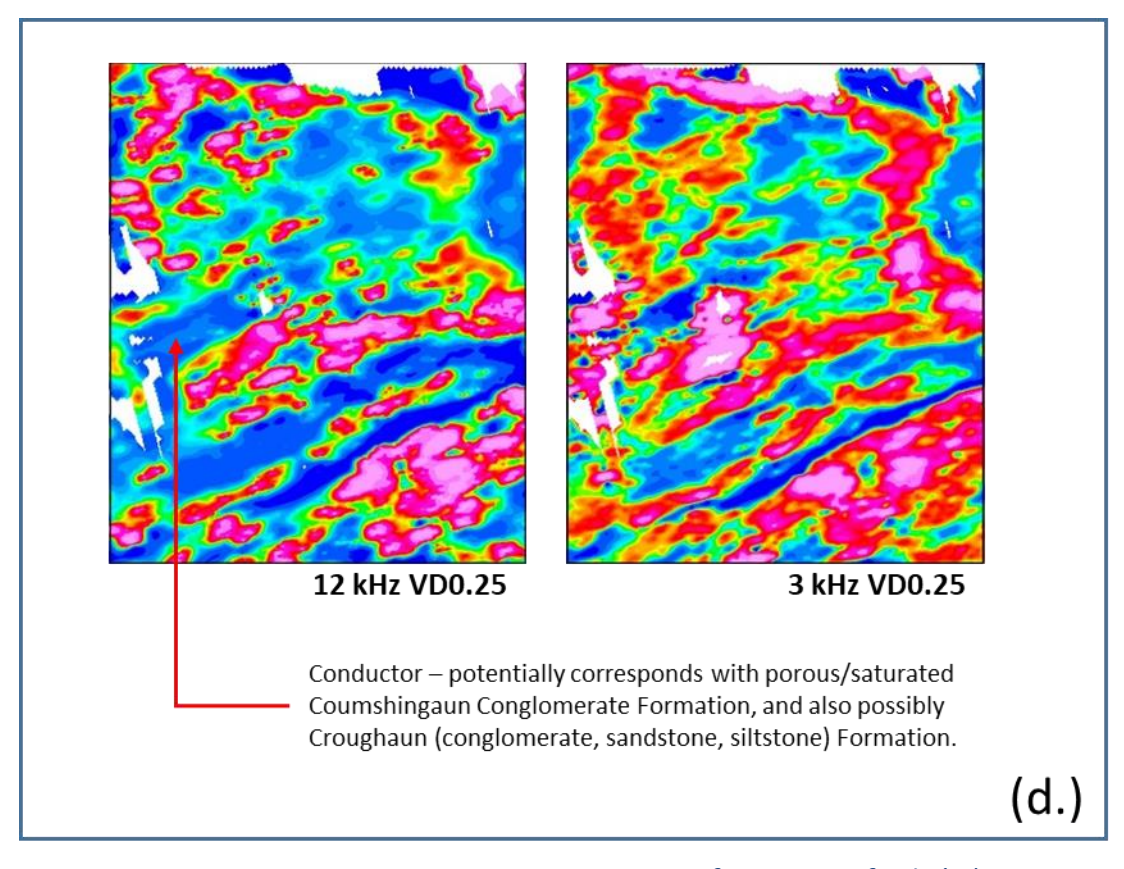


Figure 23. EM resistivity response over a portion of Co. Waterford. (a.) Extract from 1:100,000 geological map. (b.) Comparison between geological map and resistivity maps at four frequencies. (c.) Resistivity maps at four frequencies with annotated stratigraphy. (d.) Fractional vertical derivative maps (of order 0.25) at 12 and 3 kHz with annotated stratigraphy. Geological line-work (grey lines) is shown in 0.9 and 25 kHz resistivity maps to provide a geological frame of reference.

3.7. EM Inversion Resistivity Models

3.7.1. Inversion method and models

In addition to the resistivity data presented in the sections above, comprising half-space resistivity values derived at each measurement location independently for each EM frequency and then gridded to produce maps, GSI also derives a set of resistivity models through inversion of all four EM frequencies simultaneously. The resistivity models can be viewed as a series of cross-sections or depth slices, assisting interpretation of geological changes with depth.

The inversion modelling software used is the *Python* base code, *aempy* (Kiyan and Rath, 2017) and the output models have the following characteristics (more detail may be found in GSI, 2020a, 2020b and 2020c):



- One-dimensional (1-D). The resistivity structure at each measurement location is assumed to vary vertically with depth only, in the form of layers of infinite lateral extent.
- ii) Layered. The subsurface is divided into a fixed number of model layers, for which resistivity values are determined through the inversion process. Resistivity models consisting of 20 layers from surface to 62.6 m depth are released by the Tellus program. The thickness of the model layers increases logarithmically from 2.0 m at surface to 4.9 m at 62.6 m depth. Model solutions below 62.6 m depth are not released as model sensitivity and reliability is lower at greater depths.
- iii) **Smooth.** The resistivity changes from layer-to-layer are required to be smooth in the 1-D inversions (Figure 24), leading to a smoothed representation of the actual subsurface resistivity variation, which may in reality consist of sharper resistivity transitions and boundaries between distinct lithological units.

3.7.2. Enhancement of resistivity models for layer boundary identification

The 1-D inversion models are characterised by a smooth transition in resistivity across subsurface layer boundaries — as can be seen, for example, in the four discrete resistivity layers imaged in the resistivity depth profile of Figure 24 (left panel). Layer boundaries, located at the inflection points in the curves between the resistivity peaks and troughs, can be enhanced by applying a vertical derivative filter (middle panel, Figure 24). The vertical derivative has several useful characteristics:

- The position of resistivity peaks and troughs remain unchanged in the 1-D model profiles.
- ii) Layer boundaries correspond with vertical gradient values around zero, a characteristic that can be visually enhanced by taking the absolute value of the vertical derivative (right panel, Figure 24).
- iii) The vertical derivative also visually sharpens up the resistivity models, a characteristic that is particularly apparent in resistivity cross-sections (see Figure 25c).



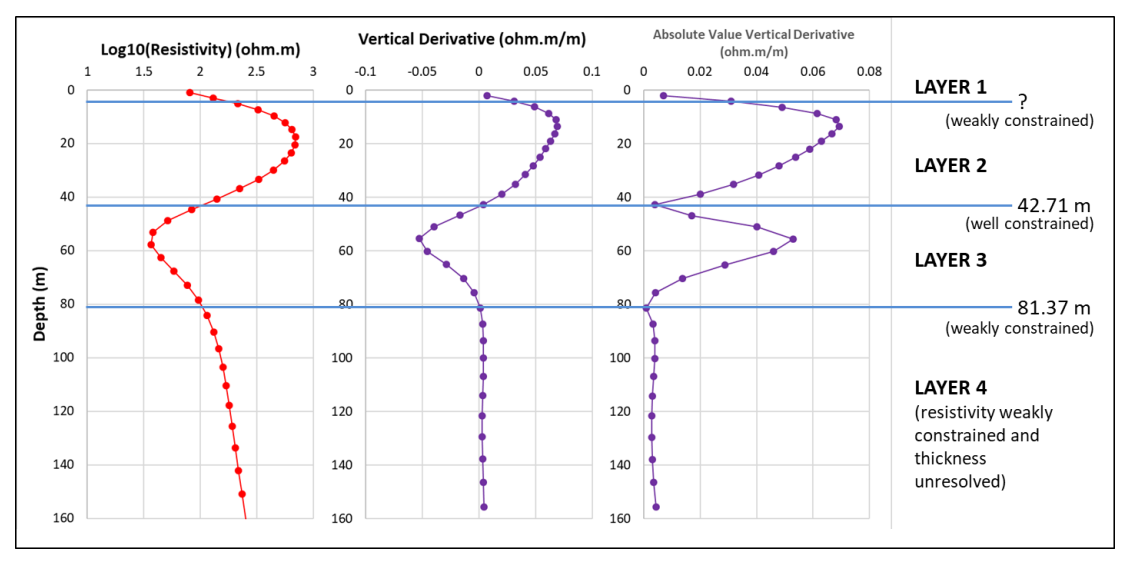
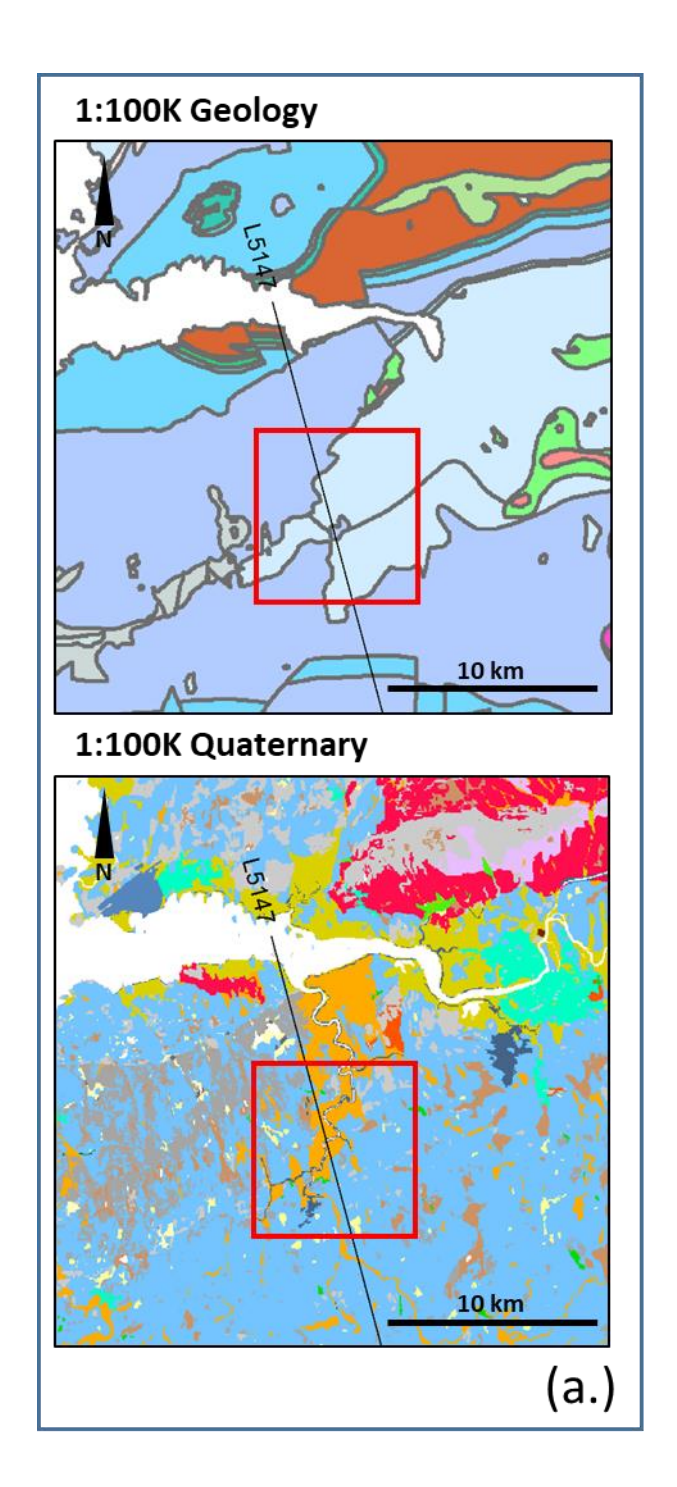


Figure 24. Example 1-D inversion model from flight-line L5264.1, at fiducial number 314, in A5 Block. (Left panel) Resistivity versus depth, with resistivity values plotted on a \log_{10} scale. (Middle) Vertical derivative of resistivity versus depth. (Right) Absolute value of vertical derivative versus depth. The resistivity structure at this location consists of four distinct layers. Boundaries between layers may be inferred from vertical derivative values close to zero.

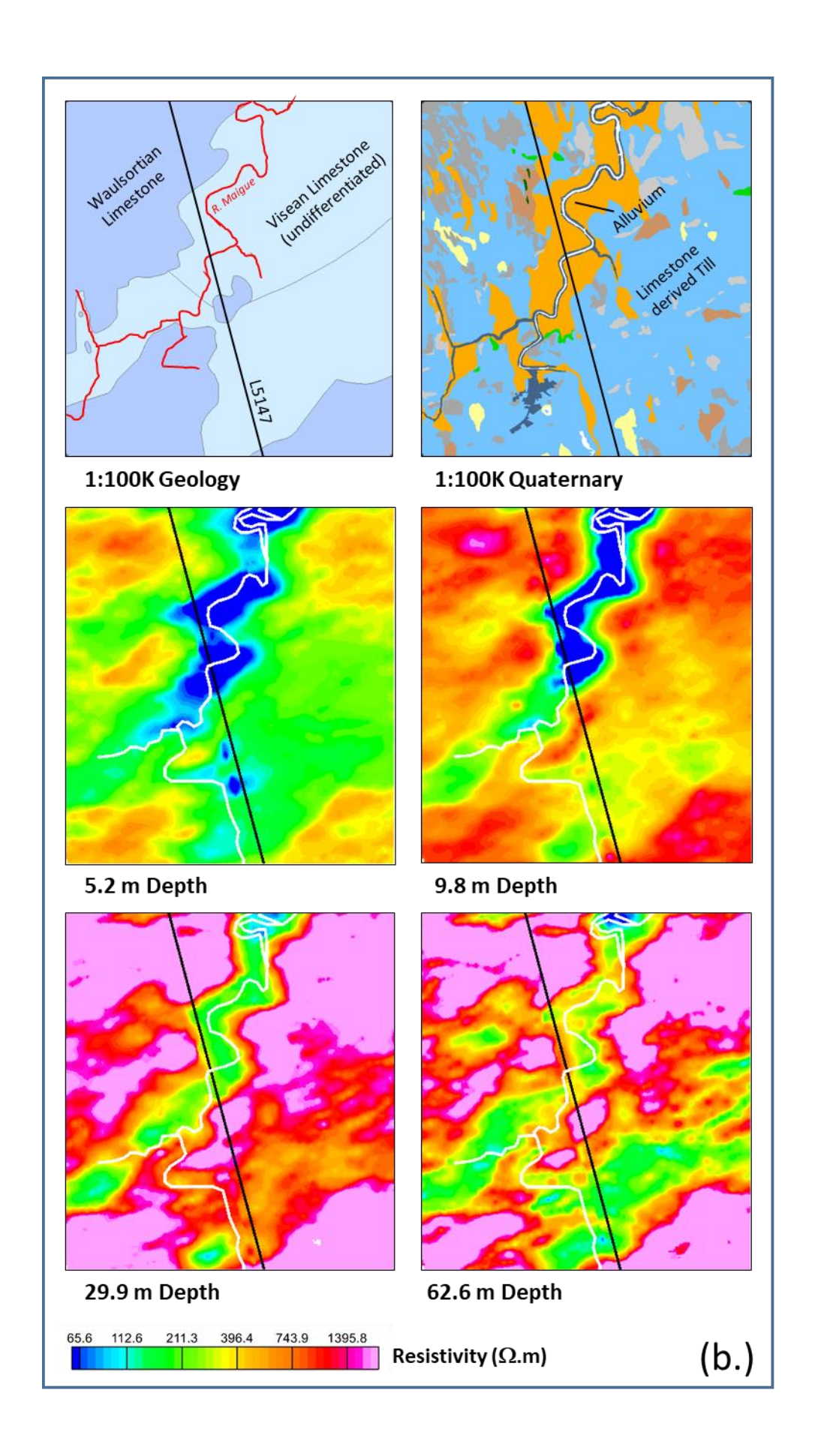
3.7.3. Case-study example: Alluvial sediments, River Maigue, Co. Limerick

The case-study illustrates resistivity imaging of bedrock geology, quaternary alluvium and weathered overburden in data from the A5 Block, acquired over the alluvial floodplain of the River Maigue, Co. Limerick. Bedrock geology in the area consists of Waulsortian and undifferentiated Visean limestones. Quaternary deposits in the area are dominated by river alluvium and limestone derived till.

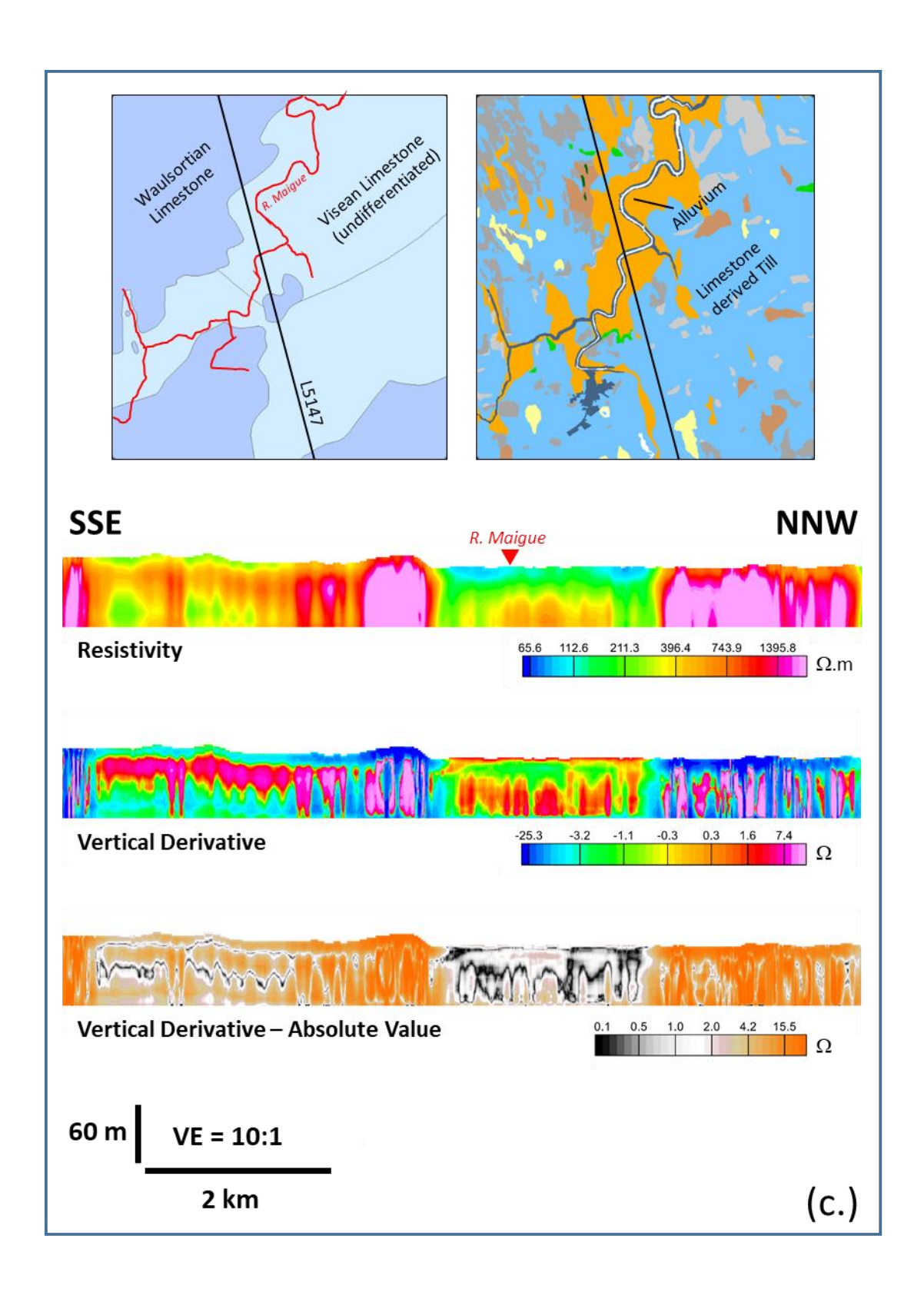














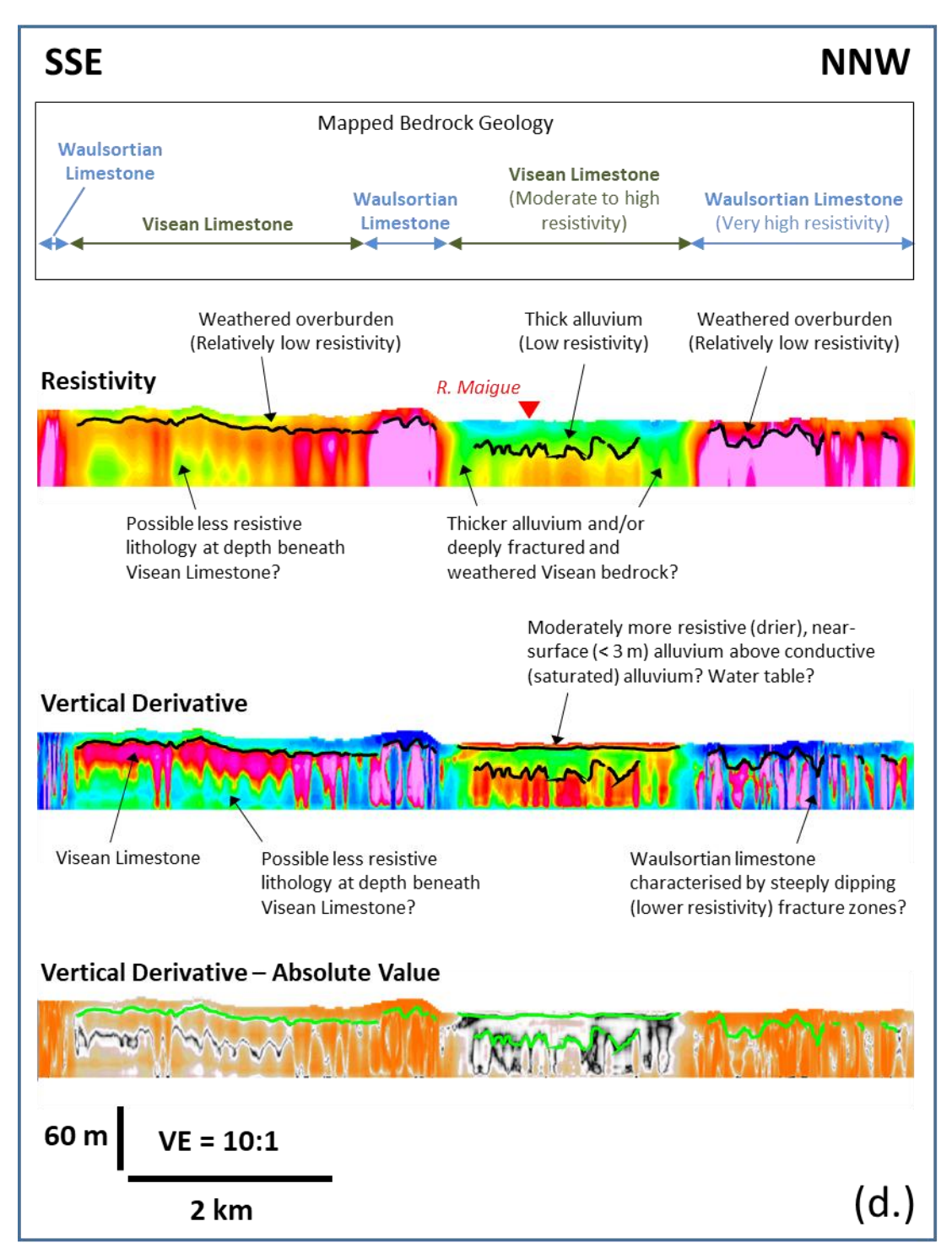


Figure 25. EM inversion resistivity models over River Maigue alluvial sediments, Co. Limerick. (a.) Extracts from 1:100,000 bedrock geology and Quaternary maps. (b.) Comparison between bedrock geology and Quaternary maps and resistivity maps at four depths. (c.) Comparison between bedrock geology and Quaternary maps and cross-sections on L5147 showing resistivity, vertical derivative and absolute value of vertical derivative. (d.) Interpretative geological sketch of line L5147 cross-sections.



4. Interpretation Guide to Radiometric Data

4.1. Introduction

While many naturally occurring elements have radioactive isotopes, only the potassium, uranium and thorium decay series have radioisotopes that produce gamma rays of sufficient energy and intensity to be measured by gamma ray spectrometry. This is because uranium, thorium and potassium are relatively abundant in the natural environment. Average crustal abundances of these elements quoted in the literature are in the range 2-2.5 % K, 2-3 ppm U and 8-12 ppm Th (IAEA, 2003), although the summary tables of concentrations derived from Tellus data and presented below indicate mean values for Irish rocks that are somewhat below these literature averages.

4.2. Measurement of Gamma Radiation

Modern gamma ray spectrometers typically record 256, 512 or 1024 channels of information in the energy range 0 to 3.0 MeV. Thus, for a 256-channel system, each channel records all gamma rays absorbed within an 11.7 keV window width. For a 1024-channel system the window width (or spectral resolution) is 2.9 keV. A typical airborne gamma ray spectrum is shown in Figure 26, together with the energy windows analysed for each of the radionuclides, as well as the total-count window.

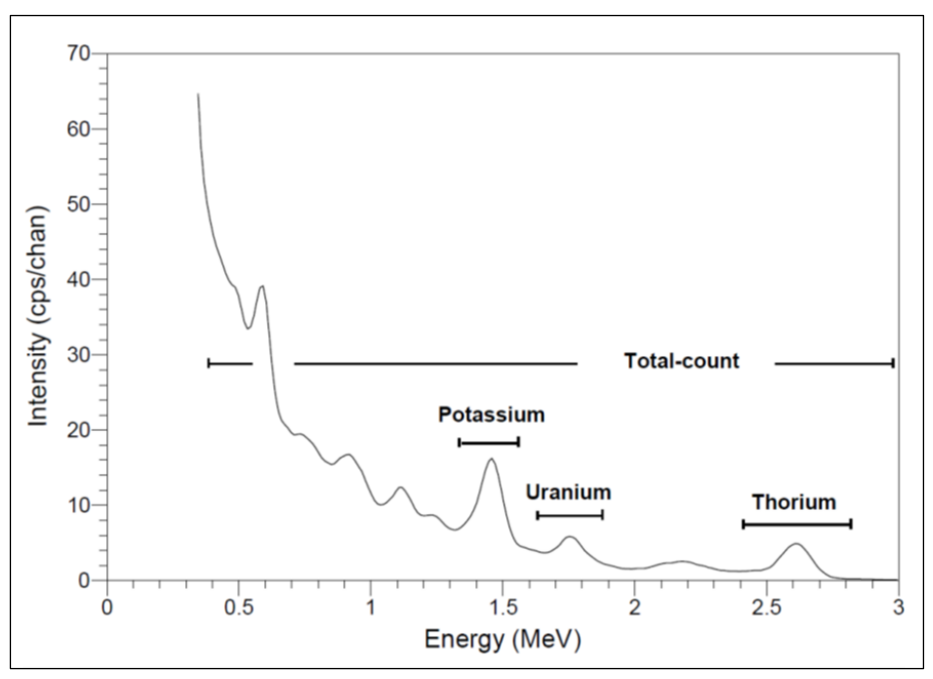


Figure 26. Typical airborne gamma ray spectrum (from IAEA, 2003).



Table 2. Gamma ray energy windows utilised in gamma ray spectrometry.

Window	Nuclide (and energy peak)	Energy Range (MeV)
Total-count		0.40 - 2.81
Potassium	⁴⁰ K (1.46 MeV)	1.37 – 1.57
Uranium	²¹⁴ Bi (1.765 MeV)	1.66 – 1.86
Thorium	²⁰⁸ Tl (2.614 MeV)	2.41 – 2.81

Different numbers of channels and crystal sizes (volumes) have been used for different vintages of Tellus airborne spectrometer data. The earlier NI, CAV, TB and TNM surveys commenced with a GR-820 spectrometer, with 256 channels and 33.56 and 8.4 L respectively of downward and upward looking crystal volume. Survey blocks A1, A2, A3, A4, A5, A6, A7 and Waterford were collected using an RS-501 spectrometer with 1024 channels and 67.2 and 12.6 L respectively of downward and upward looking crystal volume. Gamma ray energy window specifications for each of the radionuclide channels are shown in Table 2. Tellus radiometric data are recorded at a sample rate of 1 Hz, corresponding with a spatial sample interval of approximately 60 m. Standard processes and corrections are applied to Tellus radiometric data by contractor SGL, as defined in IAEA (2003) and Grasty and Minty (1995).

4.3. Radiometric Noise and Errors

- The greatest source of error in gamma ray spectrometry is statistical noise. The radioactive decay of nuclei in the source is a random process. The observed count rates in airborne gamma ray spectrometry are small, and this leads to large errors in the estimates of the radioelements. The 1 Hz sampling rate (equivalent to a 60 m spatial sampling interval) reduces statistical errors.
- Errors may result from calibration procedures. All calibrations for Tellus are done according to IAEA guide lines (1976, 1991 and 2003) to reduce calibration error.
- The height correction procedure: as the height of the aircraft increases, there is an exponential decrease in the measured count rates. This increases the fractional errors in each spectral window. However, by increasing the crystal size of the spectrometer, better results can be achieved at increased survey altitude. It is always recommended to be aware of survey altitude above ground level while carrying out any interpretation.
- Total count data are dependent on the crystal size used within the gamma-ray spectrometer (the larger the crystal volume the higher the number of gamma-rays that are intercepted and counted). Therefore, data measured over the same unit, but measured by different



instruments, may result in different total count values. Concentration values for Potassium, Thorium and Uranium are unaffected, as system calibrations used to derive these concentrations take crystal size into account.

4.4. Interpretational Tips for Radiometric Maps

A number of maps are produced from spectrometer data, including:

- i) **Total-count, TC**, measured in counts per second (cps or c/s).
- ii) Potassium concentration, %K, (percentage, %).
- iii) **Equivalent Thorium concentration**, **eTh**, (parts per million, ppm).
- iv) **Equivalent Uranium concentration**, **eU**, (parts per million, ppm).
- v) **Concentration ratio maps** (Thorium:Potassium, **RTK**; Uranium:Potassium, **RUK** and Uranium:Thorium, **RUT**).
- vi) **Ternary maps** of all three radionuclide concentrations or of all three concentration ratios.
- vii) Sum-normalized abundance maps, Kn, THn and Un, in which concentration is converted to relative abundance with respect to the sum of all three elements, for example, for potassium, Kn = K/(K+U+TH).
- viii) Radiogenic heat production maps. Heat production, A, is calculated from the three measured radio-element concentrations using the following equation (van Dam, 2007):

$$A = 0.337(0.74eU + 0.199eTh + 0.26K)$$
 (2)

where eU and eTh concentrations are in ppm units, K concentration is in % units and A is in $\mu W/m^{-3}$.

The qualitative interpretation of total-count maps may be used to classify regions into low, intermediate and high-count zones.

- High counts may indicate acidic rocks: granitic rocks, sedimentary rocks and rocks with high content of feldspar, biotite and muscovite. It is noted that higher counts may also be apparent where bedrock is exposed at surface, rather than buried under soil cover.
- **Intermediate counts** may show alkali syenite, andesite, diorite and metamorphic rocks.
- Low counts may indicate basic and ultra-basic igneous rocks and rocks with abundant pyroxene and olivine. Lower counts may also be apparent where bedrock is buried under thick soil cover and especially under peat.

Total-count data are useful for a first pass interpretation of the lithological origin of the radiometric data. Interpretation of the individual radio-element concentrations (K, eTh and eU) and of the relative proportions of the elements (in the form of ternary displays or ratio maps) provides a stronger diagnostic tool in



differentiating between different lithologies – as illustrated in several case studies below (Section 4.8) and in the statistical tables showing concentrations of the three radio-elements versus Irish lithological units (Section 4.6, Tables 3-5).

4.5. Depth of Investigation

As gamma rays are attenuated while passing through overburden, vegetation and particularly water, the depth of investigation provided by gamma rays is generally approximately 30–50 cm, i.e., the gamma rays recorded by the airborne spectrometer system do not originate from depths much greater than 50 cm below surface. However, as the soil and sediment is generally derived from the underlying geology, radiometric data provide a useful geological mapping tool.

4.6. Radionuclide Concentrations Related to 1:500K Geology

Tables 3 to 5 summarize the statistical characteristics of potassium, thorium and uranium concentrations in relation to lithological units in the 1:500K geological map. These tables may be used as an aid in the interpretation of bedrock units using radiometric data.

The tables show that a Tertiary granite (felsite) (Unit 9) is characterised by the highest mean concentrations of all three radio-elements (K: 2.4%, eTh: 16.4 ppm, eU: 2.4 ppm). A further (minor) Tertiary volcanic (Unit 78) has the second highest mean concentrations in potassium and thorium and third highest in uranium (K: 2.2%, eTh: 9.1 ppm, eU: 1.2 ppm). As a general observation, the statistical tables illustrate that the lithologies with highest concentrations of the three radio-elements include felsic volcanics, basic volcanics (but low in potassium), slates, greywackes and shales, and some sandstone units. A summary of units with particularly high concentrations in each of the radio-elements is provided below.

Units high in potassium are:

- Tertiary granite, felsite (Unit 9, mean potassium 2.4%)
- Minor Tertiary volcanic (Unit 78, 2.2%)
- Mid-Upper Ordovician acid volcanics (Unit 38, 1.8%)
- Mid-Upper Ordovician slate (Unit 39, 1.8%)
- Lower-Mid Ordovician slate (Unit 35, 1.7%)
- Cambrian slate (Unit 31, 1.6%)
- Rathkenny Formation (Unit 42, 1.6%)
- Silurian sandstone, greywacke, shale (Unit 49, 1.5%)
- Permian sandstone (Unit 73, 1.5%)

Units high in thorium are:

- Tertiary granite, felsite (Unit 9, mean thorium 16.4 ppm)
- Minor Tertiary volcanic (Unit 78, 9.1 ppm)
- Mid-Upper Ordovician acid volcanics (Unit 38, 8.4 ppm)
- Mid-Upper Ordovician slate (Unit 39, 7.9 ppm)



- Lower-Mid Ordovician slate (Unit 35, 7.3 ppm)
- Cambrian slate (Unit 31, 7.1 ppm)
- Rathkenny Formation (Unit 42, 7.1 ppm)
- Silurian sandstone, greywacke, shale (Unit 49, 6.7 ppm)
- Mid-Upper Ordovician basic volcanics (Unit 37, 6.4 ppm)

Units high in uranium are:

- Tertiary granite, felsite (Unit 9, mean uranium 2.4 ppm)
- Mid-Upper Ordovician acid volcanics (Unit 38, 1.3 ppm)
- Minor Tertiary volcanic (Unit 78, 1.2 ppm)
- Mid-Upper Ordovician basic volcanics (Unit 37, 1.1 ppm)
- Mid-Upper Ordovician slate (Unit 39, 1.1 ppm)
- Lower-Mid Ordovician slate (Unit 35, 1.1 ppm)
- Cambrian slate (Unit 31, 1.0 ppm)
- Rathkenny Formation (Unit 42, 0.9 ppm)
- Silurian sandstone, greywacke, shale (Unit 49, 0.9 ppm)
- Greenore Point (amphibolite) Group (Unit 17, 0.9 ppm)
- Namurian sandstone, shale (Unit 71, 0.9 ppm)

Table 3. Data statistics for Potassium Concentration with respect to lithological units in the 1:500K geology map. Data unit: percentage.

Potassium Concentration, K%							
Unit	11117 11117 1				Number of		
Label	UNIT NAME/Geology	Min	Max	Mean	Data		
1	Metadolerite or Amphibolite	0	2.1	0.8	6,422		
2	Serpentinite, DX	0	2.4	0.9	1,043		
3	Orthogenesis suite, Connemara	0	2.4	0.4	7,311		
4	Ordovician granite	0	2.6	1	11,957		
5	Metagabbro, metadiorite (Tyrone plu)	0	3.4	0.8	19,642		
6	Palaeozoic felsic minor intrusion	0	3.2	1.1	1,018		
7	Caledonian appinite suite	0	2.7	0.9	2,095		
8	Caledonian granite	0	6.1	1.3	285,166		
9	Tertiary granite, felsite	0.3	5.4	2.4	19,479		
10	Tertiary rhyolite (Volc & Intru)	0.1	1.8	0.8	2,408		
11	Tertiary basic intrusion	0	3.2	1.1	4,819		
13	Mullet Gneiss	0.1	2.6	1.2	1,327		
14	Cross point Gneiss	0	2.6	0.7	3,706		
15	Doolough Granite and Gneiss	0.1	2.1	0.9	193		
16	Kilmore Quay Group	0.1	1.8	1.2	1,775		
17	Greenore point Group	0.2	2.2	1.4	4,051		
18	Tyrone C1 (Corvanagh/Slishwood)	0.1	2.7	1.1	4,496		
19	Slishwood Division	0	2.5	0.7	27,048		
20	Inishkea Division	0	2.7	0.5	6,862		
21	Dalradian Grampian Group	0	3.3	0.4	40,303		



22	Dalradian Appin Group quartzite	0	2.8	0.6	13,205
23	Dalradian Appin Group	0	<i>7.3</i>	0.7	755
24	Dalradian Argyll Group Paragenesis	0	1.6	0.4	1,912
25	Dalradian Argyll Group Volcanics	0	1.8	0.6	2,748
26	Dalradian Argyll quartzite	0	5	0.7	65,152
27	Dalradian Argyll Group	0	3.1	0.8	231,623
28	Dalradian S Highland GP Volcanics	0	2.4	0.7	3,447
29	Dalradian S Highland GP	0	3.6	1	186,051
30	Cambrian quartzite	0.1	2.4	1.2	3,319
31	Cambrian slate	0	2.5	1.6	10,514
32	Cambrian greywacke, sandst, quartzite	0.1	2.7	1.4	41,171
33	Lr.Mid Ordovician basic volcanics	0	5.5	0.8	19,092
34	Lr.Mid Ordovician acid volcanics	0	2.9	0.9	3,581
35	Lr.Mid Ordovician slate	0	3.6	1.7	182,977
36	Lr.Mid Ordovician greywackes, sandstone	0	2.7	0.7	22,616
37	Mid-Up Ordovician basic volcanics	0.1	3.2	1.4	10,016
38	Mid-Up Ordovician acid volcanics	0.1	5	1.8	28,141
39	Mid-Up Ordovician slate	0.1	5.5	1.8	67,547
40	Mid-Up Ordovician g'wacke, sandstone, shale	0	10.3	1.1	117,668
41	Ordovician or Silurian melange	0	2.3	0.8	1,220
42	Rathkenny Formation	0.3	2.5	1.6	16,035
45	Croagh Patrick Succ.	0	1.7	0.5	7,748
46	Silurian quartzite	0	1.5	0.6	1,208
47	Louisburgh-Clare Island. Succ.	0.1	2.3	0.8	2,240
48	Killary-Joyces Succ.	0	2.6	1	8,709
49	Silurian sandstone, g'wacke, shale	0	3.8	1.5	493,289
50	Devo basic volcanics, minor intrus	0	3.4	1.3	3,187
52	Up Silurian-Lr Devonian ORS	0	3.7	1.1	38,760
53	Mid Devonian ORS	0	2.7	0.8	10,520
54	UP Devonian Lr Carb OSR	0.6	6.5	1	116,480
56	Dev-Lr Carboniferous volcanics & minor intrus	0	2.8	1.2	9,999
58	Lower limestone, shale	0	2.8	1.3	19,096
59	COURCEYAN "basal clastics"	0	3.2	1	83,707
60	Navan Group	0	2.7	1	39,002
61	Courceyan limestone	0	2.7	0.9	220,476
62	Waulsortian Limestone	0	2.7	0.8	226,746
63	Visean "basal clastics"	0	2.5	0.8	38,545
64	Visean shelf limestone, shale	0	3.1	0.6	1,050,477
65	Visean basinal limestone "calp"	0	2.5	0.6	400,904
66	TYRONE GP, Visean mudstone, sandstone	0	3	0.8	90,379
67	Armagh GP	0	2.1	1.2	13,389



68	LEITRIM GP, Visean mudstone, sandstone	0	1.9	0.3	71,127
69	Ballycastle Succ.	0	1.9	1	1,216
70	Late Visean-Westphalian "ORS"	0	1.9	1.1	21,760
71	Namurian sandstone, shale	0	2.5	0.8	88,631
72	Westphalian shale, sandstone	0	1.9	1.1	869
73	Permian sandstone	0.6	2.8	1.5	3,577
74	Permo-Triassic sandstone	0.3	2	1.3	1,154
75	Triassic sandstone	0	3.1	1.3	51,766
76	Lr. Jurassic mudstone	0	1.4	0.7	3,323
77	Up Cretaceous limestone	0	2.4	0.6	8,472
78	Tertiary minor volcanics	1.4	3.2	2.2	501
79	Lower basalt formation	0	2.2	0.5	175,088
80	Interbasaltic formation	0	1.1	0.3	3,558
81	Causeway Tholeiite Mbr	0	1.3	0.5	7,464
82	Upper basalt formation	0	1.2	0.4	99,510
83	Olingocene clay, sand	0	1.6	0.8	25,462

Table 4. Data statistics for Equivalent Thorium Concentration with respect to lithological units in the 1:500K geology map. Data unit: parts per million.

	Equivalent Thorium, eTh							
Unit Label	UNIT NAME/Geology	Min	Max	Mean	Number of Data			
1	Metadolerite or Amphibolite	0	10.3	3.1	6,422			
2	Serpentinite, DX	0	10.3	4.4	1,043			
3	Orthogenesis suite, Connemara	0.1	10.3	1.5	7,311			
4	Ordovician granite	0.1	19.2	4.2	11,957			
5	Metagabbro, metadiorite (Tyrone plu)	0	17.7	3.1	19,642			
6	Palaeozoic felsic minor intrusion	0.2	8.7	3.6	1,018			
7	Caledonian appinite suite	0.1	16.6	3.5	2,095			
8	Caledonian granite	0	32.3	4.4	285,166			
9	Tertiary granite, felsite	2.3	51.9	16.4	19,479			
10	Tertiary rhyolite (Volc & Intru)	0.3	8.6	3.8	2,408			
11	Tertiary basic intrusion	0.1	17.9	4.7	4,819			
13	Mullet Gneiss	0.3	7.7	2.4	1,327			
14	Cross point Gneiss	0	7.6	1.7	3,706			
15	Doolough Granite and Gneiss	0.2	7.4	2.3	193			
16	Kilmore Quay Group	0.5	7	5.1	1,775			
17	Greenore point Group	0.4	8.6	6.2	4,051			
18	Tyrone C1 (Corvanagh/Slishwood)	0.3	9.9	4.8	4,496			
19	Slishwood Division	0.1	8.1	1.7	27,048			
20	Inishkea Division	0	13.4	1.7	6,862			



21	Dalradian Grampian Group	0	11	1.3	40,303
22	Dalradian Appin Group quartzite	0.1	10.7	1.7	13,205
23	Dalradian Appin Group	0	14.8	2.6	755
24	Dalradian Argyll Group Paragenesis	0.1	8.3	2.2	1,912
25	Dalradian Argyll Group Volcanics	0.1	9	2.8	2,748
26	Dalradian Argyll quartzite	0	10.3	2.2	65,152
27	Dalradian Argyll Group	0	12.2	3.8	231,623
28	Dalradian S Highland GP Volcanics	0	7.5	2.7	3,447
29	Dalradian S Highland GP	0	16.9	4.1	186,051
30	Cambrian quartzite	0.2	11.3	5.6	3,319
31	Cambrian slate	0.3	10.9	7.1	10,514
32	Cambrian greywacke, sandst, quartzite	0.3	10.9	6	41,171
33	Lr.Mid Ordovician basic volcanics	0.1	14.2	2.9	19,092
34	Lr.Mid Ordovician acid volcanics	0.1	8.8	3.4	3,581
35	Lr.Mid Ordovician slate	0	19.9	7.3	182,977
36	Lr.Mid Ordovician greywackes, sandstone	0.1	14.6	3.1	22,616
37	Mid-Up Ordovician basic volcanics	0.4	12.2	6.4	10,016
38	Mid-Up Ordovician acid volcanics	0.4	27.1	8.4	28,141
39	Mid-Up Ordovician slate	0.2	21.6	7.9	67,547
40	Mid-Up Ordovician g'wacke, sandstone, shale	0.2	26.7	4.9	117,668
41	Ordovician or Silurian melange	0	7.4	4.2	1,220
42	Rathkenny Formation	1.4	9.8	7.1	16,035
45	Croagh Patrick Succ.	0	7.1	2.6	7,748
46	Silurian quartzite	0.2	7.1	2.9	1,208
47	Louisburgh-Clare Island. Succ.	0.1	8.9	3.4	2,240
48	Killary-Joyces Succ.	0.2	13.1	4.5	8,709
49	Silurian sandstone, g'wacke, shale	0	31.9	6.7	493,289
50	Devo basic volcanics, minor intrus	0.1	11.4	4.4	3,187
52	Up Silurian-Lr Devonian ORS	0.1	10	4.3	38,760
53	Mid Devonian ORS	0.1	8.3	3	10,520
54	UP Devonian Lr Carb OSR	0	18	4	116,480
56	Dev-Lr Carboniferous volcanics & minor intrus	0.1	9.8	4.9	9,999
58	Lower limestone, shale	0.1	9.2	4.7	19,096
59	COURCEYAN "basal clastics"	0.1	7.8	3.3	83,707
60	Navan Group	0.1	9.2	4	39,002
61	Courceyan limestone	0	9.4	3.8	220,476
62	Waulsortian Limestone	0	8	3.2	226,746
63	Visean "basal clastics"	0	9.8	2.6	38,545
64	Visean shelf limestone, shale	0	12.2	3	1,050,477
65	Visean basinal limestone "calp"	0	8.8	3	400,904



66	TYRONE GP, Visean mudstone, sandstone	0	7.2	2.7	90,379
67	Armagh GP	0	8.3	4.2	13,389
68	LEITRIM GP, Visean mudstone, sandstone	0	7.6	2.2	71,127
69	Ballycastle Succ.	0.3	6	3.4	1,216
70	Late Visean-Westphalian" ORS"	0.2	7	4.1	21,760
71	Namurian sandstone, shale	0	9.4	4.1	88,631
72	Westphalian shale, sandstone	0	9.3	5.2	869
73	Permian sandstone	1.7	9.1	5.1	3,577
74	Permo-Triassic sandstone	0.9	8.4	5.4	1,154
<i>75</i>	Triassic sandstone	0.1	17.7	4.1	51,766
76	Lr. Jurassic mudstone	0.1	5.6	2.2	3,323
77	Up Cretaceous limestone	0.1	6.2	2.1	8,472
78	Tertiary minor volcanics	5.7	14.3	9.1	501
79	Lower basalt formation	0	8.7	1.7	175,088
80	Interbasaltic formation	0.1	4.2	1.3	3,558
81	Causeway Tholeiite Mbr	0.1	5.2	1.9	7,464
82	Upper basalt formation	0	4.9	1.3	99,510
83	Olingocene clay, sand	0.1	6.8	2.8	25,462

Table 5. Data statistics for Equivalent Uranium Concentration with respect to lithological units in the 1:500K geology map. Data unit: parts per million.

Equivalent Uranium, eU							
Unit Label	UNIT NAME/Geology	Min	Max	Mean	Number of Data		
1	Metadolerite or Amphibolite	0	1.4	0.4	6,422		
2	Serpentinite, DX	0	1.8	0.5	1,043		
3	Orthogenesis suite, Connemara	0	1.8	0.2	7,311		
4	Ordovician granite	0	2.9	0.5	11,957		
5	Metagabbro, metadiorite (Tyrone plu)	0	3.2	0.4	19,642		
6	Palaeozoic felsic minor intrusion	0	1.7	0.5	1,018		
7	Caledonian appinite suite	0	2.7	0.5	2,095		
8	Caledonian granite	0	7.7	0.8	285,166		
9	Tertiary granite, felsite	0.1	9	2.4	19,479		
10	Tertiary rhyolite (Volc & Intru)	0	1.4	0.5	2,408		
11	Tertiary basic intrusion	0	2.1	0.6	4,819		
13	Mullet Gneiss	0	0.8	0.3	1,327		
14	Cross point Gneiss	0	0.9	0.2	3,706		
15	Doolough Granite and Gneiss	0	0.7	0.3	193		
16	Kilmore Quay Group	0	1.3	0.8	1,775		
17	Greenore point Group	0	1.5	0.9	4,051		
18	Tyrone C1 (Corvanagh/Slishwood)	0	1.2	0.5	4,496		
19	Slishwood Division	0	2.2	0.3	27,048		
20	Inishkea Division	0	1.3	0.2	6,862		



21	Dalradian Grampian Group	0	1.3	0.2	40,303
22	Dalradian Appin Group quartzite	0	1	0.2	13,205
23	Dalradian Appin Group	0	1.7	0.3	755
24	Dalradian Argyll Group Paragenesis	0	1.1	0.2	1,912
25	Dalradian Argyll Group Volcanics	0	1.2	0.4	2,748
26	Dalradian Argyll quartzite	0	3	0.3	65,152
27	Dalradian Argyll Group	0	5.2	0.5	231,623
28	Dalradian S Highland GP Volcanics	0	1.5	0.4	3,447
29	Dalradian S Highland GP	0	2.8	0.5	186,051
30	Cambrian quartzite	0	1.7	0.8	3,319
31	Cambrian slate	0	1.7	1	10,514
32	Cambrian greywacke, sandst, quartzite	0	1.9	0.8	41,171
33	Lr.Mid Ordovician basic volcanics	0	2.6	0.4	19,092
34	Lr.Mid Ordovician acid volcanics	0	1.3	0.5	3,581
35	Lr.Mid Ordovician slate	0	6.9	1.1	182,977
36	Lr.Mid Ordovician greywackes, sandstone	0	4	0.4	22,616
37	Mid-Up Ordovician basic volcanics	0.1	2.2	1.1	10,016
38	Mid-Up Ordovician acid volcanics	0	4.1	1.3	28,141
39	Mid-Up Ordovician slate	0	4.6	1.1	67,547
40	Mid-Up Ordovician g'wacke, sandstone, shale	0	3.8	0.6	117,668
41	Ordovician or Silurian melange	0	1	0.4	1,220
42	Rathkenny Formation	0.1	1.6	0.9	16,035
45	Croagh Patrick Succ.	0	0.9	0.3	7,748
46	Silurian quartzite	0	0.8	0.3	1,208
47	Louisburgh-Clare Island. Succ.	0.1	0.8	0.4	2,240
48	Killary-Joyces Succ.	0	5.1	0.6	8,709
49	Silurian sandstone, g'wacke, shale	0	5.1	0.9	493,289
50	Devo basic volcanics, minor intrus	0	1.7	0.6	3,187
52	Up Silurian-Lr Devonian ORS	0	1.9	0.6	38,760
53	Mid Devonian ORS	0	1.7	0.4	10,520
54	UP Devonian Lr Carb OSR	0	3	0.6	116,480
56	Dev-Lr Carboniferous volcanics & minor intrus	0	1.7	0.8	9,999
58	Lower limestone, shale	0	2.6	0.8	19,096
59	COURCEYAN "basal clastics"	0	2	0.5	83,707
60	Navan Group	0	2.1	0.7	39,002
61	Courceyan limestone	0	3.5	0.8	220,476
62	Waulsortian Limestone	0	2.1	0.7	226,746
63	Visean "basal clastics"	0	2.6	0.4	38,545
64	Visean shelf limestone, shale	0	4.2	0.8	1,050,477
65	Visean basinal limestone "calp"	0	3.4	0.8	400,904
66	TYRONE GP, Visean mudstone, sandstone	0	2.9	0.4	90,379
67	Armagh GP	0	1.9	0.6	13,389
68	LEITRIM GP, Visean mudstone, sandstone	0	4.3	0.5	71,127
69	Ballycastle Succ.	0.1	1.1	0.6	1,216
70	Late Visean-Westphalian "ORS"	0	1.3	0.5	21,760
71	Namurian sandstone, shale	0	5.9	0.9	88,631



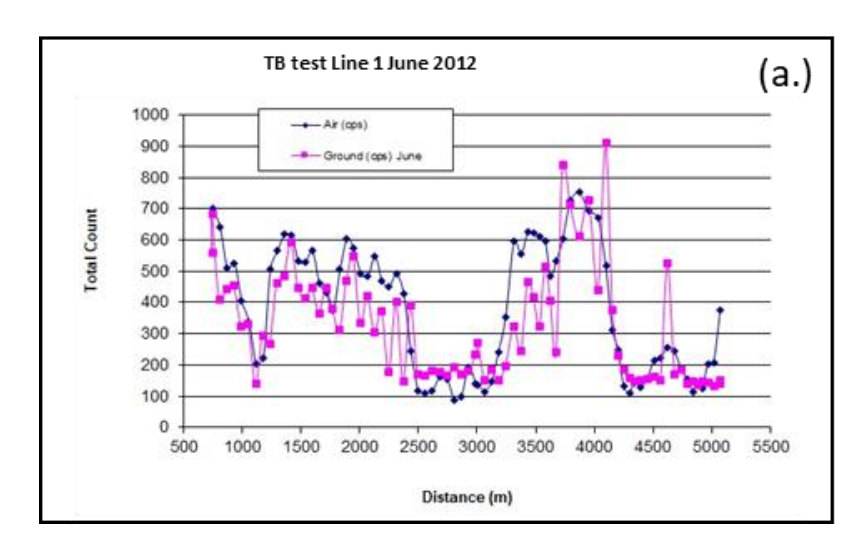
72	Westphalian shale, sandstone	0.1	1.6	0.8	869
73	Permian sandstone	0.1	1.4	0.6	3,577
74	Permo-Triassic sandstone	0.1	1.4	0.7	1,154
<i>75</i>	Triassic sandstone	0	4.3	0.6	51,766
76	Lr Jurassic mudstone	0	1.2	0.3	3,323
77	Up Cretaceous limestone	0	1.1	0.3	8,472
78	Tertiary minor volcanics	0.8	1.9	1.2	501
79	Lower basalt formation	0	1.4	0.3	175,088
80	Interbasaltic formation	0	0.8	0.2	3,558
81	Causeway Tholeiite Mbr	0	0.9	0.3	7,464
82	Upper basalt formation	0	0.9	0.2	99,510
83	Olingocene clay, sand	0	1.2	0.4	25,462

4.7. Tellus Bundoran Test Line Experiment

As part of the airborne surveys, a 6 km long test line (the Bundoran test line) has been flown at the beginning and end of each survey phase to assist with data calibration. A ground follow-up experiment was carried out on 28 June 2012 over part of the Bundoran test line (Figure 27) and has been used to compare variations in the radiometric data with variation in local quaternary and bedrock units.

Data at single ground measurement points were collected using a hand-held instrument for a 15 second integrating time and for five separate readings. The five total-count readings were then averaged for each single point to minimise statistical error. The results for a 4.2 km-long profile of data recorded in this manner are shown in Figures 27 and 28, in comparison with the airborne data. Good correlation is shown between the airborne and ground measurements.

Hand auguring was also carried out to observe soil moisture content and peat thickness at selected sites along the test profile. As illustrated in Figure 27, total-count values less than 200 c/s are associated with thick peat.





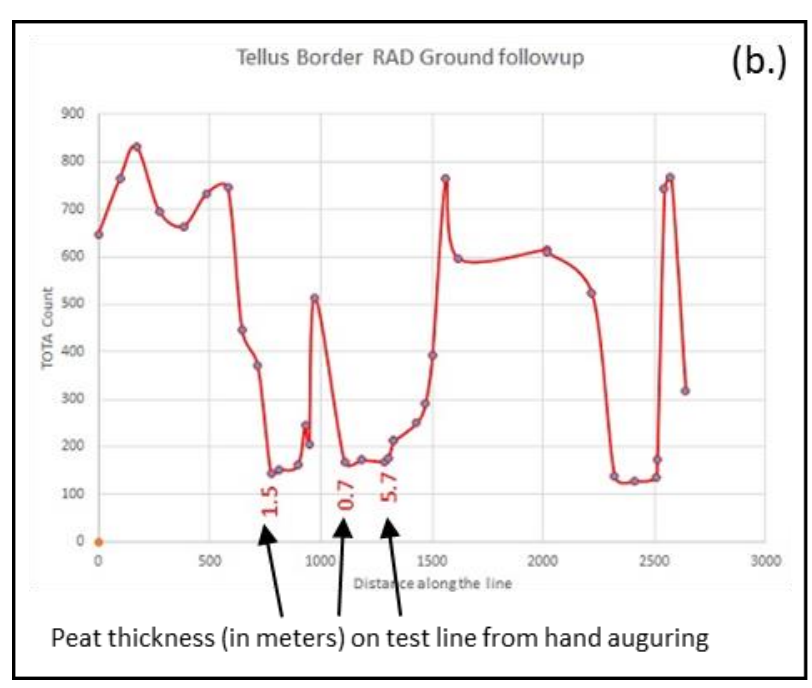
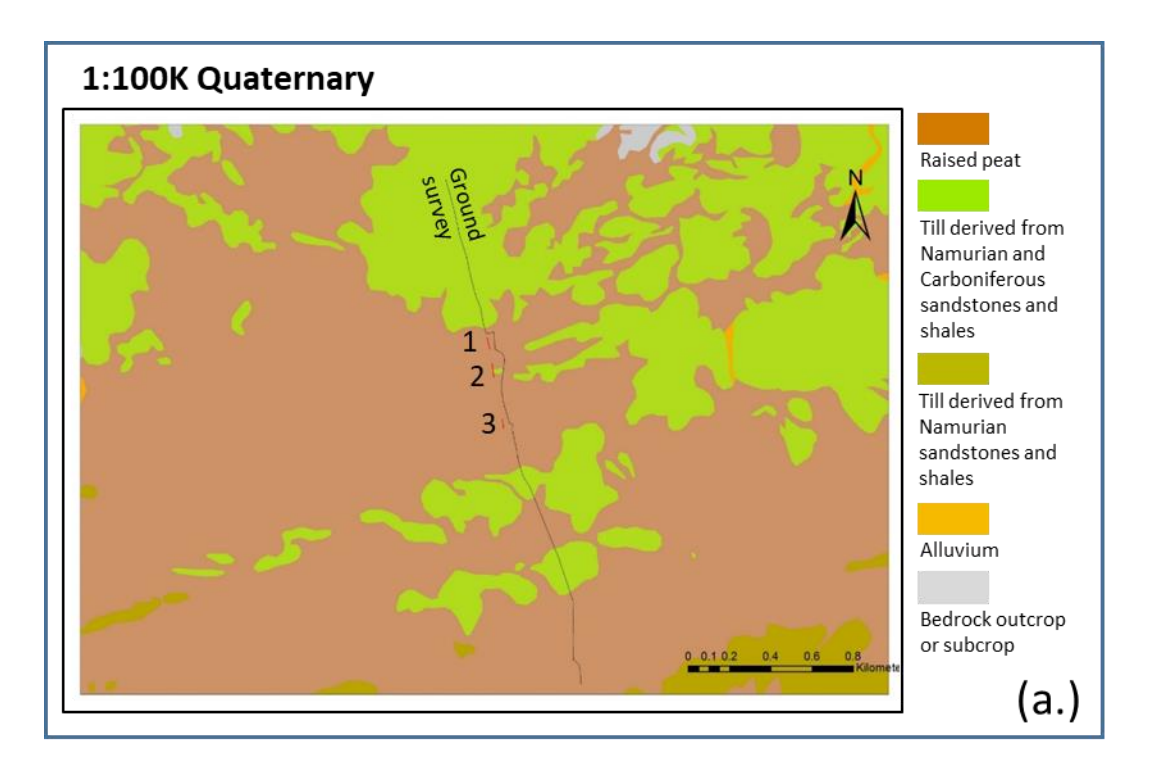
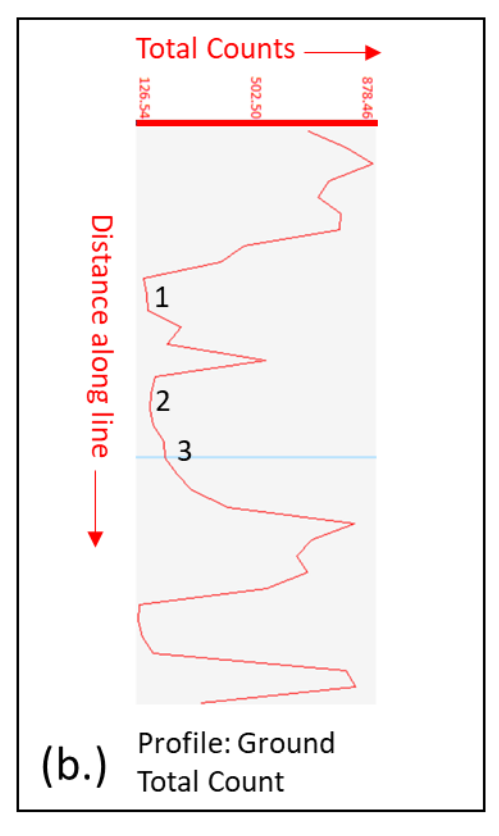
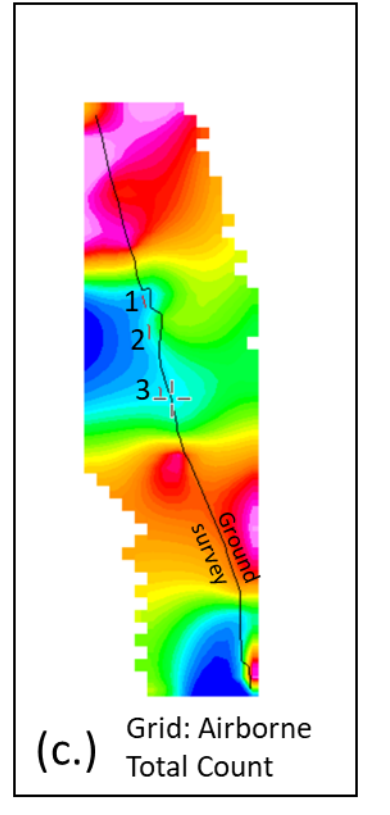


Figure 27. Bundoran Test Line gamma ray spectrometry data. (a.) Comparison of airborne and ground total-count data and (b.) ground spectrometer total-count data and measured peat thickness.









- The smaller the total-count reading, the thicker the peat deposit, assuming the peat is water saturated.
- Total counts less than 200 cps indicate thick peat bog.

Figure 28. Comparison between airborne and ground total-count radiometric data and Quaternary peat along Bundoran Test Line. (a.) Extract from 1:100,000 Quaternary geology map. (b.) Total-count measurements along ground profile. (c.) Total-count grid from airborne data, showing location of ground profile. Numbers 1, 2 and 3 indicate coincident locations in all figures.

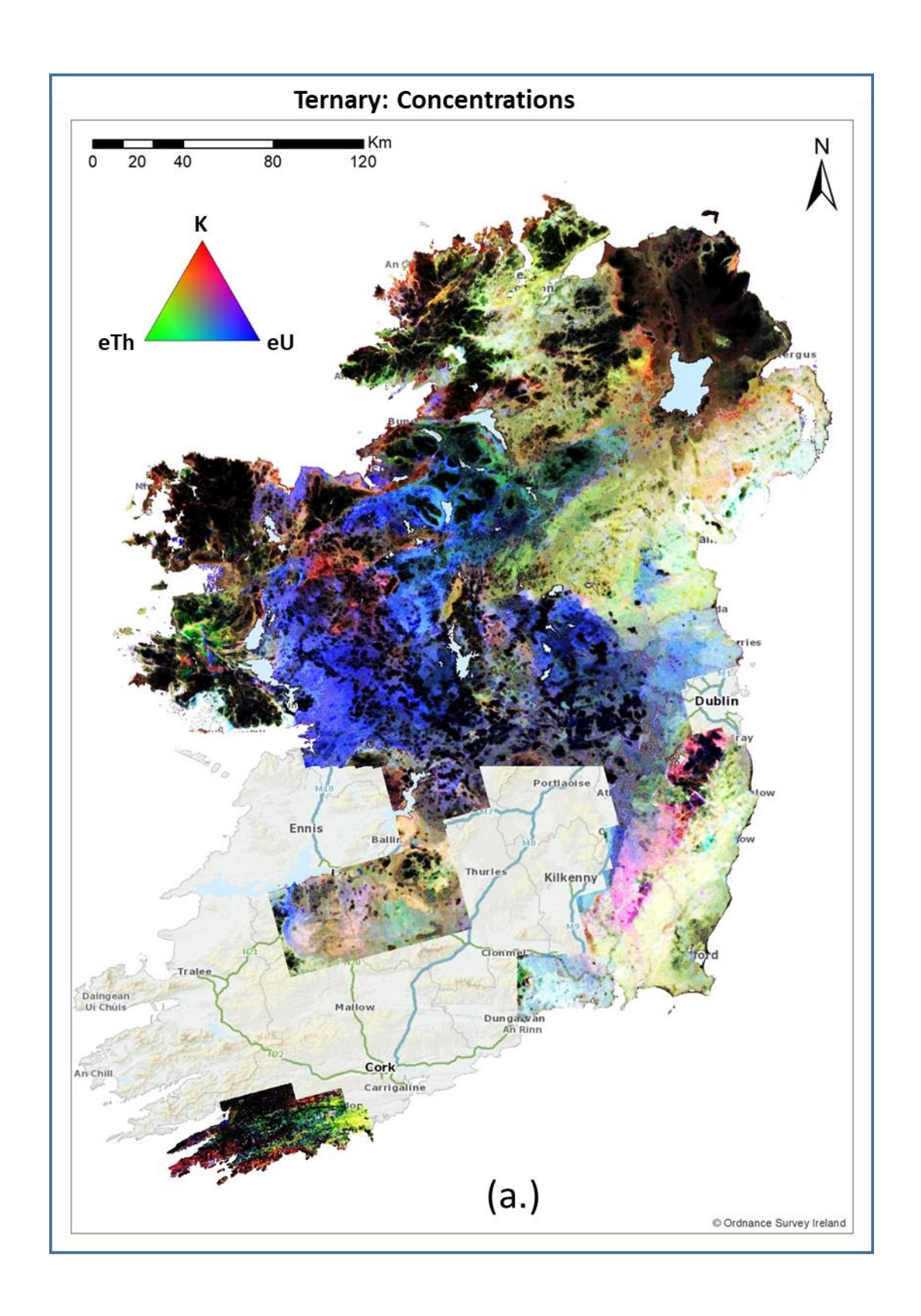
4.8. Radiometric Examples from Tellus Data

A number of case-study examples are presented that illustrate the geological mapping and resolving capabilities of the Tellus radiometric data.

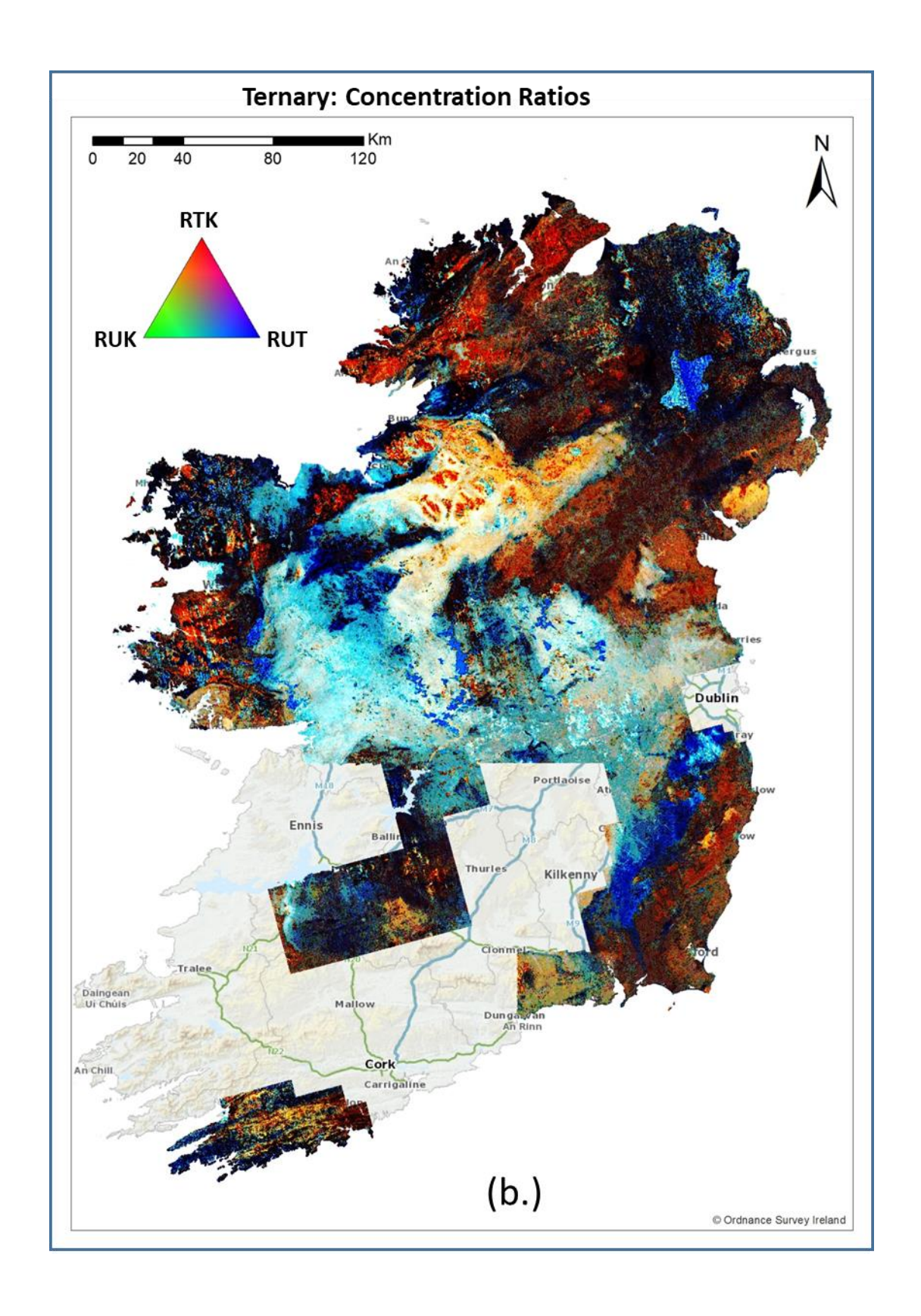
As a precursor to those examples, Figure 29 below illustrates, at a country-wide scale, the use of three different ternary images in capturing simultaneously the variations in the three radio-element concentrations. Each ternary image highlights visually different aspects of the radiometric data set. The three ternary images presented are:

- i) Radio-element concentrations: K-eTh-eU
- ii) Radio-element concentration ratios: RTK-RUK-RUT
- iii) Sum-normalised radio-element abundances: Kn-THn-Un











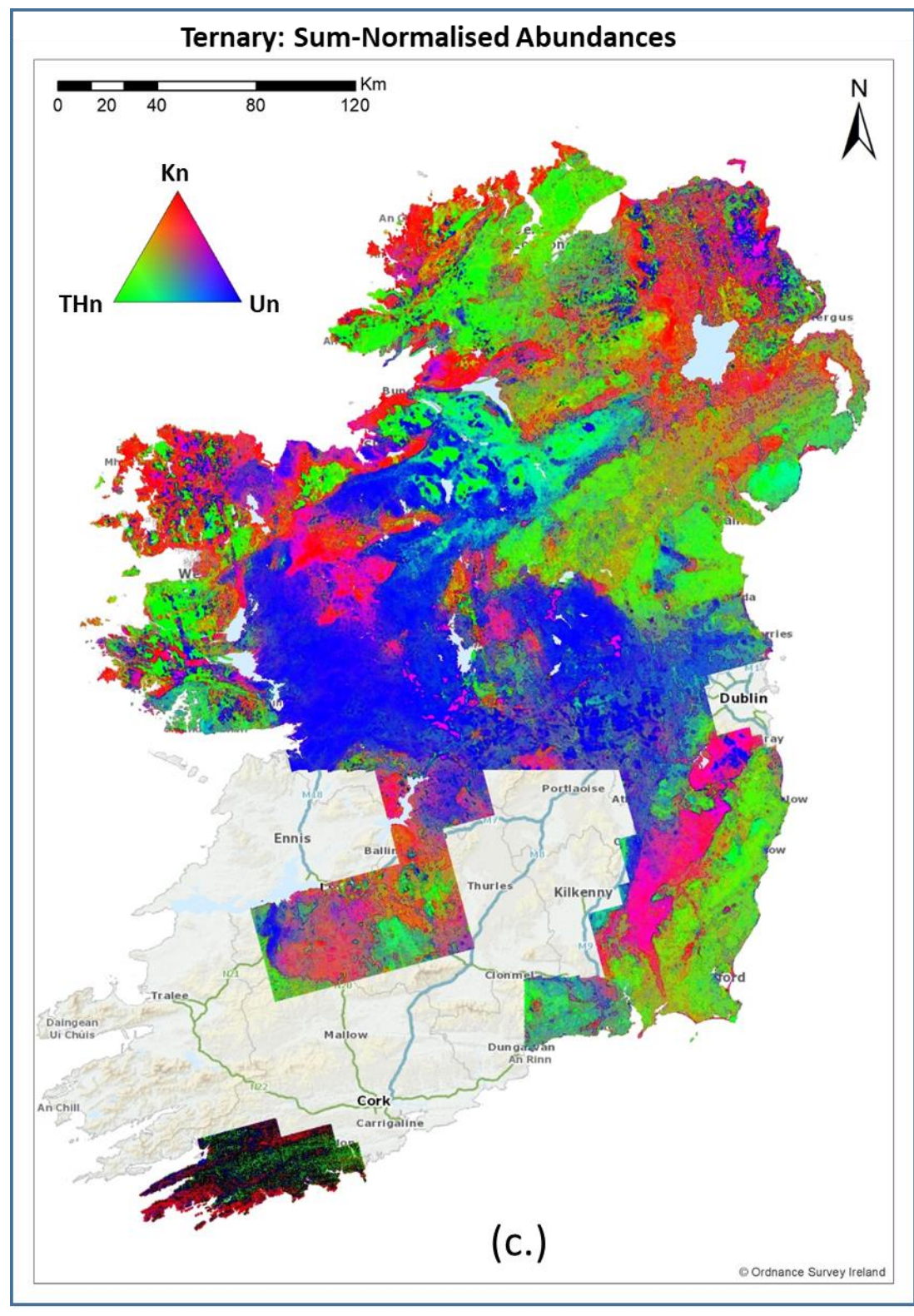


Figure 29. Ternary images of radiometric data. (a.) Concentrations: K—eTh—eU. (b.) Concentration ratios: RTK—RUK—RUT. (c.) Sum-normalised abundances: Kn—THn—Un.

The colours in the ternary image of normalised abundances (Figure 29c) tend to emphasise the most prominent of the three radio-elements at any location, leading to distinctly red, blue and green areas where potassium, thorium and



uranium are, respectively, the dominant element relative to the other two elements. The use of normalised abundances may reduce the effect of vegetation and soil moisture in the data, compared with concentration data.

Figure 30 below aims to help in understanding the colour variations that arise in the ternary images, which are all plotted using an RGB colour palette, using the case of the concentration ternary (K–eTh–eU) as an example. The colour variations exemplified in the figure may be applied to all other ternary images.

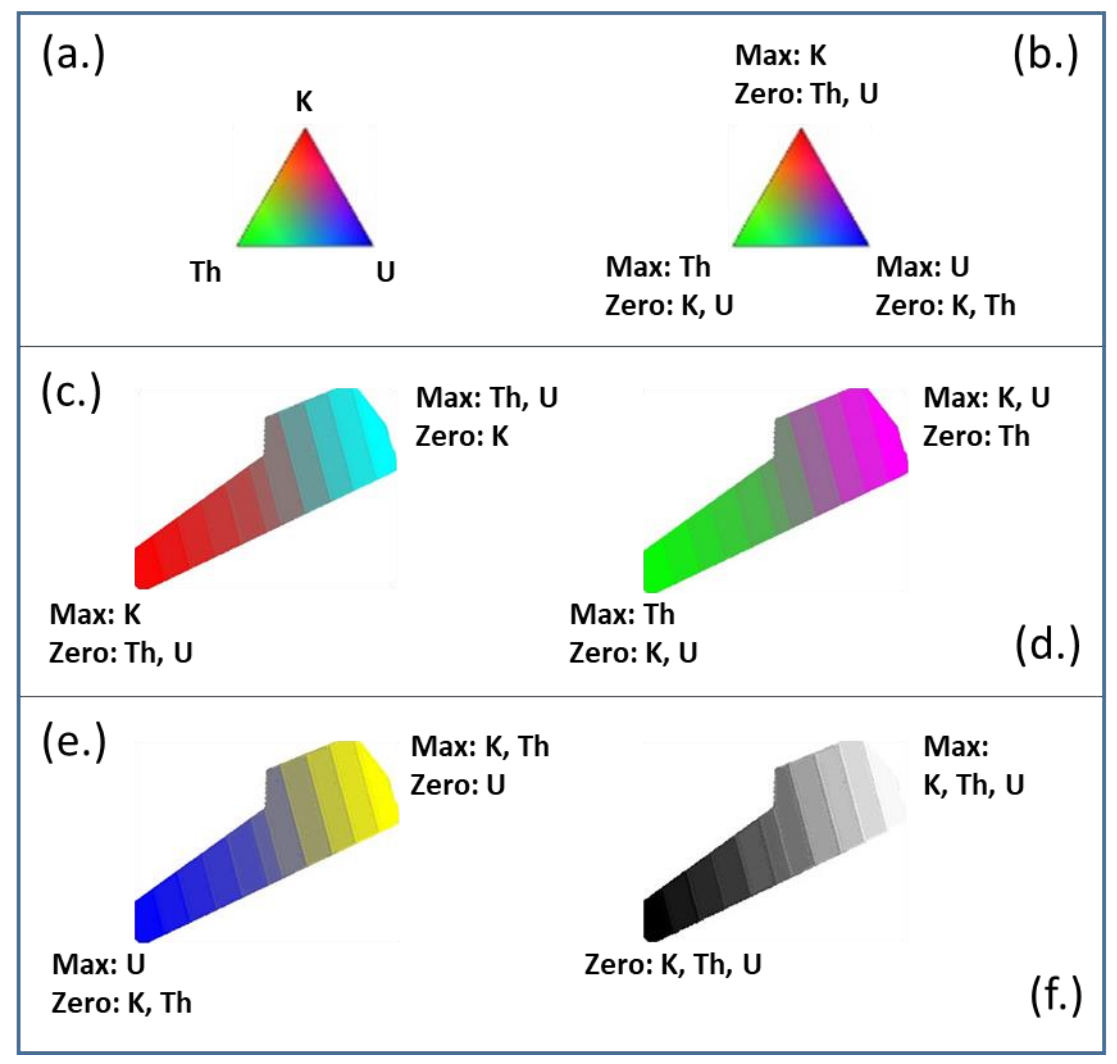


Figure 30. Guide to colours generated using RGB colour palette for ternary displays. (a. and b.) illustrate the standard colour allocation used in the concentration ternaries: red = maximum K concentration in the dataset, green = maximum thorium concentration and blue = maximum uranium concentration. (c., d. and e.) illustrate the colour variation from, on left-hand side, maximum concentration in one element and zero concentration in the other two, to, on right-hand side, zero concentration in the same one element and maximum concentration in the other two. (f.) illustrates the colour variation that arises when the concentrations in all three elements increase simultaneously from zero on left-hand side (black) to their maxima on right-hand side (white).

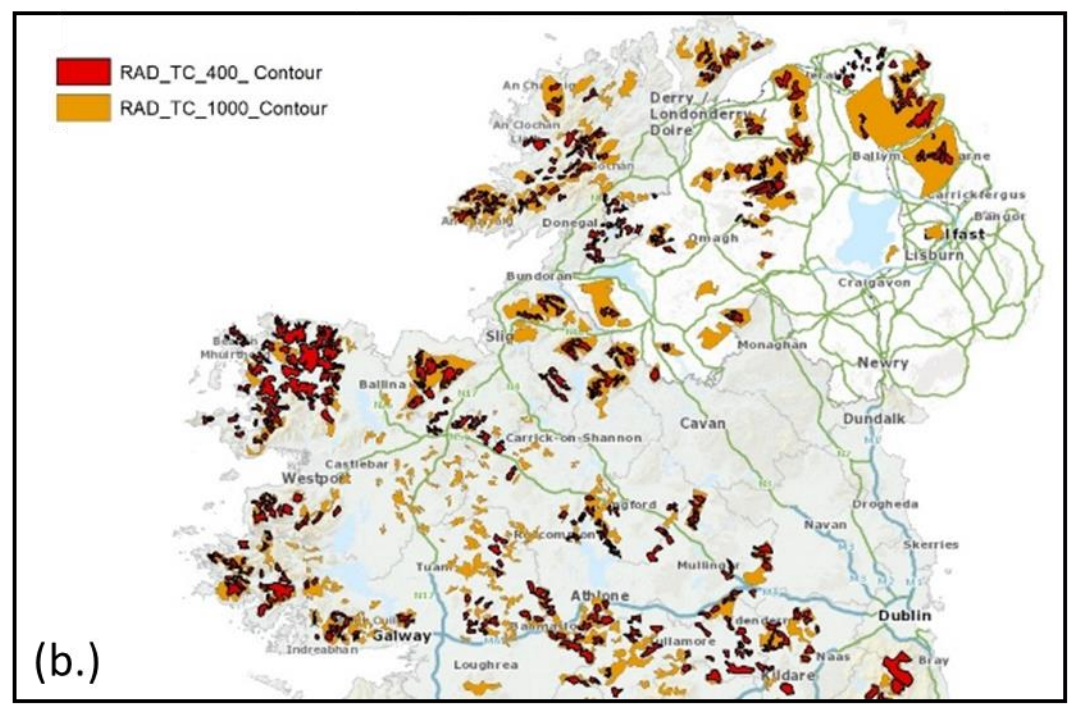


4.8.1. Quaternary sediment mapping

4.8.1.1. Peat mapping

1:100K Quaternary Peat O 12.5 25 50 75 100 Killometers (a.)

Radiometric Total-Count polygons



- Red polygons, where total-count < 400 c/s, are associated with thicker peat deposits (> 1.5 m thick).
- Orange polygons, where total-count < 1000 c/s, are associated with thinner peat.



Figure 31. Peat bogs mapped by airborne total-count data. Thick peat (red) areas are mapped where total-count ≤ 400 c/s. Orange polygons (total-count ≤ 1000 c/s) map the majority of peat deposits on the Quaternary map.

Total-count data can be used to help map peat deposits. Water, and therefore water saturated peat, cause significant attenuation of gamma rays. Low total-count measurements therefore correspond with areas of high water content, either in the form of free-standing water bodies or peat. By removing data recorded over water bodies, the remaining low value total-count data are generally all associated with peat deposits. Counts less than 400 c/s generally indicate relatively thick peat (>1 m thick), as outlined in the Bundoran Test Line experiment (Section 4.7 and Figures 27 and 28). Total-counts less than 1000 c/s correspond with almost all peat bogs shown on the Quaternary map (Figure 31). Total-count mapping could therefore be used as a proxy for approximate carbon stock calculations, although further information on peat thickness and volume is required for more precise calculations.

4.8.1.2. Alluvium and till mapping – River Maigue, Co. Limerick

Three-element composite images provide an alternative to ternary images for displaying radiometric three-element data simultaneously on one map. In the scheme, each individual element is coloured using a standard Geosoft blue-to-red-violet palette, and the composite colour is taken as the sum of each of the three colours at each map point. The composite image may reveal or draw attention to geological features not immediately apparent in each of the three individual element maps or in a ternary image.

A composite image based on sum-normalised abundances is presented in a case study over the alluvium deposits of the River Maigue, Co. Limerick (Figure 32), in comparison with the standard ternary image of radiometric concentrations.



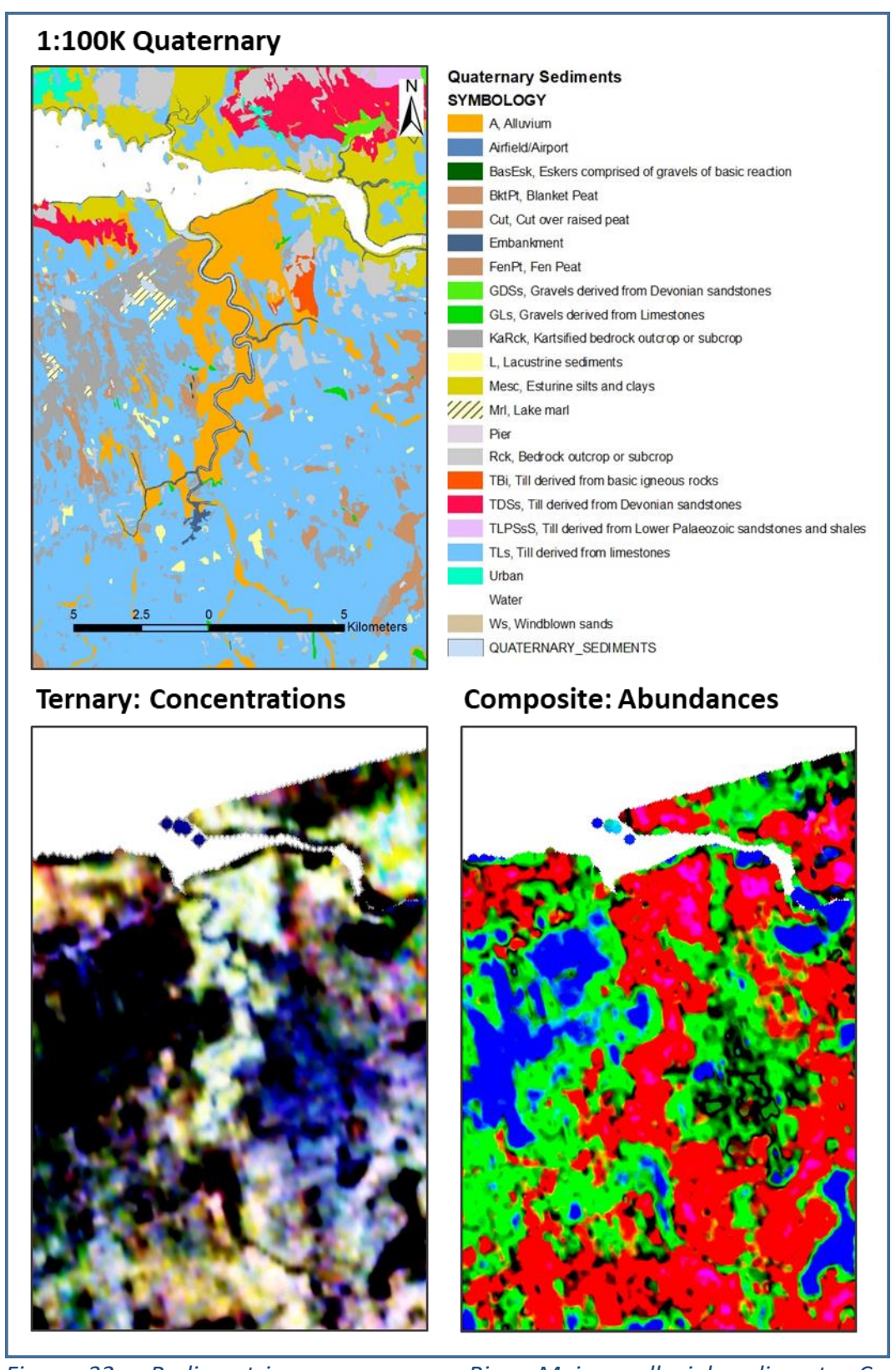
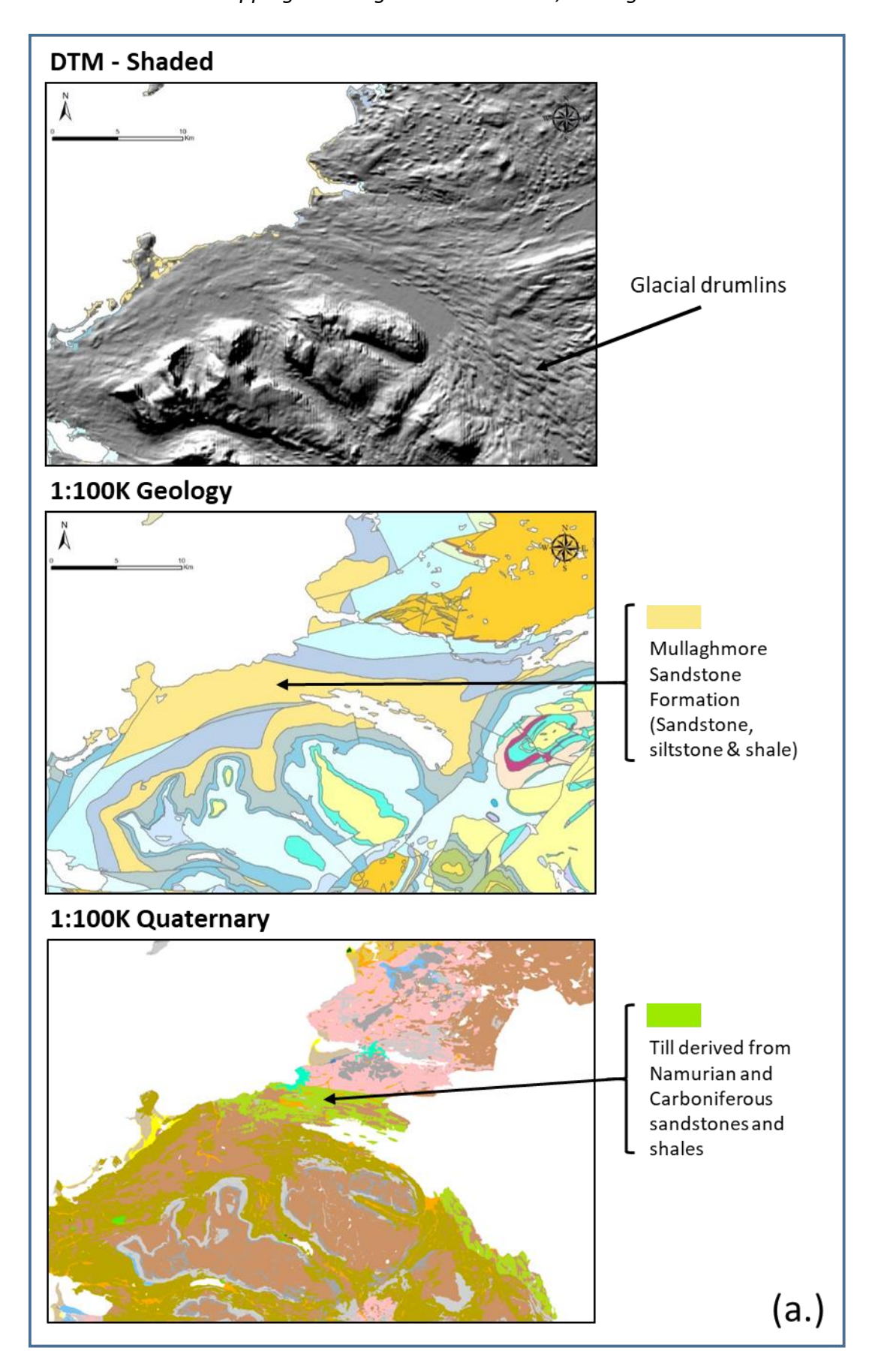


Figure 32. Radiometric response over River Maigue alluvial sediments, Co. Limerick, showing extract from 1:100,000 Quaternary geology map, ternary image of concentrations and composite image of sum-normalised abundances.







Radiometric Ternary - Concentrations Black areas (low K, Th and U eTh concentrations) correspond with water bodies (e.g., Lough Melvin) and peat. 1:100K Geology with Mullaghmore radiometrics In-situ K rich till, derived from underlying sandstones? Glacial retreat **DTM with Mullaghmore radiometrics** U and Th rich till, potentially derived and transported from surrounding carbonate successions and deposited during glacial retreat? (b.)

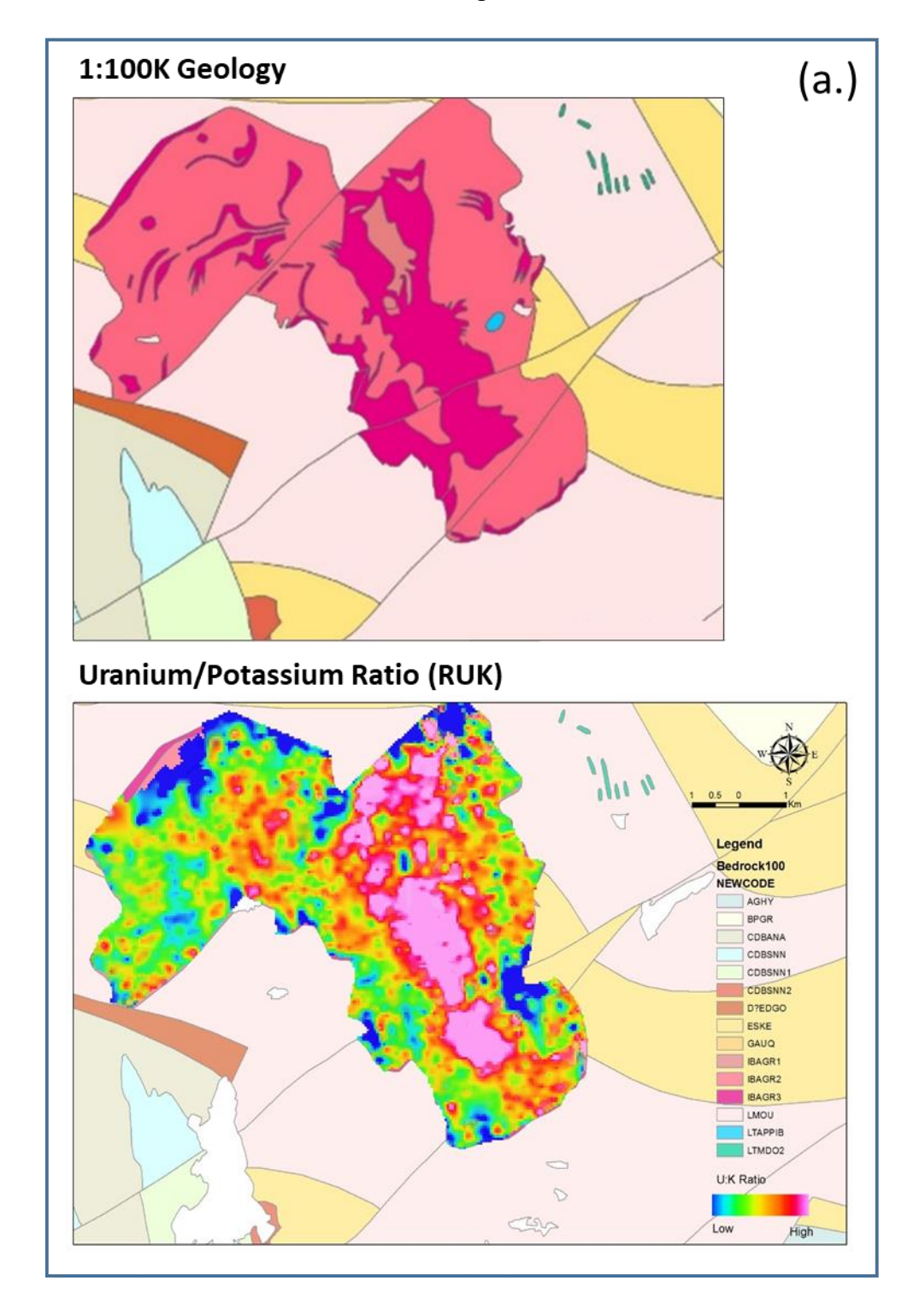
Figure 33. Radiometric response of Mullaghmore Sandstone, Co. Sligo and Co. Leitrim. (a.) Extract from high-resolution DTM, and 1:100,000 geological and



Quaternary maps. Note absence of mapped Quaternary geology in Northern Ireland. (b.) Radiometric concentration ternary map, and 1:100,000 Geology map and DTM shown with radiometric ternary data clipped to the boundary of the Mullaghmore Sandstone Formation.

4.8.2. Bedrock mapping

4.8.2.1. Barnesmore Granite, Co. Donegal – Internal zonation





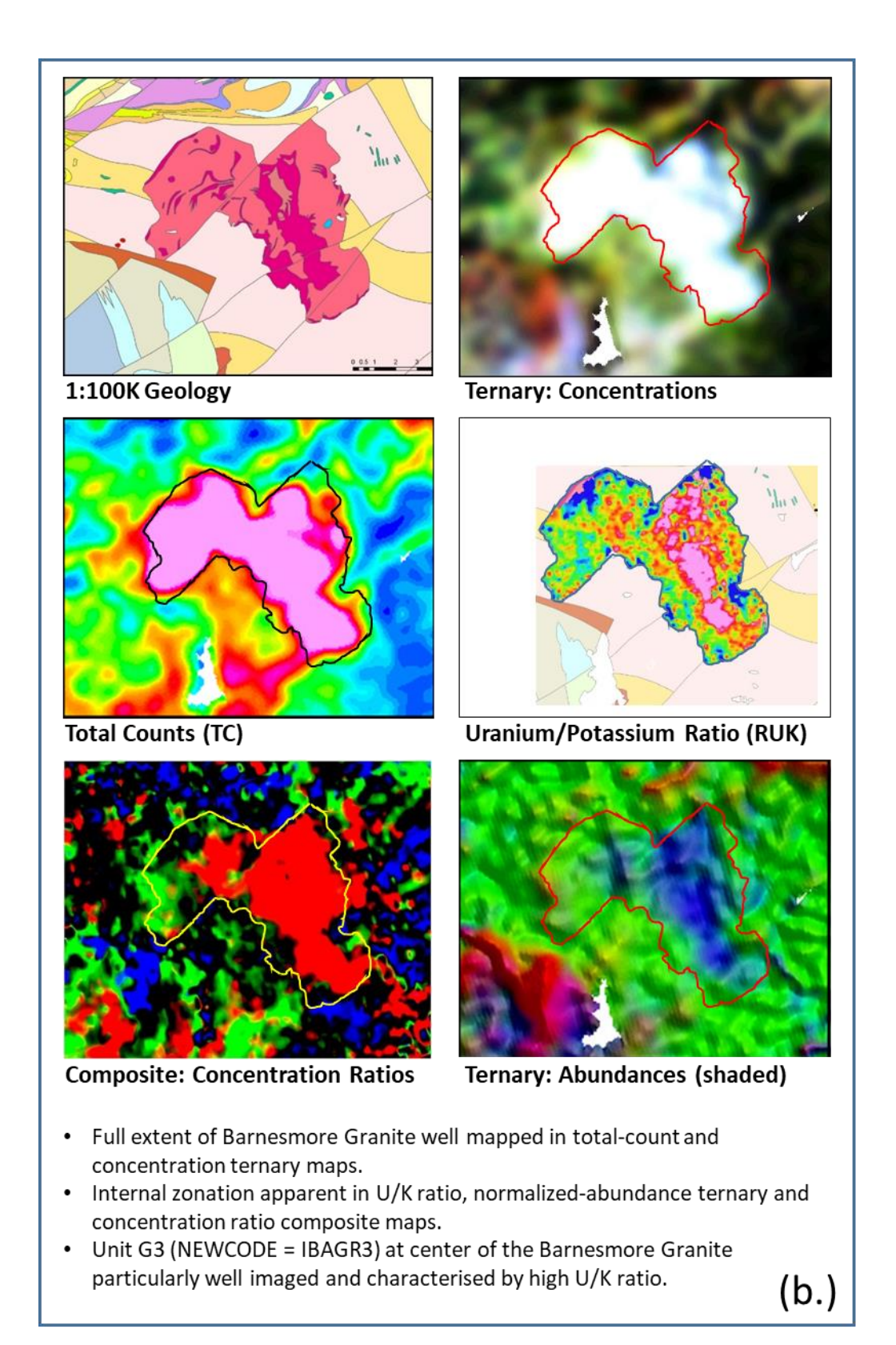
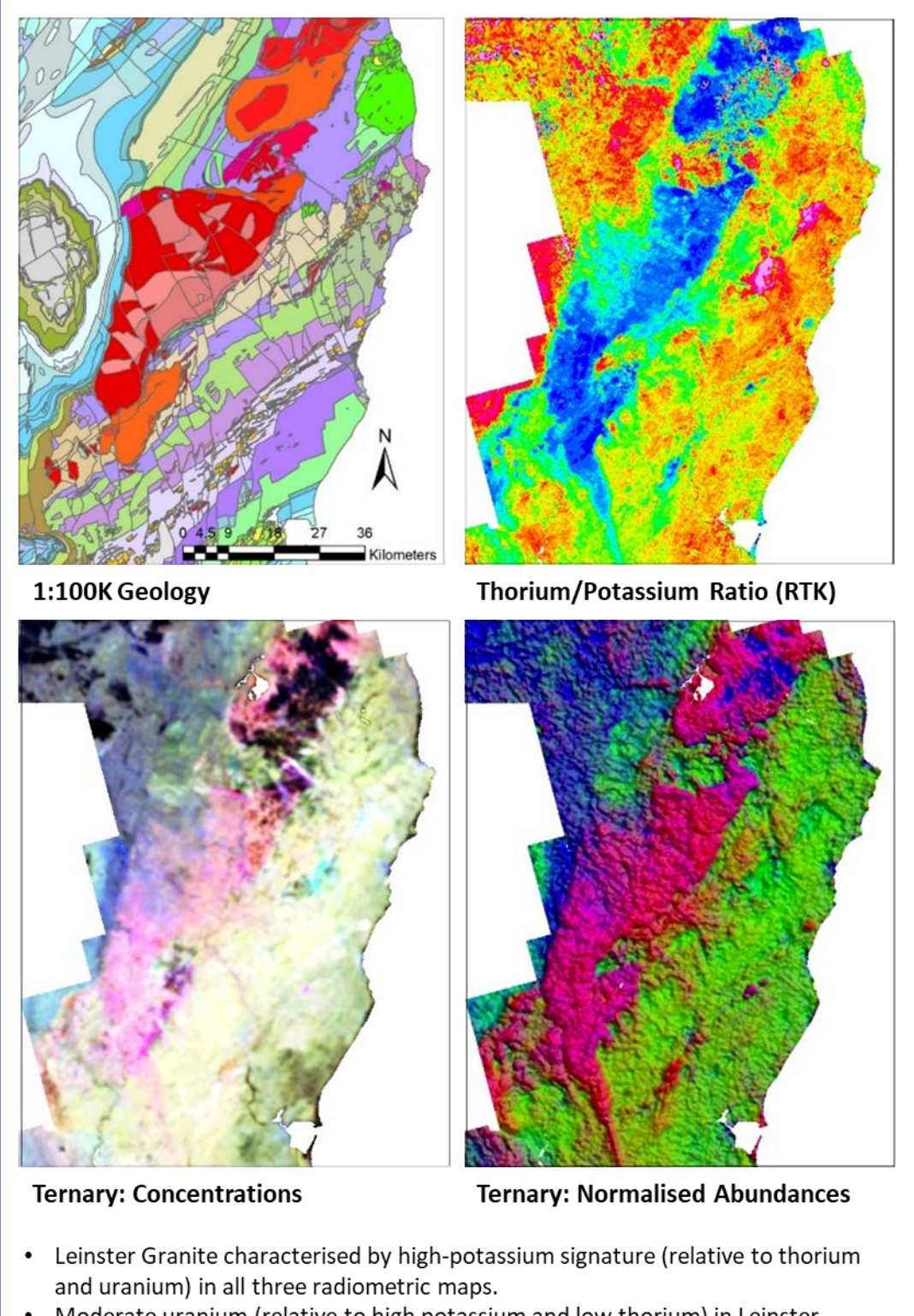


Figure 34. Radiometric response of Barnesmore Granite, Co. Donegal. (a.) Extract from 1:100,000 geological map in comparison with Uranium/Potassium concentration ratio map. (b.) Comparison between geological map and five different radiometric maps, emphasising different aspects of the internal structure of the granite. Outline of the granite displayed variously in different colours on the maps. U/K ratio map is clipped to the boundary of the granite.



4.8.2.2. Geology of South Eastern Ireland

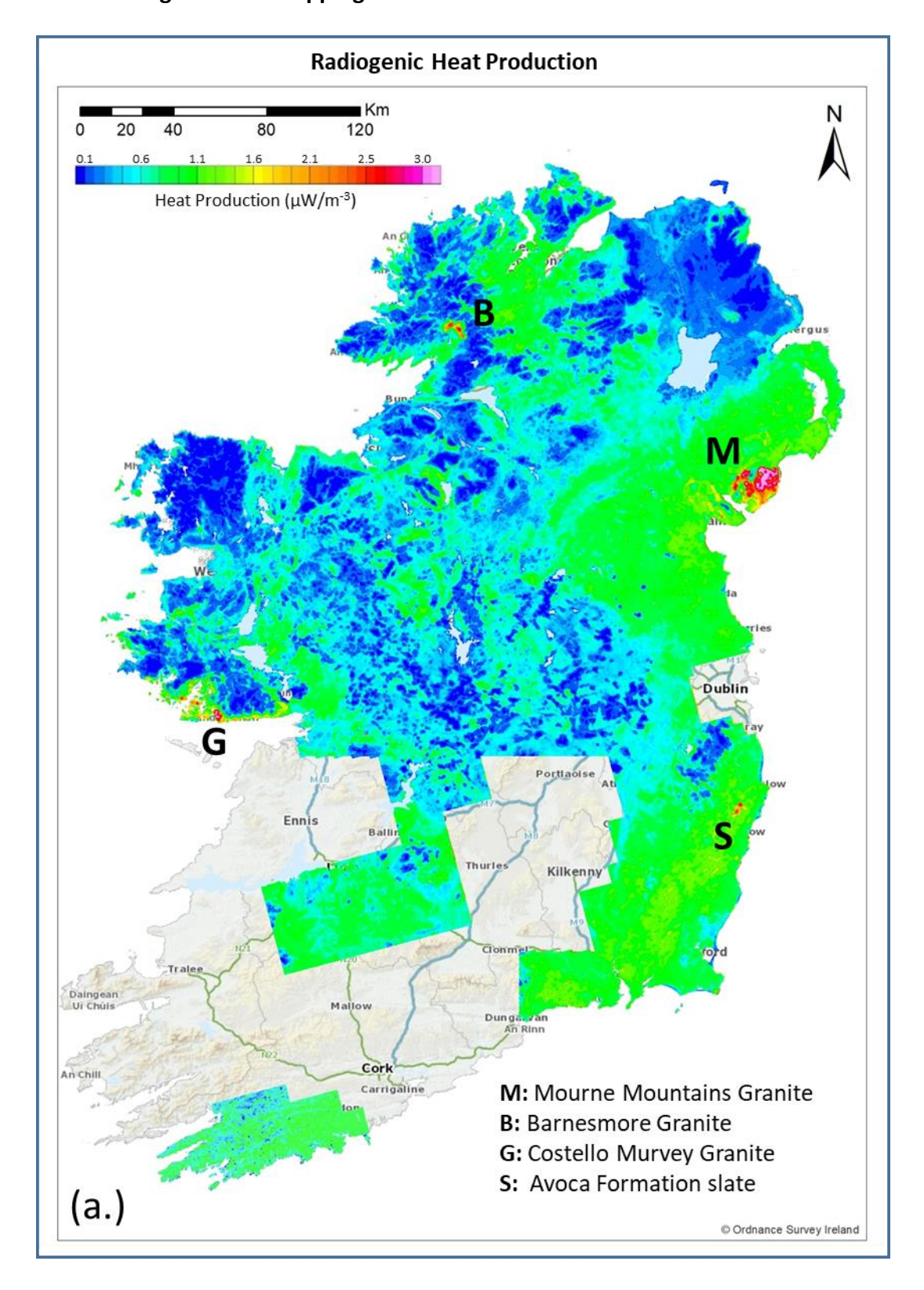


 Moderate uranium (relative to high potassium and low thorium) in Leinster Granite indicated by pinkish tone in concentration ternary and purplish tone in abundance ternary.

Figure 35. Radiometric response of South Eastern Ireland.



4.8.3. Radiogenic heat mapping





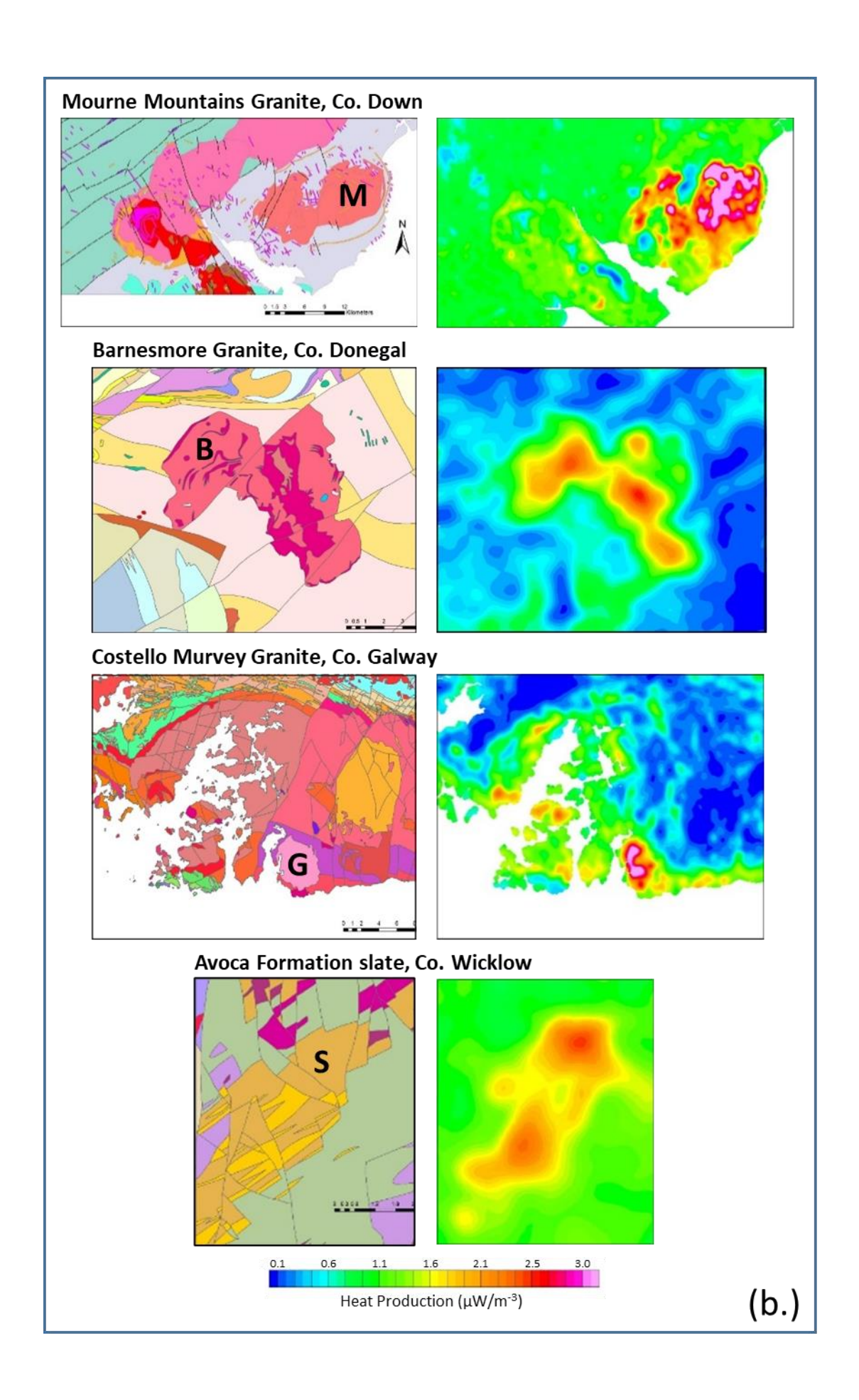




Figure 36. Radiogenic heat production of near-surface rocks in Ireland, derived from Tellus radio-element (K, U, Th) concentrations. (a.) Map of Irish radiogenic heat production, with several high heat production geological formations highlighted. (b.) Extracts from geological (left-hand side) and radiogenic heat production (right-hand side) maps at selected geological localities.

In terms of geophysical behaviour of the Earth, one of the most important applications of radiometrics is in the modelling of its thermal state. In the radioactive decay process, a portion of the mass of each decaying nuclide is converted to energy. Most of this energy resides in the kinetic energy of emitted particles or in the electromagnetic radiation of gamma rays. Radiogenic heat production in Ireland is calculated from Tellus radio-element concentrations using Equation 2 (Section 4.4). Radiogenic heat production hotspots in Ireland are associated with the Mourne Mountains, Costello Murvey and Barnesmore Granites and slates of the Avoca Formation (Figure 36).



5. References

- Beamish, D., 2013. Gamma ray attenuation in soils of Northern Ireland, with special reference to peat. *Journal of Environmental Radioactivity*, **115**, 13–27.
- Beard, L.P. and Nyquist, J.E., 1998. Simultaneous inversion of airborne electromagnetic data for resistivity and magnetic permeability. *Geophysics*, **63**(5), 1556–1564.
- Fraser, D.C., 1978. Resistivity mapping with an Airborne Multicoil Electromagnetic system. *Geophysics*, **43**, 144–172.
- Geosoft Oasis Montaj. Software for Earth Science Mapping and Processing.
- GSI, 2020a. *Tellus A5 Block: aempy Electromagnetic Inversion Report*. Technical Report, Geological Survey Ireland, February, 2020.
- GSI, 2020b. *Tellus Waterford (WFD) Block: aempy Electromagnetic Inversion Report*. Technical Report, Geological Survey Ireland, July, 2020.
- GSI, 2020c. *Tellus A6 Block: aempy Electromagnetic Inversion Report*. Technical Report, Geological Survey Ireland, July, 2020.
- Grasty, R.L. and Minty, B.R.S., 1995. The standardisation of airborne gamma-ray surveys in Australia. *Exploration Geophysics*, **26**(3), 276–283.
- Hautaniemi, H., Kurimo, M., Multala, J., Leväniemi. H. and Vironmäki, J., 2005. The 'Three-In-One' aerogeophysical concept of GTK in 2004. In: Airo, M.-L. (ed.), *Geological Survey of Finland, Special Paper*, **39**, 21–74.
- Huang, H. and Fraser, D.C., 2001. Mapping of the resistivity, susceptibility, and permittivity of the earth using a helicopter-borne electromagnetic system. *Geophysics*, **66**(1), 148–157.
- Huang, H. and Fraser, D.C., 2003. Inversion of helicopter electromagnetic data to a magnetic conductive layered earth. *Geophysics*, **68**(4), 1211–1223.
- International Atomic Energy Agency (IAEA), 2003. Guidelines for radioelement mapping using gamma ray spectrometry data.
- Kiyan, D. and Rath, V., 2017. Inverse Methods for Airborne Electromagnetic Data from the Tellus Surveys: The aempy Toolbox. Unpublished Report and User Manual, Dublin Institute for Advanced Studies, Ireland, March 21, 2017.
- Milligan, P.R. and Gunn, P.J., 1997. Enhancement and presentation of airborne geophysical data. *AGSO Journal of Australian Geology and Geophysics*, **17**(2), 63–75.
- Nabighian, M.N., 1972. The Analytic Signal of two-dimensional magnetic bodies with polygonal cross-section: Its properties and use for automated anomaly interpretation. *Geophysics*, **37**, 507–517.
- Parasnis, D.S., 1986. *Principles of Applied Geophysics, Fourth Edition*. Chapman and Hall Ltd., London.
- Salem, A., Williams, S., Fairhead, J.D., Ravat, D. and Smith, R., 2007. Tilt-depth method a simple depth estimation method using first-order magnetic derivatives. *The Leading Edge*, **26**, 1502–1505.



- Sengpiel, K.-P., 1988. Approximate Inversion of Airborne EM Data from a Multilayered Ground. *Geophysical Prospecting*, **36**, 446-459.
- Sengpiel, K.-P. and Siemon, B., 1998. Examples of 1D Inversion of Multifrequency AEM Data from 3D Resistivity Distributions. *Exploration Geophysics*, **29**, 133–141.
- SGL, 2019. Fixed-Wing High-Resolution Aeromagnetic, Gamma-ray Spectrometric and Frequency-Domain Electromagnetic Survey, Tellus A5 Block, Republic of Ireland, 2019. Unpublished Technical Report, Sander Geophysics Limited, Canada, August, 2019.
- Telford, W.M., Geldart, L.P., Sheriff R.E. and Keys D.A., 1976. *Applied Geophysics*. Cambridge University Press, Cambridge.
- van Dam, C.L., 2007. *Radiogenic Thermal Heat Potential of Northern Ireland*. Unpublished Internal Report to Geological Survey of Northern Ireland.
- Verduzco, B., Fairhead, J.D., Green, C.M. and MacKenzie, C., 2004. New insights into magnetic derivatives for structural mapping. *The Leading Edge*, **23(2)**, 116–119.



Appendix 1. Supplementary Information - Magnetics

1. First Vertical Derivative

The first vertical derivative (FVD) is given by equation:

$$FVD = \frac{\partial T}{\partial z}$$

where T is total magnetic field intensity and z is vertical distance. The measurement unit is nT/m.

2. Second Vertical Derivative

The second vertical derivative (SVD) is defined as:

$$SVD = \frac{\partial^2 T}{\partial^2 z}$$

where T is total magnetic field intensity and z is vertical distance. The measurement unit is nT/m²

3. Analytic Signal

The analytic signal (AS) (Nabighian, 1972) is defined as:

$$AS = \sqrt{\left(\frac{\partial T}{\partial x}\right)^2 + \left(\frac{\partial T}{\partial y}\right)^2 + \left(\frac{\partial T}{\partial z}\right)^2}$$

where T is total magnetic field intensity and x and y are distances in the two horizontal grid directions and z is vertical distance. The measurement unit is nT/m.

4. Tilt Derivative

The tilt derivative (or tilt angle, θ , or local phase) (Verduzco et al., 2004) of a magnetic anomaly, T, is given by:

$$\theta = \tan^{-1} \frac{VDR}{THDR}$$

where the numerator and denominator are the vertical and horizontal derivatives of the anomaly, respectively. The vertical derivative is given by (cf. section 6.1):

$$VDR = \frac{\partial T}{\partial z}$$

and the total horizontal derivative is given by:



$$THDR = \sqrt{\left(\frac{\partial T}{\partial x}\right)^2 + \left(\frac{\partial T}{\partial Y}\right)^2}$$

The measurement unit is degrees or radians, where 1 degree = $\pi/180$ radians or 1 radian = $180/\pi$ degrees.

5. Total Horizontal Derivative of Tilt Derivative

The total horizontal derivative of the tilt derivative is defined as:

$$HD_TDR = \sqrt{\left(\frac{\partial TDR}{\partial x}\right)^2 + \left(\frac{\partial TDR}{\partial y}\right)^2}$$

The measurement unit is radians/m or degrees/m.



Appendix 2. Supplementary Information - Electromagnetics

1. EM Method

A transmitter coil is excited by a time-varying electric current and produces an alternating magnetic field in space so that currents are then induced in any nearby conductors (e.g., ground, sea water). These induced currents in turn produce a secondary magnetic field which is sensed by the receiver coil and recorded. A part of the transmitting current is fed into the recording electronics to buck out the primary magnetic field at the receiver. Using this technique, the secondary field can be measured with high precision so that its in-phase and quadrature components are recorded in parts per million (ppm) of the primary magnetic field with a precision of one ppm.

2. Electrical Conductivity of Porous Rocks

The conductivity of porous rock varies with the volume and physical arrangement of the pores and with the conductivity and amount of contained water (fluid). Archie's empirical formula provides one means of describing and estimating the resistivity of porous rocks (Archie, 1942):

$$\rho_r = \frac{a\rho_w}{\phi^m S^n}$$

where ρ_r is the bulk rock resistivity, ρ_w is resistivity of water in pores, φ is porosity, S is fraction of pore spaces filled by water, and a, m and n are empirical constants such that typically $n \approx 2$, $0.5 \le a \le 2.5$ and $1.3 \le m \le 2.5$. Note that the bulk rock resistivity in Archie's formulation is independent of the resistivity of the rock matrix itself. The resistivity of the pore water depends on the concentration of dissolved solids (ions).

3. Depth of Investigation

Conceptually, the depth of investigation can be defined as the maximum depth at which a buried target can be detected by a measurement system. The EM response of the target should be sufficiently large compared to the strength of the primary field transmitted by the AEM system and to the noise of the system. Although the depth of penetration is mainly controlled by the subsurface resistivity and the frequencies of investigation (as illustrated by Equation 1 in Section 3.3), transmitter moment, noise-levels (both system and cultural) and flight height in AEM surveys also affect depth of investigation. Quantification of the depth of investigation, or depth of sensitivity, of an AEM system is not straight-forward as the EM signal strength, and hence sensitivity to geological structures, decays gradually with depth and is not lost suddenly and entirely at



any particular depth. Comprehensive numerical simulation and modelling of both observed and synthetic EM response data is ideally required to quantify reliably the depth of investigation for any particular subsurface resistivity structure and flight altitude.

In the absence of such detailed numerical modelling, approximate measures of depth of investigation based on the EM skin-depth (P, Equation 1) are commonly used, for example, the half-skin-depth (P/2) (SGL, 2019). While alternative approximations based on the skin-depth are also used (e.g., Sengpiel, 1988 and Sengpiel and Siemon, 1998) they do not differ significantly from P/2. Typically for the Tellus survey, the reliable maximum depth of EM investigation and sensitivity is of the order of 60 m below ground level.

4. EM Noise

System noise

System noise refers to the noise that is intrinsic to the EM measurement system as a whole. Geological signals with amplitudes lower than the amplitude of the system noise cannot be measured. While much of the system noise relates to the electronics of the transmitter, receiver and recording systems, other sources of noise may also be regarded as 'system' noise. For example, thunderbolts and lightning create EM pulses that can be measured with an EM system from long distances. However, due to their characteristic shapes, these signals can be filtered out during data processing. Motion noise due to thermal expansion of the aircraft wings is also a source of time varying noise in the data. If the distance between the EM transmitter and receiver loops located on the wing-tips is reduced by about 2 mm then it causes an in-phase anomaly of about 280 ppm in the recorded EM responses. As an aluminium rod of 20 m length will shorten by 2 mm if the temperature drops about 4°C (Hautaniemi et al., 2005), thermal noise of the order of 280 ppm may arise during the course of a daily survey flight. Drift corrections applied during data processing aim to correct for temperature effects on the recorded data.

Cultural noise

Cultural noise is recorded when flying over buildings, industrial complexes, railways, motorways and power-lines. Noise in the EM data may create negative values in the EM responses. The number of negative values is generally higher for the in-phase components than the quadrature components and the number of negative values in the data is generally an indication of the level of cultural noise. Typically, the percentage of negative values decreases with increasing frequency, i.e., the higher frequency data tend to have lower levels of cultural noise.



Rock petrophysical parameters

Beard and Nyquist (1998) and Huang and Fraser (2001, 2003) demonstrated the effects and the interactions of three earth parameters (magnetic permeability, dielectric permittivity and conductivity) on frequency domain EM data. Interpretation of AEM data is commonly resistivity/conductivity under the assumption that the magnetic permeability (susceptibility) is that of free space and dielectric permittivity ignored. In reality, the data contain information about magnetic permeability, dielectric permittivity and conductivity and variation in these parameters affects the data. Practically, variation in dielectric permittivity has very little effect on the data at the frequencies used for the Tellus program. However, when surveying over strongly magnetic rocks, subsurface imaging may benefit from the inclusion of magnetic permeability in the modelling.

Flight altitude

EM measurements at high altitude correspond with low signal-to-noise ratios as the geological signal strength is attenuated with increasing altitude. The low signal-to-noise ratios at high altitude reduce the reliability of the transformation of the EM response data into resistivity values. While the modelling algorithms used in deriving resistivity values from the EM response data take into account the variation in flight altitude, when flight altitude becomes too high, noise dominates and reliable resistivity values cannot be computed. Experience and assessment of Tellus airborne EM data shows that usable resistivity data is achieved below altitudes of about 150 m and above which the signal-to-noise ratio is too low. Therefore, data above 150 m altitude are often clipped from the published maps.

Processing noise

Most processing noise is related to levelling of data between different blocks (i.e., at the boundaries of blocks) or between different flight-lines within a block. Levelling errors are clearly observed as stripes in the flight-line direction or as breaks or steps across the boundaries of survey blocks.

